

https://dspace.org/

Surface enhanced raman scattering dependence on chain-length of 1-alkanethiols on gold and silver nanoparticles

Shumbula, Ndivhuwo Prince

2018

https://hdl.handle.net/10539/25874

Shumbula, Ndivhuwo Prince (2018) Surface enhanced Raman scattering dependence on chain-length of 1-alkanethiols on gold and silver nanoparticles, University of the Witwatersrand, Johannesburg, <http://hdl.handle.net/10539/25874>

Downloaded from a DSpace repository. https://dspace.org/

Surface enhanced Raman scattering dependence on chain-length of 1-alkanethiols on gold and silver nanoparticles



A dissertation submitted for the partial fulfilment of the requirements for the degree of Master of Science in Chemistry

Faculty of Science

University of the Witwatersrand

Private Bag X03

Wits

By

Ndivhuwo Prince Shumbula

(Student number: 677753)

Signed by

_____on this_____ day of _____

Student: Mr N.P. Shumbula

Signed by

_____on this _____ day of _____

Supervisor: Prof N. Moloto

Co-Supervisors: Dr M.M. Mlambo, Dr P.S. Mdluli

Declaration

I declare that this dissertation “Surface enhanced Raman scattering dependence on chain-length of 1-alkanethiols on gold and silver nanoparticles” was my own work carried out under the supervision of Prof N. Moloto, Dr M. Mlambo and Dr P. Mdluli. This work is being submitted for the degree of masters of Science (chemistry) to the school of Chemistry, Faculty of Science, University of the Witwatersrand, Johannesburg and has not been submitted before for any degree or examination at any university.

Name : Ndivhuwo Prince Shumbula Date : ___/___/2017

Signature : _____

Abstract

Surface enhanced Raman spectroscopy (SERS) is a surface sensitive technique through which the Raman signal of molecules adsorbed on a metallic surface is enhanced. It is a molecular vibrational technique which has evolved from the classic Raman spectroscopy in early 1970s. This technique is widely used for identification of solid, liquid and gas analytes. It also enables a sensitive detection of single molecule and also provides its distinguished chemical fingerprints. This technique has the ability to improve the Raman cross section by orders of up to 10^{15}. The enhancement of local magnetic field due to localised surface plasmon resonance (SPR) is greatly dependent on SERS substrates (i.e. metal nanoparticles) used and the molecule (Raman reporter) attached to the substrate. In the current project, we report on the effect that the chain-length of 1-alkanethiol functionalized on gold and silver nanoparticles (AuNPs and AgNPs) has on the Raman scattering enhancement.

AuNPs and AgNPs were synthesized by the reduction of chloroauric acid and silver nitrate respectively, using tri-sodium citrate as a reducing agent. Citrate capped nanoparticles were obtained and further functionalized with 1-alkanethiols of different chain-lengths, i.e. pentanethiol (PT), decanethiol (DT), dodecanethiol (DDT), and pentadecanethiol (PDT). The 1-alkanethiols were chosen as Raman reporters because they are able to form self-assembled monolayer (SAM) systems on the surface of metals, thus influencing their stability. The optical properties of both functionalized (SAMs) and unfunctionalized AuNPs and AgNPs were studied using ultraviolet-visible (UV-Vis) spectroscopy. A red shift of the SPR bands of AuNPs and AgNPs prior to functionalization with 1-alkanethiols was observed from the UV-Vis spectra. AuNPs and AgNPs which were monodispersed and spherical-like morphology with the average diameters of 14 and 25 nm respectively were obtained as was evidenced from the transmission electron microscopic (TEM) analysis. The obtained negative zeta

potential indicated negatively charged surfaces for both AuNPs and AgNPs. AuNPs were more stable and well dispersed in the colloidal solution as compared to AgNPs since they possessed a strong negative zeta potential. The effect of chain-length on Raman scattering was evaluated using Raman spectroscopy and the enhancement factor (EF) was calculated from the intensities of symmetric stretch vibrations of C-H observed in the region of about 2900 to 3000 cm^{-1} in all SERS spectra. SERS spectra for all 1-alkanethiols (Raman reporters) showed more intense characteristic peaks as compared to their classical Raman spectra. Some vibrational modes which were not observed in classical Raman spectra where observed from the SERS spectra. The shorter chain-length PT possessed a higher enhancement factor (EF) of the Raman cross-section as compared to the longer chain-lengths 1-alkanethiols. DFT and Molecular Dynamic studies were done to establish the influence of the chain length on the EF. The geometry of the RR adsorbed on the metal surface as well as the position in which the RR was adsorbed on the metal surface was found to influence the charge density transfer hence the SERS spectra obtained. From the calculations, it was evident that the adsorption of the RRs on both Ag and Au metals resulted on an enhanced Raman spectra however other factors influenced the observed EF trend.

Acknowledgements

- Foremost, I would like to thank the God Almighty for giving me the courage, strength and His endless Grace to accomplish this task. I would like to extend my sincere gratitude to my supervisors Prof Nosipho Moloto, Dr Mbuso Mlambo and Dr Phumlane Mdluli for the continuous support of my MSc research, for their patience, motivation, enthusiasm and immense knowledge. Their guidance helped me through all the time of research and writing of this dissertation. I couldn't have imagined having best supervisors and mentors for my MSc.
- My sincere thanks also go to my brother Dr Poslet Shumbula for his eye opening advices, guidance, support and motivations.
- I would like to thank my fellow lab mates in 'The MOLOTO group' (lab 330) for their advices, comments, hard questions, stimulating discussions, sleepless nights we were working together before deadlines and for all the fun we had. I would like to further extend my gratitude to CATOMAT for valuable suggestion, positive criticisms and encouraging spirit.
- I thank the microscopy and microanalysis unit (MMU) at the University of the Witwatersrand for training and allowing me to use their most valuable and expensive techniques. Special thanks go to Prof Alexander Ziegler, Dr Manoko Maubane, and Dr Zikhona Tetana, for their patience and help.
- I would also like to thank the School of Chemistry at the University of the Witwatersrand for great research facilities and some research based lectures I was provided with.
- This project wouldn't be possible without financial support from DST-NRF.
- Last but not least, I would like to pass my gratitude to my parents and siblings for supporting me morally and spiritually throughout my entire life.

List of Publications

1. Mbuso Mlambo, Richard A. Harris, Philani Mashazi, Myalowenkosi Sabela, Suvardhan Kanchi, Lawrence M. Madikizelae, **Ndivhuwo P. Shumbula**, Nosipho Moloto, Thulani T. Hlatshwayoa, Phumlani S. Mdluli. Computational and experimental evaluation of selective substitution of thiolated coumarin derivatives on gold nanoparticles: Surface enhancing Raman scattering and electrochemical studies. Applied Surface Science 396 (2017) 695-704.
2. Francis Otieno, **Shumbula N. Prince**, Mildred Airo, Mlambo Mbuso, Nosipho Moloto, Rudolph Erasmus, Alex Quandt and Daniel Wamwangi, Improved efficiency of organic solar cells using Au NPs incorporated into PEDOT: PSS buffer layer. AIP Advance 7 (2017) 085302.
3. **Ndivhuwo P. Shumbula**, Nosipho Moloto, Mbuso Mlambo, Phumlane S. Mdluli, Experimental and theoretical study of the effect of 1-alkanethiol chain-length functionalized on gold and silver nanoparticles on surface enhanced Raman scattering. (To be submitted).

Presentations

1. “Surface enhanced Raman scattering (SERS) dependence on chain-length of 1-alkanethiols on gold and silver nanoparticles” Oral presentation. Group seminar, University of the Witwatersrand, South Africa. 30th March 2016.
2. “Synthesis and characterization of silver nanoparticles using chemical reduction method” Oral presentation. Group seminar, University of the Witwatersrand, South Africa. 05th April 2016
3. “Experimental and theoretical study of the effect of 1-alkanethiol chain-length functionalized on gold and silver nanoparticles on surface enhanced Raman scattering” Oral presentation. Group seminar, University of the Witwatersrand, South Africa. 08th September 2017
4. “Dependence of Raman signal enhancement on chain-lengths of 1-alkanethiol adsorbed on gold nanoparticles” Poster presentation. South African chemical institute (SACI). Cape Town, South Africa. 25th-29th June 2017

TABLE OF CONTENTS

DECLARATION ..... **III**

ABSTRACT ..... **IV**

ACKNOWLEDGEMENTS ..... **VI**

LIST OF PUBLICATIONS ..... **VII**

PRESENTATIONS ..... **VIII**

LIST OF FIGURES ..... **XI**

LIST OF TABLES ..... **XIII**

APPENDICES ..... **XIV**

ABBREVIATIONS ..... **XV**

CHAPTER 1 ..... **1**

SYNOPSIS **1**

1.1 BACKGROUND 1
1.2 PROBLEM STATEMENT 3
1.3 MOTIVATION 4
1.4 AIM AND OBJECTIVES 5
1.4.1 Aim *5*
1.4.2 Objectives *5*
1.5 OUTLINE 5
1.6 REFERENCES 7

CHAPTER 2 ..... **9**

LITERATURE REVIEW **9**

2.1 GENERAL INTRODUCTION 9
2.2 SERS ENHANCEMENT MECHANISMS AND ENHANCEMENT FACTOR 10
2.2.1 Electromagnetic enhancement mechanism *10*
2.2.2 Chemical enhancement mechanism *11*
2.2.3 SERS substrate *14*
2.2.3.1 Metallic electrodes *14*
2.2.3.2 Metallic nanoparticles *16*
2.3.4 Raman reporter *24*
2.4 SERS APPLICATIONS 27
2.5 REFERENCES 34

CHAPTER 3 ..... **42**

THE EFFECT OF CHAIN-LENGTH ON THE SERS OF 1-ALKANETHIOLS FUNCTIONALIZED ON AUNPS **42**

3.1 INTRODUCTION 42
3.2 EXPERIMENTAL 44

3.2.1 Chemicals *44*
3.2.2 Synthesis of and functionalization of AuNPs with 1-alkanethiols *44*
3.2.3 Characterization *45*
3.3 COMPUTER SIMULATION 46
3.3.1 Molecular Adsorption *46*
3.4 RESULTS AND DISCUSSION 46
3.5 CONCLUSION 64
3.6 REFERENCES 65

CHAPTER 4 67

THE EFFECT OF CHAIN-LENGTH ON THE SERS OF 1-ALKANETHIOLS FUNCTIONALIZED ON AGNPS 67

4.1 INTRODUCTION 67
4.2 EXPERIMENTAL 68
4.2.2 Instrumentations *69*
4.2.3 Synthesis and functionalization of AgNPs *69*
4.3 RESULTS AND DISCUSSION 70
4.4 CONCLUSION 85
4.5 REFERENCES 86

CHAPTER 5 88

GENERAL CONCLUSIONS AND RECOMMENDATIONS 88

5.1 CONCLUSIONS 88
5.1.1 Synthesis and functionalization of Au and Ag nanoparticles *88*
5.1.2 The dependence of Raman scattering cross-section on the chain-length of 1-alkanethiols *88*
5.2 RECOMMENDATIONS AND FUTURE WORK 89

APPENDIX 90

SUPPLEMENTARY INFORMATION 90

List of figures

Figure 1.1: Energy states diagram depicting the manner through which the incident photons are scattered in Raman spectrometry. 2

Figure 1.2: comparison between (a) classical Raman and (b) SERS effects on the analyte.....3

Figure 2.1: Illustration of the electromagnetic enhancement mechanism in SERS [15]. 11

Figure 2.2: Illustration of the three different types of chemical enhancement mechanism in SERS [15]. 13

Figure 2.3: Scheme illustrating the oxidation–reduction cycle of a silver electrode in electrolyte (KCl) solution. Modified from [15]. 16

Figure 2.4: Approximate wavelength ranges where Ag, Au, and Cu have been well-characterized and are established to support SERS [33]. 17

Figure 2.5: SPR absorption spectra of (a) spherical AuNPs and (b) gold nanorods (AuNR) of different aspect ratio; scheme illustrating the collective oscillations of conduction electrons in response to an external field for nanospheres (c) and nanorods (d). [15]. 21

Figure 2. 6: The effect of (a) sizes and (b) shapes of nanoparticles on the SPR. 22

Figure 2. 7: Illustration of the effect of RR molecules on the EF [98]. 27

Figure 2. 8 Schematic representation of some applications of SERS. 28

Figure 2. 9: SERS based immunoassay for early detection of diseases [40]. 29

Figure 2. 10: A schematic for designing Sensitive and selective gas sensing devices [41]. ...31

Figure 2. 11: Schematic representation for fabrication of the electrochemical-SERS based devices for bio-analysis applications [46].....32

Figure 2. 12: SERS spectra from the reaction suspension collected at different reaction times [50]. 33

Figure 3.1: Schematic diagram representing the synthesis and functionalization of AuNPs. .45

Figure 3.2: UV-Vis absorption spectra of citrate capped and 1-alkanethiols functionalized AuNPs. 47

Figure 3. 3: Particle size distribution of citrate capped and 1-alkanethiols functionalized AuNPs. 50

Figure 3.4: TEM images of (a) citrate-capped, (b) PT, (c) DT, (d) DDT, (e) PDT functionalized AuNPs. 51

Figure 3.5: Raman spectra of 1-alkanethiols (black) and their corresponding SERS spectra (red). * denotes υ(C-H) *sym*, # denotes υ(C-H) *asym* and & denotes υ(Au-S). 54

Figure 3.6: Relationship between the enhancement factor and chain-length of 1-alkanethiols. 56

Figure 3.7: The modelled 1-alkanethiols and their chain-lengths (a) 1-PT, (b) 1-DT, (c) 1-DDT, (d) 1-PDT. 58

Figure 3.8: DFT calculated Raman spectra of (a) PT, (b) DT, (c) DDT, and (e) PDT together with the insert of the zoomed lower region of the spectra. 60

Figure 4.1: UV-Vis absorption spectra of citrate capped and 1-alkanethiols functionalized AuNPs. 71

Figure 4.2: Particle size distribution of citrate capped and 1-alkanethiols functionalized AgNPs 74

Figure 4.3: TEM images of (a) citrate-capped, (b) PT, (c) DT, (d) DDT, (e) PDT functionalized AgNPs. 75

Figure 4.4: Raman spectra of 1-alkanethiols (black) and their corresponding SERS spectra (red). 77

Figure 4. 5: Relationship between the enhancement factor and chain-length of 1-alkanethiols. 79

Figure 4. 6: The modelled 1-alkanethiols and their chain-lengths (a) 1-PT, (b) 1-DT, (c) 1-DDT, (d) 1-PDT. 80

Figure 4.7: Optimized geometries of (a) Ag-PT, (b) Ag-DT, (c) Ag-DDT and (d) Ag-PDT.. 80

Figure 4.9: The calculated molecular geometry on the surface of AgNPs and their effect on the charge density 84

List of tables

Table2. 1: Colloidal metal nanoparticles used for SERS and synthesis methods.....19

Table 3.1: Summary of SPR bands of citrate capped and 1-alkanethiols functionalized AuNPs and their corresponding FWHM values.....48

Table 3.2: The values of zeta potentials of citrate capped and 1-alkanethiols functionalized AuNPs.....52

Table 3.3: A Summary of the experimental and theoretical bands assignment of PT adsorbed on AuNPs.....54

Table 3. 4: A Summary of the experimental and theoretical bands assignment of DT adsorbed on AuNPs.....54

Table 3.5: A Summary of the experimental and theoretical bands assignment of DT adsorbed on AuNPs.....55

Table 3. 6: A Summary of the experimental and theoretical bands assignment of PDT adsorbed on AuNPs.....55

Table 3. 7: DFT calculated nucleophilic centres of PT, DT, DDT, and PDT.....61

Table 4.1: Summary of SPR bands of citrate capped and 1-alkanethiols functionalized AuNPs and their corresponding FWHM values.....71

Table 4. 2: The values of zeta potentials of citrate capped and 1-alkanethiols functionalized AgNPs.....75

Table 4. 3: A Summary of the experimental and theoretical bands assignment for PT adsorbed on AgNPs.....77

Table 4. 4: A Summary of the experimental and theoretical bands assignment for DT adsorbed on AgNPs.....77

Table 4. 5: A Summary of the experimental and theoretical bands assignment for DDT adsorbed on AgNPs.....77

Table 4. 6: A Summary of the experimental and theoretical bands assignment for PDT adsorbed on AgNPs.....78

Table 4. 7: DFT calculated nucleophilic centres of PT, DT, DDT, and PDT.....83

Appendices

Supplementary materials

List of figures

Figure S3. 1: Zeta potentials of AuNPs stabilized by tri-sodium citrate. 90

Figure S3. 2: Zeta potentials of AuNPs stabilized by PT. 90

Figure S3. 3: Zeta potentials of AuNPs stabilized by DT.....91

Figure S3. 4: Zeta potentials of AuNPs stabilized by DDT.....91

Figure S3. 5: Zeta potentials of AuNPs stabilized by PDT. 91

Figure S4. 1: Zeta potentials of AgNPs stabilized by tri-sodium citrate. 92

Figure S4. 2: Zeta potentials of AgNPs stabilized by PT. 92

Figure S4. 3: Zeta potentials of AgNPs stabilized by DT.....92

Figure S4. 4: Zeta potentials of AgNPs stabilized by DDT.....93

Figure S4. 5: Zeta potentials of AgNPs stabilized by PDT. 93

Abbreviations

Ag	Silver
AgNPs	Silver nanoparticles
a.u	arbitrary units
Au	Gold
AuNPs	Gold nanoparticles
AuNRs	Gold nanorods
CCD	Charged coupled device
DT	Decanethiol
DDT	Dodecanethiol
CE	Chemical enhancement
EF	Enhancement factor
EM	Electromagnetic
EME	Electromagnetic enhancement
FT-Raman	Fourier transform Raman
HOMO	Highest occupied molecular orbital
LOD	Limit of detection
LUMO	Lowest unoccupied molecular orbital
ml	millilitre
MPCs	Monolayer protected clusters
mV	Millivolt
NR	Normal Raman
NIR	Near-infrared
nm	Nanometres

NPs	Nanoparticles
PT	Pentanethiol
PDT	Pentadecanethiol
RR	Raman reporter
SERRS	Surface-enhanced resonant Raman scattering
SERS	Surface enhanced Raman scattering
SPR	Surface plasmon resonance
TEM	Transmission electron microscope
UV-Vis	Ultraviolet–visible spectroscopy

Chapter 1

Synopsis

1.1 Background

Raman spectroscopy is a molecular vibrational technique that is widely used for identification of solids, liquids and gasses [1, 2]. Like infrared spectrometry, this technique gives an idea on the structural features of analytes based on their molecular vibrations. However, Raman spectrometry doesn't require an elaborate sample preparation which is one of its advantages over infrared spectroscopy [1]. This technique is mainly based on the scattering of incident radiation by various vibrational modes of molecules within the sample [3]. The incident photons are simultaneously scattered elastically (Rayleigh) and inelastically (stokes or anti-stokes) as shown in **Figure 1.1** [3]. The elastic scattered photons possess the same energy as that of incident radiation and vice versa for inelastic scattered photons. The energy of inelastic scattered photons is either small (stokes scattering) or large (anti-stokes) as compared to incident radiation [4-5]. Therefore, in Raman spectroscopy the inelastic scattered photons also known as Raman scattering are the ones that contains most important information about the structural features of the molecules within the sample. Since only a small fraction of photons will be scattered inelastically, the Raman cross-sections are extremely low [5].

Various Raman spectroscopic instruments have been developed in order to improve the weak Raman scattered radiation. There are two types of Raman spectrometers, dispersive and Fourier transform (FT) Raman spectrometer. FT Raman spectrometer was developed to improve the shortcomings of dispersive spectrometer. The problem of fluorescence impingement was solved with FT Raman. However, this technique continued to lack

sensitivity due to high signal to noise ratio, stability of the instrument and resolution; more especially to trace analytes and complex structures [6-8].

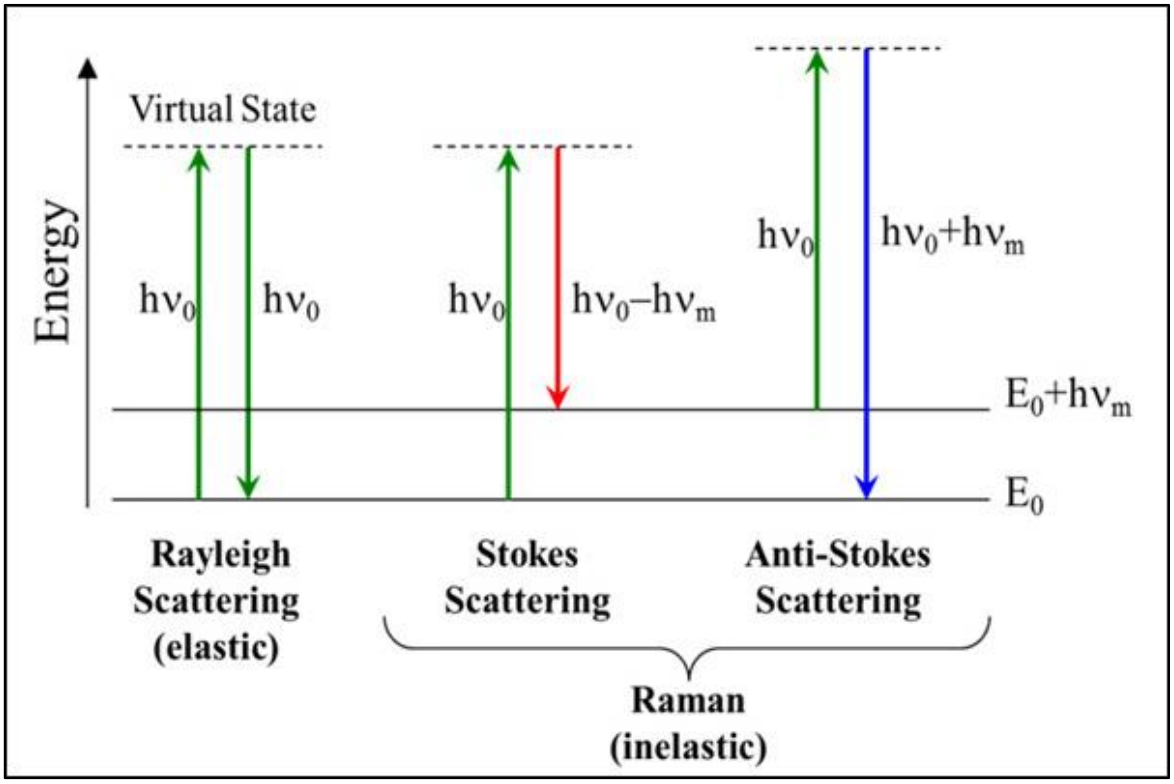


Figure 1.1: Energy states diagram depicting the manner through which the incident photons are scattered in Raman spectrometry [3].

Raman spectroscopy has gained its popularity as a means of chemical fingerprinting due to technology advancement such as the use of mercury lamps, lasers, and charged coupled detectors (CCD) [9-11]. The signal enhancement method gave Raman spectroscopy even more popularity. This enhancement was first observed in 1974 by Fleischmann and co-workers. They discovered that the adsorption of pyridine on a roughened silver electrode resulted in a significantly enhanced Raman spectrum [12]. This enhancement was later named surface-enhancement Raman scattering/spectroscopy (SERS). SERS can now enhance

the weak Raman scattering cross section by the factor of up to 10^{16} as compared to the classical Raman spectroscopy, both dispersive and FT.

SERS still applies the same principles as classical Raman spectroscopy, however with the molecule of interest being adsorbed on a rough metal, semiconductor or metal nanostructured materials [13-15]. This technique has been applied in various fields of science ranging from biochemistry to biology [16-18]. The classic application of SERS is the direct sensing of various analytes attached onto a metallic substrate, yielding both qualitative and quantitative information as shown in **Figure 1.2** [19].

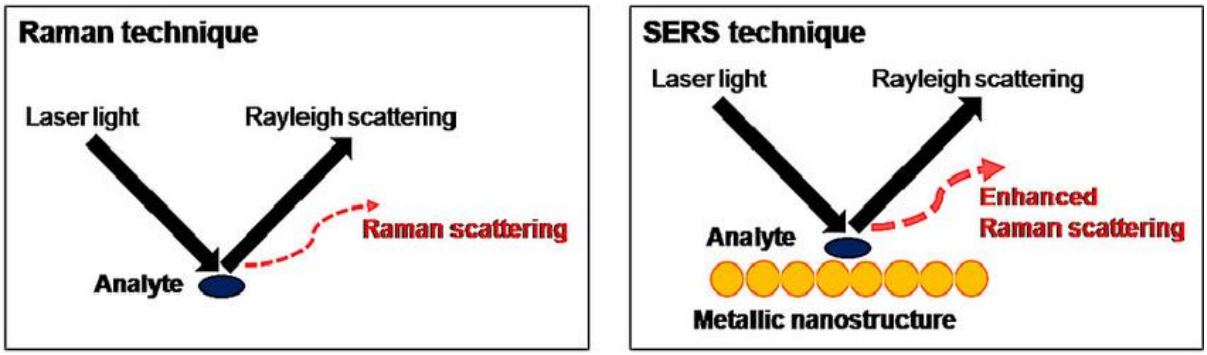


Figure 1.2: comparison between (a) classical Raman and (b) SERS effects on the analyte.

1.2 Problem statement

High mortality rate in our society is directly caused by the complexity in diagnosis of diseases (e.g. cancer, malaria, TB, and HIV/Aids) while they are still in their early treatable stage. A host of immunoassay detection techniques (enzyme immunoassay, radioimmunoassay, fluoroimmunoassay) have been implemented and applied for early diagnosis of diseases while they are still in their asymptomatic stage, with no sign and symptoms [1-3]. Raman spectroscopy has also become one of those techniques, playing a vital role in structural analysis. However, this technique shows a lack of detection sensitivity

towards various molecules and macromolecules [4]. Together with some diagnosis procedures, they lack sensitivity towards macromolecules and trace analytes; and some of these procedures are too expensive, complex and time consuming. SERS has a potential to be a significant analytical technique even in complex biological environments, owing to its sensitivity and easy data interpretation. Hence its application is thwarted by an understanding of a combination of its properties which contribute to the Raman signal enhancement [5]. The importance of the studies to look into properties of combining the SERS substrate (metallic nanoparticle) and Raman reporter (1-alkanethiols) will provide a better understanding on optimising parameters for SERS application.

1.3 Motivation

Colloidal nanoparticles are interesting materials that have gained a vast attention in the field of science and technology due to their electronic, optical and structural properties [6-7]. These materials include metal nanostructures (e.g. gold and silver), metal oxides, and other semiconductors. Gold and silver nanoparticles (AuNPs and AgNPs) exhibit various native size-dependent properties such as surface energy and light scattering or absorption as compared to their bulk materials. These interesting properties are attributed to a phenomenon known as surface plasmon resonance (SPR) [8-9]. The ease of synthesizing AuNPs and AgNPs and their surface modification with various molecules and polymers in ambient environment has led to their vast application in photovoltaic, electronics, drug delivery systems and water treatment [7-11]. More recently, the synthesis and functionalization of Au and Ag nanoparticle with 1-alkanethiols and their application in SERS has been reported [9]. In addition, 1-alkanethiol functionalized AuNPs and AgNPs yield a prototypical self-assembled monolayer (SAM) system, with potential of biological applications. SAMs are better scaffolds to study SERS since they give out uniform Raman signal, and have proven to

be stable at different ionic strengths [6-7]. However, the effect that the chain-length of 1-alkanethiols adsorbed on the surface of Au and Ag nanoparticles have on SERS has not been investigated. Thus, we seek to investigate the possible effects of varying chain-length of 1-alkanethiols on the surface chemistry of AuNPs and AgNPs and the SERS enhancement factor (EF).

1.4 Aim and objectives

1.4.1 Aim

The main aim of the project was to synthesize and functionalize gold and silver nanoparticles with 1-alkanethiols of different chain-lengths and evaluate the enhancement factor dependency.

1.4.2 Objectives

- Synthesize AuNPs and AgNPs of smaller sizes.
- Functionalize AuNPs and AgNPs with 1-alkanethiols of different chain-lengths.
- Investigate SERS dependence on chain-length using Raman spectroscopy.
- Evaluate chain-dependence of SERS using DFT and Molecular Dynamics.

1.5 Outline

Chapter 1: Synopsis

Chapter one gives the problem statement and the motivation of the study, together with the aim and objectives of the project.

Chapter 2: Literature review

This chapter will present the whole outline of the dissertation; it will briefly describe the Raman spectroscopic technique (history/theory), its applications and progression towards surface enhanced Raman scattering (SERS). The chapter will further explain the fundamentals and the significance of SERS. This chapter will further present a critical review on SERS; basically it will focus more on the main parameters of SERS (SERS substrate and Raman reporter), how they affect or the role they play in Raman scattering enhancement. It will then specifically present the reported findings on gold and silver nanoparticles as SERS substrate and the formation of 1-alkanethiols SAMs on the surface of gold and silver nanoparticles. This chapter will finally introduce the gap and will be concluded by the main focus of the current project.

Chapter 3: Synthesis and functionalization of gold nanoparticles with 1-alkanethiols (Raman reporter) of various chain-lengths

This chapter focuses on the synthesis and functionalization of gold nanoparticles with 1-alkanethiols of different chain-lengths. It will further give a full discussion on how the chain-lengths of 1-alkanethiols affect the enhancement factor of Raman signal.

Chapter 4: Synthesis and functionalization of silver nanoparticles with 1-alkanethiols (Raman reporter) of various chain-lengths

This chapter focuses on the synthesis and functionalization of silver nanoparticles with Raman reporter molecules. It will then give a full discussion on how the chain-lengths of 1-alkanethiols on silver nanoparticles affect the enhancement factor of Raman signal.

Chapter 5: Conclusion and future study

This chapter will summarize the whole project and provide the general conclusion based on the aim of the project.

1.6 References

1. Ferraro, J.R., 2003. ***Introductory Raman spectroscopy***. Academic press.
2. McCreery, R.L., 2005. ***Raman spectroscopy for chemical analysis*** (225). John Wiley & Sons.
3. Flasar, F.M., Kunde, V.G., Abbas, M.M., Achterberg, R.K., Ade, P., Barucci, A., Bézard, B., Bjoraker, G.L., Brasunas, J.C., Calcutt, S. and Carlson, R., 2004. **In *The Cassini-Huygens Mission*** (pp. 169-297). Springer Netherlands.
4. Jayasooriya, U.A. and Jenkins, R.D., 2002. **In *An Introduction to Laser Spectroscopy*** (pp. 77-104). Springer US.
5. Sivaprakasam, V. and Killinger, D.K., 2003. ***JOSA B***, *20*(9), pp.1980-1989**.**
6. Devi, R.V., Doble, M. and Verma, R.S., 2015. ***Biosens. Bioelectron***, *68*, pp.688-698.
7. Xu, J., Butler, I.S., Gibson, D.F.R. and Stangel, I., 1997. ***Biomat***, *18*(24), pp.1653-1657.
8. Khalil, S.K., Allam, M.A. and Tawfik, W.A., 2007. ***Eur J Dent***, *1*(2), p.72.
9. Voller, A., Bartlett, A. and Bidwell, D.E., 1978. ***J. Clin. Pathol***, *31*(6), pp.507-520.
10. Chikkaveeraiah, B.V., Bhirde, A.A., Morgan, N.Y., Eden, H.S. and Chen, X., 2012. ***ACS nano***, *6*(8), pp.6546-6561.
11. De Peinder, P., Vredenbregt, M.J., Visser, T. and De Kaste, D., 2008. ***J Pharm Biomed Anal***, *47*(4), pp.688-694.
12. Le Ru, E. and Etchegoin, P., 2008. ***Elsevier***.

13. Kelly, K.L., Coronado, E., Zhao, L.L. and Schatz, G.C., 2003. ***J. Phys. Chem. B***, *107* (3), pp 668–677

14. Howes, P.D., Chandrawati, R. and Stevens, M.M., 2014. ***Science***, *346*(6205), p.1247390.

15. Malinsky, M.D., Kelly, K.L., Schatz, G.C. and Van Duyne, R.P., 2001. ***J. Am. Chem. Soc***, *123*(7), pp.1471-1482.

16. Hu, M., Chen, J., Li, Z.Y., Au, L., Hartland, G.V., Li, X., Marquez, M. and Xia, Y., 2006. ***Chem. Soc. Rev***, *35*(11), pp.1084-1094.

17. Daniel, M.C. and Astruc, D., 2004. ***Chem. rev***, *104*(1), pp.293-346.

18. Sarkar, A., Shukla, S.P., Adhikari, S. and Mukherjee, T., 2010. ***Int. J. Nanotechnol***, *7*(9-12), pp.1027-1037.

19. Banholzer, M.J., Millstone, J.E., Qin, L. and Mirkin, C.A., 2008. ***Chem. Soc. Rev***, *37*(5), pp.885-897.

Chapter 2

Literature Review

2.1 General introduction

Surface enhanced Raman scattering/spectroscopy (SERS) is a phenomenon/technique in which the Raman signal of molecules adsorbed on a metallic substrate is enhanced by several orders of magnitude. The Raman signal in SERS is primarily driven by the interaction of laser incident radiation and metallic substrate. This interaction produces more enhanced laser field as a result of the coherent oscillation of the excited conduction electrons; a phenomenon known as surface plasmon resonance (SPR). In fact, SERS is a surface sensitive technique since a molecule has to adsorb or be in closer proximity to the SERS substrate in order to acquire the enhanced field of electromagnetic (EM) radiation. The adsorption of molecule on the SERS substrate is very critical in SERS applications because the enhanced laser field decay with increasing distance from the substrate.

To date, SERS has become a versatile spectroscopic technique/phenomenon that has been exploited in a large number of scientific fields. Ever since its discovery in 1977 [1], SERS has become the most significant method to amplify Raman scattering efficiency over some stimulated Raman processes and electronic resonance enhancement [2, 3]. For the past few decades, innovative studies on Raman signal enhancement have been in progress. The enhancement of a weak Raman signal by a factor of up to 10^{16} has been independently reported by several research groups [4-7]. Despite such enhancement of Raman signal, which has improved SERS sensitivity than that of classical Raman spectroscopy, SERS was not fully utilized to its maximum potential until recently. SERS experiments were previously disadvantaged from irreproducible SERS signatures due to little understanding and ill-defined

fabrication of electrochemical roughened substrates. The discovery of single molecule SERS in 1997 by Kneipp and co-workers have attracted new research and have transformed SERS from just being a physical phenomenon to an effective and robust analytical technique [5]. Recently, SERS has been applied to many analytical systems such as anthrax detection, chemical warfare–stimulant detection, in vitro and in vivo sensing, environmental monitoring and monitoring of heterogeneous catalytic reactions [6-9].

The enhancement factor (EF) of a Raman signal is mainly driven by manipulation of various parameters such as SERS substrates and Raman reporter (RR) molecules. Besides the importance of substrates and RR molecules, the energy/wavelength of laser radiation and the concentration of RR molecules must be thoroughly controlled in order to obtain significant EF. Nevertheless, SERS substrates are the most critical parameter in SERS experiments due to their ability to enhance the incoming EM radiation through a phenomenon known as SPR [1, 10]. Therefore, the choice of SERS substrates and their fabrication methods is one of the most critical aspects in SERS experiments. Secondary to the substrates, RR molecules were also found to play a significant role on SERS effects; this was proven to be due to the charge transfer between the substrate and the RR molecules [11].

2.2 SERS enhancement mechanisms and enhancement factor

2.2.1 Electromagnetic enhancement mechanism

The ability of a weak Raman scattering to be enhanced to several order of magnitude by a molecule adsorbed on a metallic substrate was of a great advantage in Raman applications. Jeanmaire and Van Duyne first attributed this enhancement to electromagnetic field enhancement (EME) possessed by surface plasmons (SP) on SERS substrates [1]. EME mechanism arises from the excitation of SPR which further strengthens the EM field around

the metallic surface as in **Figure 2.1**. This mechanism relies more on the plasmonic behaviour of metallic surfaces or SERS substrates which is driven by either their morphology or size [13]. The enhancement contribution by this mechanism can reach a magnitude of up to 10^{14} or more [10, 12]. However, the mechanism is chemically non-selective, and it is distance dependent. It requires a molecule to be either adsorbed on or be in a close proximity to the metal surface for greater SERS enhancement.

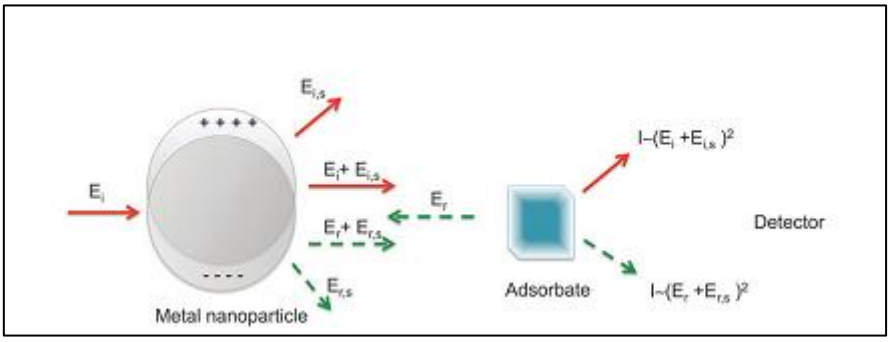


Figure 2.1: Illustration of the electromagnetic enhancement mechanism in SERS [15]**.**

Generally, the incident EM radiation (E_i) of certain energy excites the conduction electrons on the surface of a substrate, and induces the oscillation dipole of the conduction electrons (SPR). The local field ($E_{i,\,s}$) is then generated on the surface of the metallic substrate [14]. It is this local field that causes a strong vibrational transition in the molecule thus resulting in an enhanced Raman scattered radiation (E_r). The enhanced E_r can also polarize the metal substrate resulting in a highly intensified radiation ($E_{r,\,s}$) to be easily detected.

2.2.2 Chemical enhancement mechanism

Albrecht and Creighton further explained the chemical enhancement mechanism (CE) brought about by the adsorbed molecule on Raman scattering enhancement [11]. CE is known to give an order or two to the enhancement magnitude of Raman signal. This

mechanism doesn't involve SP effects, but charge transfer (CT) between the highest occupied molecular orbital (HOMO) of the adsorbed molecule (or the conduction band (CB) of a metallic surface) and the lowest unoccupied molecular orbital (LUMO) of a chemisorbed species as shown in **Figure 2.2**. Three distinct contributions that may happen separately are possible in this mechanism [15]. The first contribution involves ground state chemical interactions between the adsorbates and the metal surface without any excitation of metal-adsorbate system. This contribution is more likely to occur in a situation where there is no strong interaction between the metal and the adsorbate. For the second contribution, the excitation wavelength and the molecular transition have to be in resonance which then promote the resonance Raman scattering (RRS). This happens mostly when the dye molecules are being used as RRs. The last contribution involves a strong CT between covalently bonded molecules to the metal surface. Molecules that have a strong chemical affinity (e.g. 1-alkanethiols and amines) with metal substrate promote this mechanism.

Unlike EME, this model is chemically selective, more especially to those molecules with lone pair of electrons and other functional groups, through which they can bond to the metallic surface [11]. Plenty of experiments have confirmed that both mechanisms play key roles in SERS effects [13, 14 17]. However, it is believed that the total EF of Raman scattering is the results of the coupling of the two mechanisms with EME contributing more to the enhancement of SERS signal than CE [18].

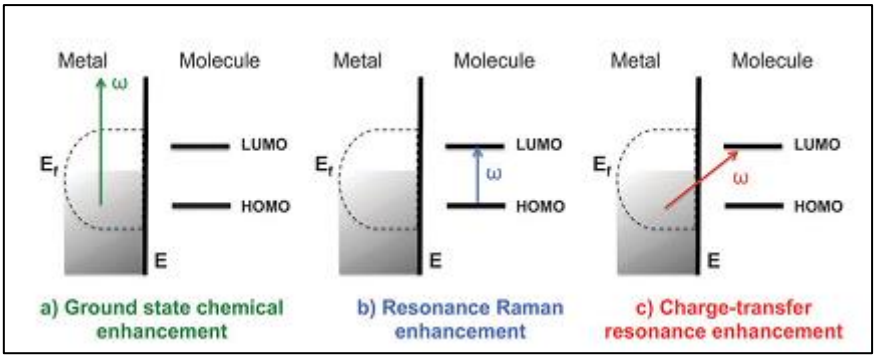


Figure 2.2: Illustration of the three different types of chemical enhancement mechanism in SERS [15].

2.2.2.1 Enhancement factor

The multiplicative product of the EME and CE mechanisms (EF =EM × CE), constitute the total EF of the SERS signal. However, there is not enough scientific support and universally accepted standards to quantify experimental EF for SERS-active substrates. Le Ru *et al.* thoroughly discussed this problem of the multiple definitions of the EF [19]. The most used and maybe simplest way for calculation of SERS EF is done using equation 1.

$$EF = \frac{I_{SERS}/N_{NR}}{I_{NR}/N_{SERS}} \quad (1)$$

Where I_{SERS} and I_{NR} are the intensities of the vibrational modes in SERS and normal Raman spectrum respectively. N_{NR} represents the number of molecules probed on the Raman spectrum (free molecules), while N_{SERS} represents the number of molecules probed using SERS (1-alkanethiol with Au substrate). Most researchers use this equation to calculate EF. However, varying conditions in which the calculations are performed have been reported; causing the difficulties in consistency and comparing the activity of various SERS substrate and RRs used. Three considerations to be noted before the calculations of EF have been proposed by Van Duyne *et al.* [19]. This include (i) the complete description of the conditions and how EF is calculated, (ii) the molecule of RRs within the excitation environment must carry the same weight in enhancement and (iii) to use RRs that have a

well-defied spectrum and a good chemical affinity to a selected SERS substrate. These considerations play a significant role in consistency or reproducibility of calculating the EF. Most calculated EF are over estimated because the precise number of molecules are not determined, the signal intensities are not normalised and the signals are selectively measured from the hot spot instead of large region scanning [19]. In case of the current studies, we focussed more on the second and third considerations since the first one has been thoroughly investigated separately by Mlambo and co-workers and other research groups [19-23].

2.2.3 SERS substrate

SERS effect is heavily dependent on a metallic substrate (SERS substrate) and their properties. In a nut shell, good SERS substrates are those metallic structures that support the strongest SPRs and provide the largest enhancement or amplification of Raman signal. Therefore, the choice of SERS substrate, their shapes and sizes are among the most critical aspects that influence SERS effect. This is because different metals with different shapes and sizes possess different electronic and optical properties that further affect the SPR and the manner through which the molecules adsorb on the surface. A SERS substrate is thus a common denomination for any plasmon-resonance-supporting structure that yields a significant Raman signal. There are two main and commonly used classes of SERS substrates that have been reported in SERS experiments so far [19].

2.2.3.1 Metallic electrodes

Electrochemically roughened electrodes have played a critical role in the historical development of SERS and its discovery. It is therefore important to note that SERS started as a discipline of electrochemical science. Electrochemically roughened electrodes produced by oxidation-reduction circles (ORC) provide superb optical and chemical properties which are

necessary for Raman signal enhancement [20]. In addition, these electrodes are untimely and one of the most stable SERS substrates that produce uniform and reproducible EF of up to 10^5 [20]. Several methods for preparing such substrates have been reported in literature. Current-controlled ORC and double potential ORC are the commonly [21-23] used methods amongst galvanostatic methods, [24] template deposition in membranes [25-28] and cyclic voltammetry [27]. These methods result in the formation of particles with typical sizes of 20-500 nm on the surface of the electrode. The final structure of the surface depends on the hydrogen bubbling before the roughening process and the irradiation of the electrode during the process [21, 29-32].

Silver electrode prepared by one of the above mentioned procedures (**Figure 2.3**) was the first substrate to be utilised in SERS experiments, although other metal surfaces have been evaluated as active SERS substrates in electrochemical cells. [28, 33-35]. The intense Raman spectrum of pyridine molecules adsorbed on the surface was observed [1, 14]. It was further realised that the Raman signal of the ring-stretching modes of pyridine was enhanced five times more than that of liquid pyridine. Similar results were obtained by Albrecht and Creighton where it was revealed that the Raman spectrum of pyridine remained enormously intense even after a single ORC [11]. This effect was attributed to the roughness at the Ag electrode surface, which facilitated the adsorption of molecules on the surface and further achieved a strong SERS signal after irradiation [20].

Although the pyridine molecule SERS spectrum was the first to be observed, the enhancement of Raman signal of other molecules adsorbed on the surface of rough metal electrodes have also been observed. Bukowska and Michota studied the Raman spectrum of 4-mercaptobenzoic acid (PMBA) adsorbed on the roughened surface of gold (Au) and silver

(Ag) electrodes. The Raman signal enhancement was evidenced by intense peaks of most of the vibrational modes of PMBA [36-40]. It was suggested that the enhancement was due to the roughness of the surface. Philpott *et al.* also argued convincingly that the induced Raman scattering of molecules adsorbed on the surface of plasmonic material was due to the broadening of their electronic energy levels [41].

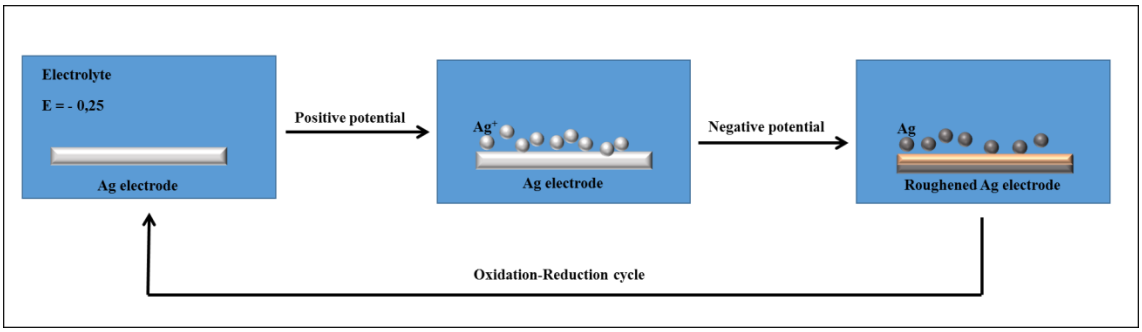


Figure 2.3: Scheme illustrating the oxidation–reduction cycle of a silver electrode in electrolyte (KCl) solution. Modified from [15].

2.2.3.2 Metallic nanoparticles

Once the roughened electrodes became a routine SERS substrate, a plethora of research started to focus more on the development of reliable and effective SERS substrate with tuneable plasmon resonance and a wide range of EF [5, 6]. Thanks to the development and good progress in the field of nanoscience and nanotechnology, synthesis and fabrication of SERS substrate with great potential in Raman signal enhancement has been achieved. The new substrates have found application in drug delivery, catalysis, gas sensors etc. [42-44]. Noble metal nanomaterials have shown a great potential in Raman signal enhancement over their electrochemical roughened counterparts due to their ability to enhance electromagnetic field on their surface.

Noble metals such as gold (Au), silver (Ag), and copper (Cu) are the most used SERS substrates. This is because they possess a strong interband transition which results in the oscillation of conduction electrons hence the formation of SPR at the infrared-visible (IR-Vis) range of EM spectrum [1, 45-47]. **Figure 2.4** shows the wavelength range in which the SPR bands of Cu, Au and Ag occur. With Cu nanoparticles known to be less stable in ambient environment, AuNPs and AgNPs have been endorsed as best SERS substrates. Therefore, current studies employ AuNPs and AgNPs as SERS substrates due to the aforementioned advantages.

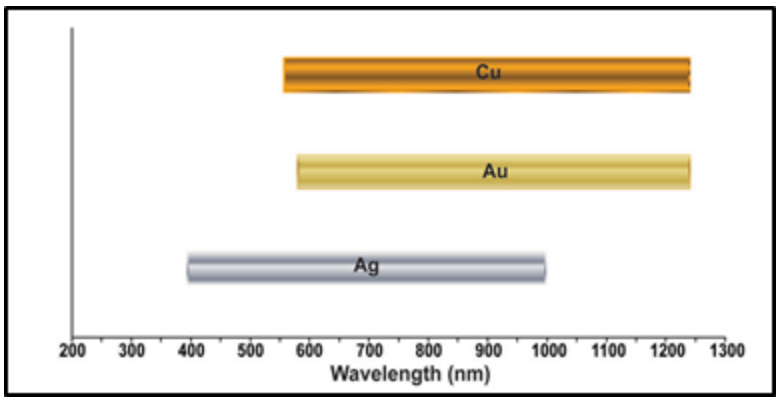


Figure 2.4: Approximate wavelength ranges where Ag, Au, and Cu have been well-characterized and are established to support SERS [33].

2.2.3.3 Synthesis and properties of AuNPs and AgNPs

Au and Ag nanoparticles are probably the most remarkable metallic NPs and have attracted considerable attention in research. In particular, these metallic NPs have unique properties which have driven a variety of applications in the field of science [45, 46]. Their stability in ambient environment, simple synthetic methods and importantly, their plasmonic character are the most fascinating properties which make them considerable in all of these applications. Au and Ag colloids are typically prepared by chemical reduction of their inorganic salts in

solution through several chemical routes [5, 6, 47]. The coulombic repulsive forces among the particles facilitate the stability of these colloids in solution. These coulombic repulsive forces require the presence of a stabilizing agent that protects the colloids and further prevent them from aggregating. Most of the time the reducing agent also play a role as a stabilizing agent, which is the case in sodium-citrate-reduced colloidal nanoparticles. These types of colloids are the most commonly utilized SERS substrates [44-47]. Other methods (e.g. laser ablation and photoreduction) for synthesizing SERS-active colloids (Au an Ag) have been reported in literature [48-53]. Various methods for preparation of SERS-active colloids of various morphology and composition are listed in **Table 2.1**.

Brust-Schiffrin method has been the most implemented method for synthesizing AuNPs with the sizes below 10 nm [70]. This method involves the reduction $HAuCl_4.2H_2O$ using sodium borohydride as a reducing agent in the presence of 1-alkanethiols. The advantage of this method is the formation of AuNPs which are assembled by the monolayer of 1-alkanethiols [70]. However, AuNPs which are prepared by this method cannot be utilised in biological applications (unless ligand exchange of hydrophobic molecules is performed) since they are hydrophobic. Currently, researchers have reported on the synthesis of AuNPs by the reduction of $HAuCl_4.2H_2O$ using tri-sodium citrate (Turkevich method). In this case tri-sodium citrate acts as both reducing and capping agent. This synthetic method results in biocompatible, good size distributed AuNPs with long term stability. These NPs can be used in a wide range of applications, including bio-analytical chemistry since they are water soluble [71-73].

Table2. 1: Colloidal metal nanoparticles used for SERS and synthesis methods

Particle morphology	Method used	Colloidal nanoparticles	Citation
Spheres	Creighton method (borohydride method)	Ag Au	54
	Lee–Meisel method (citrate method)	Ag (Ag and Au)	55 56
	Other reduction method	Ag Cu	57 58
	Laser ablation	Ag, Au and Cu	48
	Seed-mediated method	Au	59
	Photoreduction	Ag	5
Cubes	Polyol method	Ag	60
	Seed-mediated method	Ag Au	61 62
Pyramids	Seed-mediated method	Au	63
	Oxidative etching process	Ag	64
Wires	Polyol method	Ag Au	65 66
Stars	Seed-mediated method	Au	67
Rods	Electrochemical method	Au Ag	62 68
	Electrochemical method	Au	69

On the other hand, various methods for the preparation of AgNPs have been implemented. Lee and Meisel method is currently the most common method for preparation of AgNPs. This method involves the reduction of $AgNO_3$ with tri-sodium citrate in aqueous solution [56]. However, this method is not capable of yielding NPs which are monodispersed with respect to size and shape. Lee and Meisel method was recently modified (Steinigeweg *et al.*) by employing glycerol-water solution as a solvent for Ag-salt instead of using only water [73]. The increased monodispersity of NPs was attributed to the presence of hydroxyl groups of glycerol, which acts as a co-stabilizing agent and prevent them from oxidation and ripening.

The electronic and optical properties of Au and Ag NPs are very important during their application. These properties are mainly driven by their size and shape, dielectric properties of the surrounding medium, inter-particle distance and the adsorbed surfactants [74-78]. The understanding of the effect of these properties has been utilized to evolve SERS substrates with various morphological characteristics that yield a well-defined SERS signal. For example, the optical responses for Au or Ag nanorods which are anisotropic depend on the direction of the rod with respect to the electric field component of the incident radiation (**Figure 2.5**). Nanorods, possess two resonance frequencies, a longitudinal mode for the oscillation of the electron cloud along the long axis and a transverse mode when the oscillation occurs in a perpendicularly direction of this axis. Unlike nanorods, spherical nanoparticles possess only one resonance frequency. This is because the conduction electrons on the spherical nanoparticles oscillate in one direction with respect to the incident radiation. The SPR band of spherical nanoparticles occurs in the same range as the SPR for the transverse mode in the nanorods (**Figure 2.5**). These properties are also highly suitable for applications in photovoltaic, photo-catalysis and some bio-applications [69, 79-82].

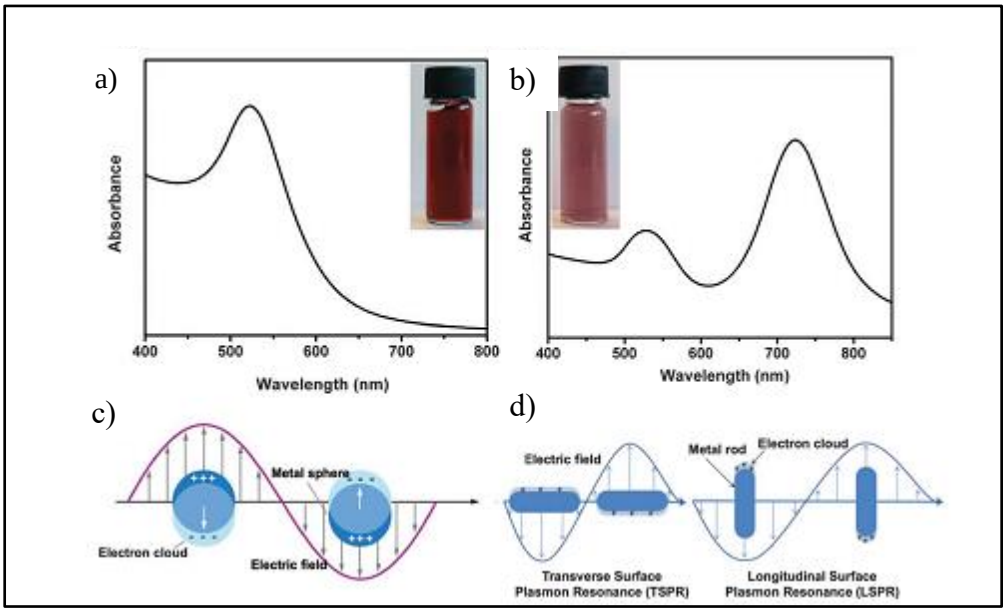


Figure 2.5: SPR absorption spectra of (a) spherical AuNPs and (b) gold nanorods (AuNR) of different aspect ratio; scheme illustrating the collective oscillations of conduction electrons in response to an external field for nanospheres (c) and nanorods (d). [15].

2.2.3.4 AuNPs and AgNPs as SERS substrates

Since Raman signal enhancement based on SERS is widely dependent on SPR excitation, it is therefore critical to control all the aspects that influence the SPR to maximize the strength of Raman signal and reproducibility. The sizes, shapes and inter-particle spacing ("hot spot") of AuNPs and AgNPs are the main characteristic to be controlled since they play a major role in optical properties of the material and hence affect their plasmonic character [83]. **Figure 2.6** shows the effect of size and shape on the SPR of AuNPs. Quester *et al.* evaluated the performance of AuNPs of various sizes and shapes for SERS application using methylene blue as a target molecule (Raman reporter) [83]. Even though the synthesised AuNPs were not monodispersed, they still possessed strong SERS capacity due to the availability of hot spots between nanoparticles which result in more intense surface plasmons resonance. AuNPs which were dominated by mixed morphology (triangles, hexagonal, cubes and spheres)

somehow showed a stronger Raman signal enhancement as compared to the quasi-spherical nanoparticles. The strong enhancement by mixed morphological nanoparticles was attributed to the high concentration of conduction electrons density at the edges of irregular NPs which will further results in strong SPR. On the other hand, the quasi-spherical NPs with the average diameter ranging from 3 to 12 nm showed less SERS capacity than those with the diameter range of 6 to 23 nm and 10 to 200 nm. However, the importance of uniform enhancement was not considered in this study since their substrates were not uniformly dispersed. It is important to utilize SERS substrates which are uniform and reproducible in order to acquire a good understanding of SERS enhancement mechanisms.

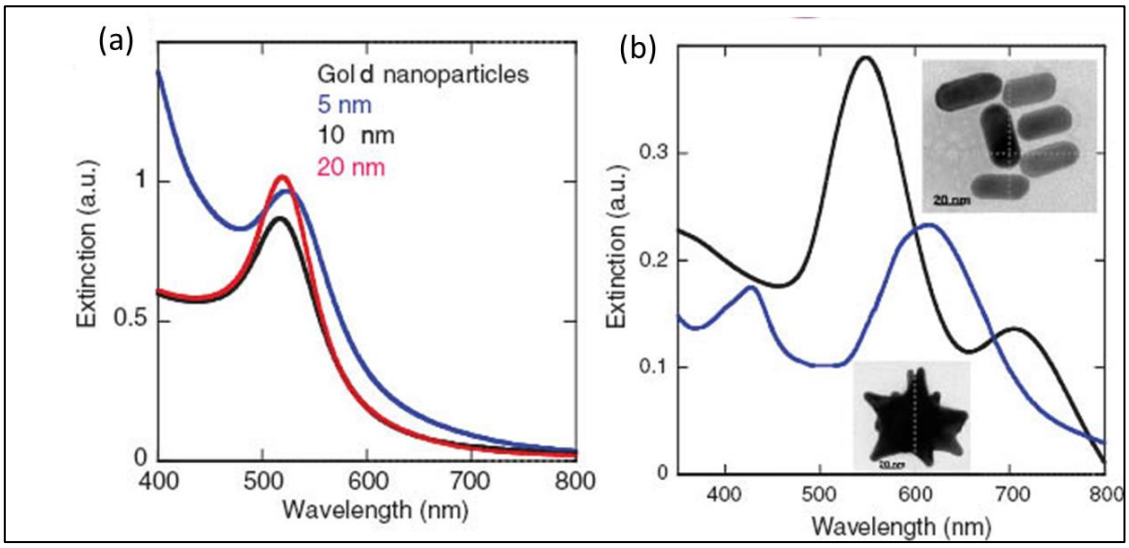


Figure 2. 6: The effect of (a) sizes and (b) shapes of nanoparticles on the SPR.

Various researchers have reported on the effect of NPs size towards Raman signal enhancement. Kalmodia *et al.* tested the effect of size of AuNPs on Raman signal enhancement [84]. AuNPs of large size were found to enhance Raman signal stronger than smaller sizes NPs. The calculated enhancement factor (EF) of 3.4 x10^7 due to AuNPs of 61 nm was reported. Several researchers concluded that spherical AuNPs with the average diameter of approximately 50 nm yield the maximum SERS EF [44]. The optimal size of NPs

ranging from 30 to 100 nm was reported to provide best SERS enhancement. NPs with small Average diameter (< 10nm) are considered to have inefficient SERS activity due to their very small scattering cross-section [86].

As far as the shape of nanostructures is concerned, gold and silver nanorods, nanostars, and truncated-triangular nanoparticles have appeared to be more effective for SERS enhancement and other related applications. Kottmann *et al.* have shown that the EM field resulting from metallic SPR is more intense at the corners of triangular nanoparticles [86]. Similar study was conducted by Sau *et al.* from which they observed strongly enhanced EM field at the edges of colloidal nonspherical (triangular) noble metallic nanoparticles. The enhancement of EM field of up to 400 times stronger than that of spherical nanoparticles was observed from decahedral nanostructures [87]. Raman signal of Rhodamine 6G on silver nanoflowers was found to be more enhanced as compared to the one on silver nanosphere [88]. Similar studies by Xie *et al* also showed that Raman signal of Rhodamine 6G on gold nanoflowers was 10 times more intense than that from AuNPs [89]. The multiple non-degenerate dipole modes of complex structure results in a broad SPR absorption band, unlike in the spherical nanoparticles where there is only one dipolar plasmon resonance since they are symmetrical. The high multipolar charge distribution are clearly induced in nonspherical nanoparticles since their induced electronic cloud is not distributed homogenously [89]. However, spherical nanoparticles are still considered to be suitable for many applications either in colloidal or immobilized state. This is because spherical NPs are easy to synthesize and are mostly biocompatible, therefore can cover a wide range of applications [90].

2.2.4 Raman reporter

The intrinsic properties of RR molecules also play a major role on Raman signal enhancement. It is by far the most important aspects that RR molecules should be located within a range of enhanced electromagnetic field generated by the excited SPR. Therefore a logical selection of RR molecules is an important key in developing an effective and sensitive SERS based methods. This is specifically for analysis of complex structures (proteins, cells, DNA, etc.) even in their minute/trace concentrations. In essence, RR molecules should be able to produce intense Raman signal (high Raman scattering cross-section) prior to mixing with plasmonic nanostructured or electrochemically roughened materials, and of far most importance they must have functional group/s that possess strong chemical affinity to the metal nanostructures. In addition, RR molecules should at least have high symmetry for spectral multiplexing, and low photo-bleaching for signal stability. RR molecules can still acquire strong EM field from SPR even if they are not in close proximity to the substrate [1]. However, the distance between RR molecules shouldn't be that large since the enhanced EM field decays exponentially, with a decay length of approximately 2 nm [13].

Various RR molecules and their structural effects on Raman signal enhancement have been reported so far. Fluorescent dyes adsorbed on the SERS substrate were reported to show an extra Raman signal enhancement due to their fluorescence properties which lead to surface enhanced resonance Raman scattering (SERRS) [91-93]. Dyes also offer more advantage of spectral multiplexing wherein spectrally distinct molecules can be detected simultaneously [92]. Mirkin *et al.* used R6G dye as RR to perform multiplexed experiments for the detection of DNA sequences with high sensitivity and specificity [90]. Graham and co-workers also used benzotriazoles and other commercial dyes to perform multiplexed experiment for DNA detection [93]. However, in some cases dye molecules showed chemical and photo instabilities which lead to photobleaching and spectral overlap. Researchers have also

investigated the effect of structure in terms of bulkiness and the symmetry of RR molecule on Raman enhancement. For instance, Schlucker and co-workers looked at how RR molecules of different sizes influence the Raman signal. In particular the effects of R6G dye and MBA adsorbed on Au/Ag nanoshells were investigated [94]. The Raman spectrum of small MBA showed few but intense peaks. This was attributed to the high symmetry of MBA which lead to spectral multiplexing. On the other hand R6G yielded more peaks as compared to MBA, and this lead to spectral overlapping. **Figure 2.7** shows some of the commonly used RR molecules, their chemical structures and their effect on the EF. The decrease in SERS EF with an increase in the size of the RR molecules was observed. These observations were attributed to the fact that small molecules easily fit between the hot spots (crevices) formed by the aggregated colloids.

Alkanethiol coordinated AuNPs and AgNPs have attracted significant research in fundamental technology and science. This is because alkanethiols on AuNPs and AgNPs form a prototypical self-assembled monolayer (SAM) system [21, 95]. In addition, alkanethiols possess strong chemical affinity towards Au and Ag through Au-S or Ag-S covalent bond, which results in a formation of densely packed and uniformly orientated cluster. The adsorption of alkanethiol results in covalent interaction between thiol head and Au and Ag metal, with alkyl chain stabilising the cluster through Van der Waals interaction. The formation of Au-S bond from alkanethiol and metal surface was found to involve hydrogen evolution. This was evidenced by oxidative addition of S-H to the metal then followed by reductive elimination of hydrogen as shown in equation 2.

$$RS\text{-}H + Au/Ag \longrightarrow RS\text{-}(Au/Ag) + 1/2H_2 \qquad (2)$$

The alkanethiolate monolayer also shields the particles from agglomeration and scaffolds the attachment of some moieties. The replacement of capping agents from the cluster by strong ligands is possible. This is similar to the way in which alkanethiol replaces weakly attached citrate ions from Au or Ag surface. Mixed monolayer protected cluster (MMPCs) results from this multifunctionalisation of MPCs as shown in equation 3.

$$(RS)nMPC + x(R'SH) \longrightarrow x(RSH) + (R'S)x(RS)n\text{-}1MPC \quad (3)$$

In SERS experiments, the densely packed structures of alkanethiol SAMs on SERS substrates tend to reduce or minimize spectral interferences from other molecules in the medium solution. In addition, SAM of RRs molecules offer great advantage on reproducible SERS signatures [96]. Wang and co-workers demonstrated the use of 2-aminobenzenethiol functionalized AgNPs for SERS detection of living cells [17]. Levin *et al.* also studied SERS spectra of 1-alkanethiol SAMs of various chain-lengths on gold nanoshells substrates [97]. The main idea was to study vibrational resonance of 1-alkanethiol SAMs while varying chain length. SERS spectra of 1-alkanethiol SAMs were found to be more intense (revealing sharp resonance) as compared to those from native Raman spectroscopy. Moreover, long-chains 1-alkanethiols showed low vibrational frequency of Au-S stretch as compared to shorter chains. This was attributed to an increase in Van der Waals interaction with increasing chain, thus reducing the chain mobility on the planar facets of NPs. Beside their influence in SERS studies alkanethiols SAMs also help in maintaining the stability of SERS substrates; this helps to prevent the agglomeration and aggregation in nanostructured substrates (i.e. AuNPs and AgNPs).

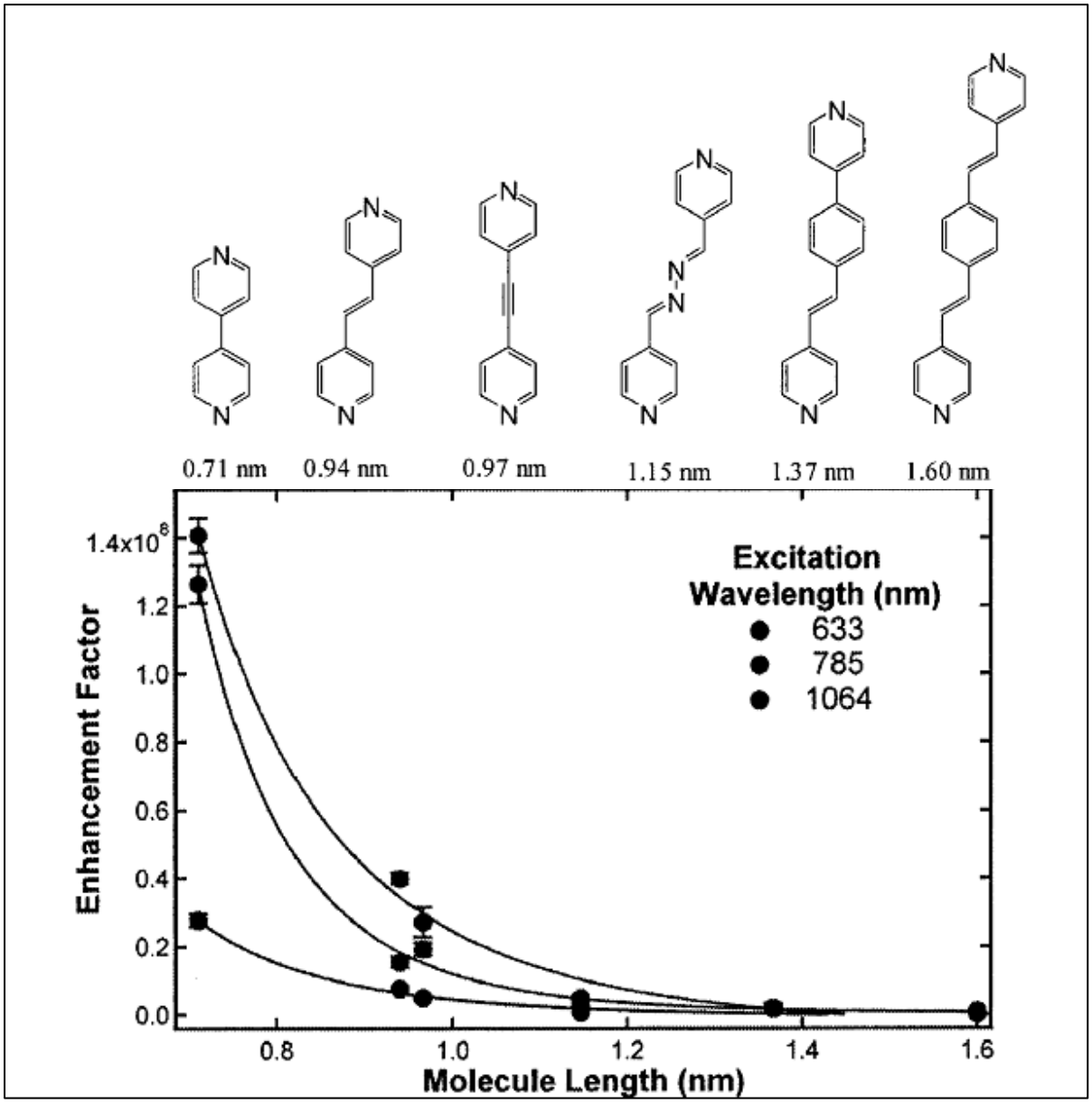


Figure 2. 7: Illustration of the effect of RR molecules on the EF [98].

2.3 SERS applications

SERS is a sensitive and selective technique for molecular identification and detection. The signals from this technique reveal a distinct spectrum with more informative characteristic peaks. In addition, SERS spectrum provides molecule fingerprints that can be utilized for analytical purposes. The fingerprinting ability of Raman spectroscopy makes it more special and lot more specific than other commonly utilized techniques like infrared and fluorescence

spectroscopies. This technique combines the high specificity and other advantages of classic Raman technique with high sensitivity, possibly better than that of fluorescence and infrared. Due to this, Raman spectroscopy has already been exploited in variety of applications ranging from scientific to industrial areas. Some of the main applications of SERS are shown in **Figure 2.8**.

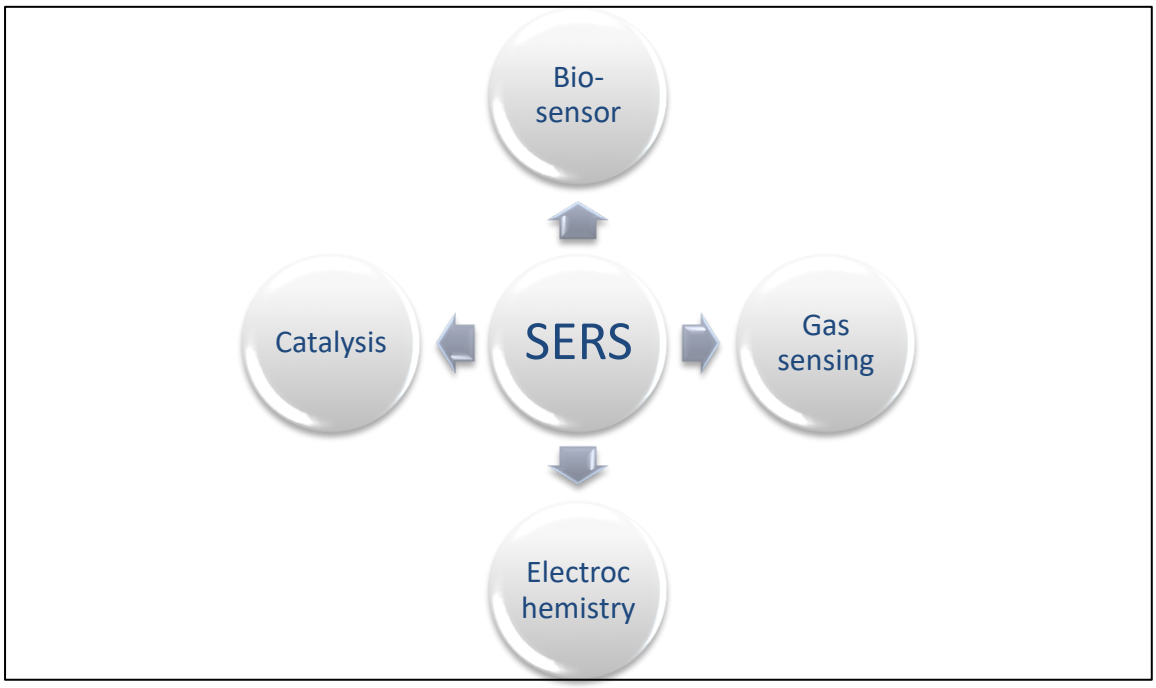


Figure 2. 8 Schematic representation of some applications of SERS.

2.3.1 SERS in detection of diseases

The strong Raman signal provided by SERS can simply increase the sensitivity or lower the limit of detection of the technique. This makes it simply to use Raman to investigate systems that could not be investigated by the classical Raman spectroscopy and other related techniques. SERS has recently been used to detect biological samples due to its sensitivity and selectivity. The SERS based biosensors are utilized mostly as immunoassays (as shown in **Figure 2.9**) for diseases diagnosis, including cancers, malaria and TB [61, 62]. For

instance, Matousek *et al.* have reported on SERS-based immunoassay using metallic nanoparticles conjugated with antibodies as SERS probes. This SERS-based technique is portable, with rapid response, low limit of detection, and simple instrumentation. Furthermore, Grubisha *et al.* also reported on the diagnosis of prostate specific antigen (cancer) in human serum at a very low concentration (~1pg/ml) using SERS based readout method [63]. Sha *et al* on the other hand have identified breast cancer cells from blood sample by combining anti-her2 antibody conjugated SERS tags with epithelial cell-specific antibody functionalized magnetic nanoparticles [64]. Guo *et al.* used hollow gold nanospheres and magnetic microspheres as SERS tags and SERS substrates, respectively [40]. Hence Synthesizing SERS probes which are stable and possess strong Raman signal can lead to most reliable and effective SERS based immunoassay with a very low limit of detection towards various antigen.

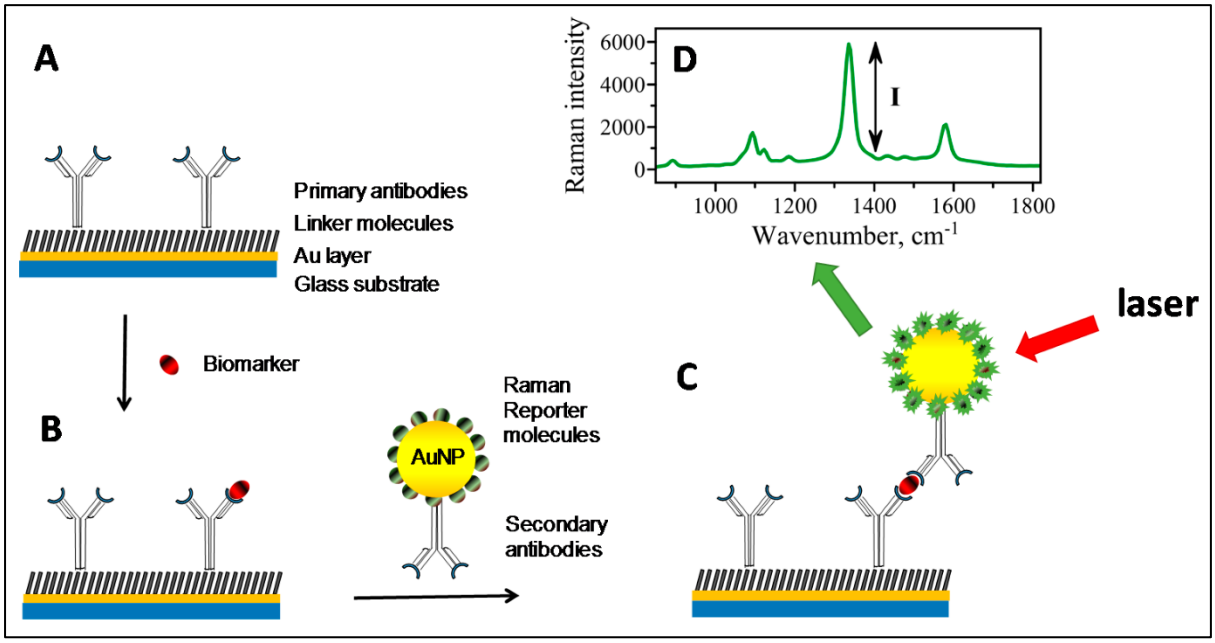


Figure 2. 9: SERS based immunoassay for early detection of diseases [40].

2.3.2 SERS gas sensor

The modelling and designing of devices for efficient detection and selective towards explosives, volatile organic compounds and other toxic gases have attracted a great research which is of a notable interest in security and environmental monitoring agencies. To date, various gas sensing devices including SERS have been manufactured and showed critical importance for detecting highly toxic gasses such as chemical warfare agents (CWAs) and toxic industrial chemicals (TICs). However, SERS analysis requires analyte molecules to bind with or be in close proximity to the SERS substrate in order to acquire more specific and representable results. Due to this requirement, SERS measurements are quite challenged because of lack of interaction between substrate and the analyte. Despite this challenge, various explosives such as dinitrobenzene, half-mustard agents etc. have been detected using SERS-based gas detectors. **Figure 2.10** shows a simple SERS device for gas toxic gas sensing. Piorek and co-workers circumvented this challenge by using water soluble gasses that can be converted to liquid and detected by Microfluidic SERS sensor. By using this SERS based technique, 4-aminobenzenethiol (4-ABT) gas with a concentration as low as 300 µM was able to be detected [41]. Similar study by Gibbs et al also revealed successfully the detection of benzenethiol (BT) using SERS as a gas sensor with the detection limit of 6ppb [42]. Other gas phases such as Nerve agent simulants, dimethyl methylphosphonate and diisopropyl methylphosphonate, have been detected by SERS using electrochemically roughened silver oxide substrate [43, 44]. Detection of half-mustard gas was also achieved by SERS analysis using a portable Raman spectrometry and silver film over nanosphere (AgFON) as a substrate [45].

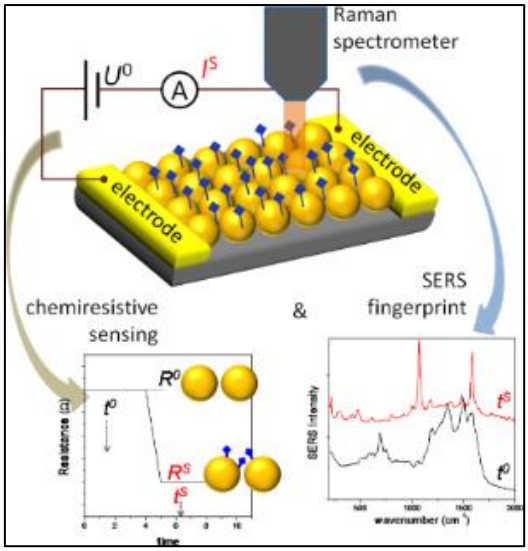


Figure 2. 10: A schematic for designing Sensitive and selective gas sensing devices [41].

2.3.3 SERS is electrochemistry

Besides being a detection technique, SERS has been utilized in electrochemistry to study and analyse the behaviour of various molecules in various oxidation states. The compatibility of the two techniques (SERS and electrochemical techniques) is solidated by the fact that they both use metals as substrates (SERS) and electrodes (electrochemical techniques) respectively. Abdelsalam et al. demonstrated the use of electrochemically prepared Au surface for electrochemical SERS by recording the pyridine spectra as a function of the electrode potential. In this case, Raman signal of pyridine was found to decrease as the electrode potential become more negative (-1.2 V). At the electrode potential of -1.6 V Raman signal was very low, as this was attributed to the formation of hydrogen in the pores of electrode (also acted as substrate) [46]. Electrochemical SERS was used to gather the chemical information for the derivation of Tetrathifulvalene (TTF) during potential sweep. TTF is a compound which is rich in electrons and has been utilized most extensively in electronic devices such as solar cells and super-capacitors. The electrochemistry of TTF is characterized by two reversible one-electron processes at 0.34 and 3.68 eV [47]. Paxton *et al* studied the structural change and redox properties of TTF using electrochemical SERS. In this case they used AuFON as a SERS-active substrate and working electrode.

A change in vibrational energy due to change in oxidation state was observed together with the dramatic change of signal as the potential was swept [48]. In general, Electrochemical SERS offers the ability to study electrochemical changes of a specific molecule spectroscopically, and can be further used for molecular switches and electronic stimulation.

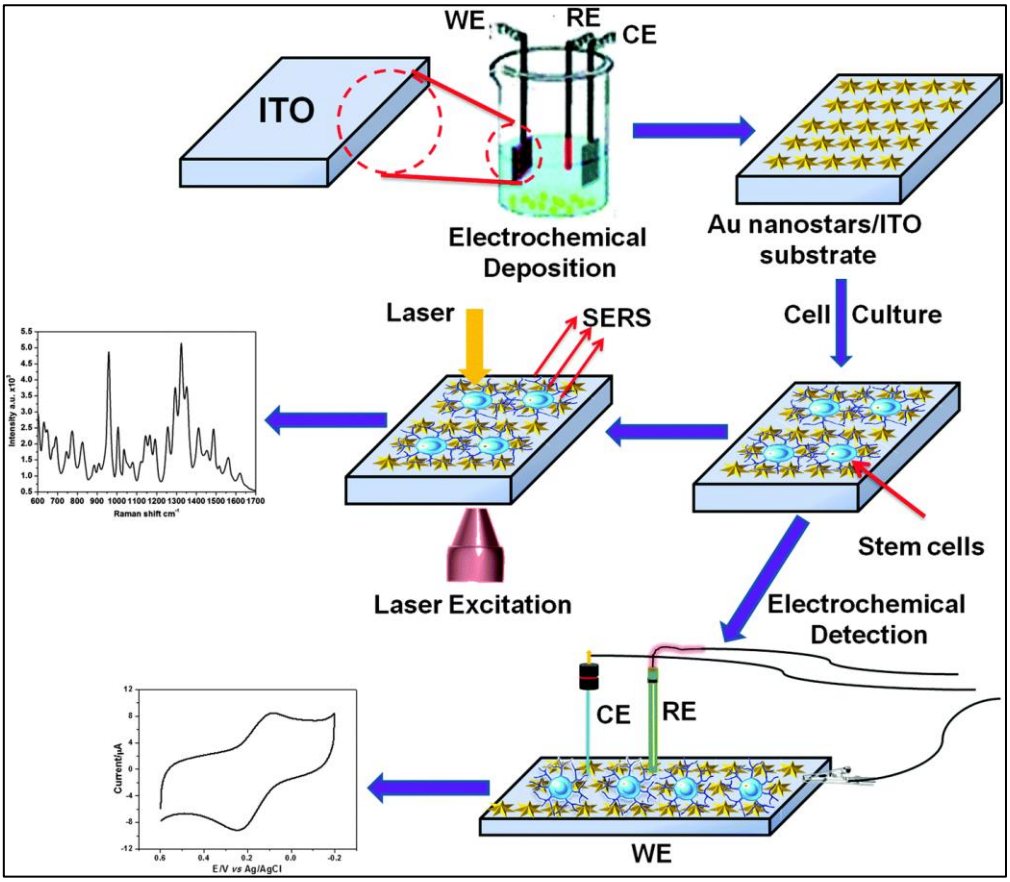


Figure 2. 11: Schematic representation for fabrication of the electrochemical-SERS based devices for bio-analysis applications [46].

2.3.4 SERS in catalysis

Various techniques have been so far used to monitor chemical reactions during catalysis processes. Analytical techniques such as Uv-Vis, XRD, and IR have been good candidates for in situ studies of catalysed reactions. However, Uv-Vis is not surface selective and provide limited information, IR on the other hand is complicated due to strong water absorption band if aqueous system (i.e. colloidal catalyst) is employed. SERS can therefore fulfil the entire requirement for monitoring molecular transformation in heterogeneous catalysis, owing to its advantages of chemical specificity, selectivity and sensitivity. Xie *et al* demonstrated the significance of SERS on Au-catalysed reduction of 4-nitrothiophenol (4-NTP) to aniline derivative (4-ATP). The mild catalytic activity of gold allowed the successful monitoring of reaction by collecting aliquots (for SERS analysis) from direct colloidal solution at different reaction times. The SERS spectrum of the last aliquot showed the spectral features which are comparable to that of 4-ATP [50]. The successful monitoring of Au-catalysed reduction of 4-NTP using SERS technique is clearly indicated in **figure 2.12.** Similar studies by the same group was conducted for monitoring platinum (Pt)-catalysed reduction of 4-NTP by sodium borohydride ($NaBH_4$) using SERS. The conversion of 4-NTP to 4-ATP was evidenced by the disappearance of nitrous (NO_2) peak at 1560 cm^{-1} as the reaction progress with time. Additionally, the new peak which appeared at around 1615 cm^{-1} confirms the formation of 4-ATP [51].

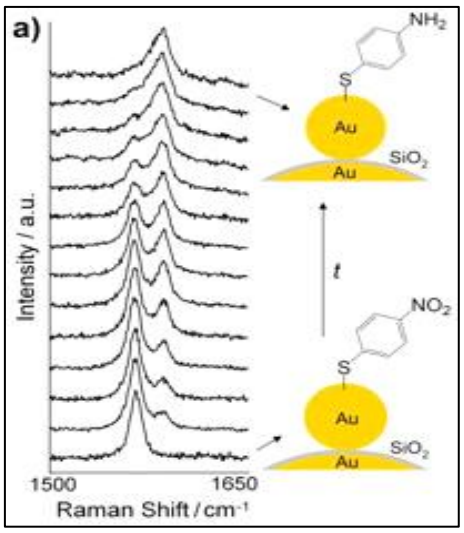


Figure 2. 12: SERS spectra from the reaction suspension collected at different reaction times [50].

2.4 References

1. Jeanmaire, D.L. and Van Duyne, R.P., 1977. *Journal of* ***J. Electroanal. Chem,*** *84*(1), pp.1-20.
2. Dieringer, J.A., McFarland, A.D., Shah, N.C., Stuart, D.A., Whitney, A.V., Yonzon, C.R., Young, M.A., Zhang, X. and Van Duyne, R.P., 2006. ***Faraday discuss***, *132*, pp.9-26.
3. Stiles, P.L., Dieringer, J.A., Shah, N.C. and Van Duyne, R.P., 2008. ***Annu. Rev. Anal. Chem***., *1*, pp.601-626.
4. Guo, P., Sikdar, D., Huang, X., Si, K.J., Xiong, W., Gong, S., Yap, L.W., Premaratne, M. and Cheng, W., 2015. ***Nanoscale***, *7*(7), pp.2862-2868.
5. Kneipp, K., Wang, Y., Kneipp, H., Perelman, L.T., Itzkan, I., Dasari, R.R. and Feld, M.S., 1997. ***Phys rev lett***, *78*(9), p.1667.
6. Zhang, X., Young, M.A., Lyandres, O. and Van Duyne, R.P., 2005. ***J. Am. Chem. Soc***, *127*(12), pp.4484-4489.
7. Zhang, X., Shah, N.C. and Van Duyne, R.P., 2006. ***Vib spectrosc***, *42*(1), pp.2-8.
8. Yonzon, C.R., Stuart, D.A., Zhang, X., McFarland, A.D., Haynes, C.L. and Van Duyne, R.P., 2005. ***Talanta***, *67*(3), pp.438-448.
9. Stuart, D.A., Haes, A.J., Yonzon, C.R., Hicks, E.M. and Van Duyne, R.P., 2005. **In *IEE Proceedings-Nanobiotechnology*** (Vol. 152, No. 1, pp. 13-32). IET Digital Library.
10. Lyandres, O., Shah, N.C., Yonzon, C.R., Walsh, J.T., Glucksberg, M.R. and Van Duyne, R.P., 2005. ***Anal chem***, *77*(19), pp.6134-6139.
11. Albrecht, M.G. and Creighton, J.A., 1977. ***J. Am. Chem. Soc,*** *99*(15), pp.5215-5217.
12. Morelli, L., Zór, K., Jendresen, C.B., Rindzevicius, T., Schmidt, M.S., Nielsen, A.T. and Boisen, A., 2017. ***Anal Chem***, *89*(7), pp.3981-3987.

13. Schatz, G.C. and Van Duyne, R.P., 2002. ***Handbook of vibrational spectroscopy***.

14. Jain, P.K., Huang, X., El-Sayed, I.H. and El-Sayed, M.A., 2007. ***Plasmonics***, *2*(3), pp.107-118.

15. Fateixa, S., Nogueira, H.I. and Trindade, T., 2015. ***Phys. Chem. Chem. Phys***, *17*(33), pp.21046-21071.

16. Jensen, L., Aikens, C.M. and Schatz, G.C., 2008. ***Chem. Soc. Rev***, *37*(5), pp.1061-1073.

17. King, F.W., Van Duyne, R.P. and Schatz, G.C., 1978. ***J. Chem. Phys***, *69*(10), pp.4472-4481.

18. Moskovits, M., 1978. ***J. Chem. Phys***, *69*(9), pp.4159-4161.

19. Goad, D.G. and Moskovits, M., 1978. ***J. Appl. Phys***, *49*(5), pp.2929-2934.

20. Le Ru, E. and Etchegoin, P., 2008. ***Elsevier science***.

21. Kleinman, S.L., Frontiera, R.R., Henry, A.I., Dieringer, J.A. and Van Duyne, R.P., 2013. ***Phys. Chem. Chem. Phys***, *15*(1), pp.21-36.

22. Vo-Dinh, T., 1998. ***TrAC, Trends Anal. Chem***, *17*(8), pp.557-582.

23. Mlambo, M., Harris, R.A., Mashazi, P., Sabela, M., Kanchi, S., Madikizela, L.M., Shumbula, P.N., Moloto, N., Hlatshwayo, T.T. and Mdluli, P.S., 2017. ***Appl Surf Scie***, *396*, pp.695-704.

24. Tian, Z.Q., Ren, B. and Wu, D.Y., 2002. ***J. Phys. Chem. B***, 106(37), pp. 9463–9483

25. Weaver, M.J., Hupp, J.T., Barz, F., Gordon, J.G. and Philpott, M.R., 1984. ***J. Electroanal. Chem***, *160*(1-2), pp.321-333.

26. Zhu, C., Meng, G., Huang, Q., Zhang, Z., Xu, Q., Liu, G., Huang, Z. and Chu, Z., 2011. ***Chem. Commun***, *47*(9), pp.2709-2711.

27. Gu, G.H. and Suh, J.S., 2010. ***J. Phys. Chem***, *114*(16), pp.7258-7262.

28. Gu, G.H., Kim, J., Kim, L. and Suh, J.S., 2007. ***J. Phys. Chem. C***, *111*(22), pp.7906-7909.

29. Zheng, J., Li, X., Gu, R. and Lu, T., 2002. ***J. Phys. Chem. B***, *106*(5), pp.1019-1023.

30. Gómez, R., Pérez, J.M., Solla-Gullón, J., Montiel, V. and Aldaz, A., 2004. ***J. Phys. Chem. B***, *108*(28), pp.9943-9949.

31. Brolo, A.G., Irish, D.E. and Lipkowski, J., 1997. ***J. Phys. Chem. B*** *101*(20), pp.3906-3909.

32. Wu, D.Y., Xie, Y., Ren, B., Yan, J.W., Mao, B.W. and Tian, Z.Q., 2001. ***PhysChemComm***, *4*(18), pp.89-91.

33. Zhu, C., Meng, G., Huang, Q., Li, Z., Huang, Z., Wang, M. and Yuan, J., 2012. ***J. Mater. Chem***, *22*(5), pp.2271-2278.

34. Wang, X., Shi, W., She, G. and Mu, L., 2012. ***Phys. Chem. Chem. Phys***, *14*(17), pp.5891-5901.

35. Hulteen, J.C. and Van Duyne, R.P., 1995. ***J vac sci technol A***, *13*(3), pp.1553-1558.

36. Chursanova, M.V., Germash, L.P., Yukhymchuk, V.O., Dzhagan, V.M., Khodasevich, I.A. and Cojoc, D., 2010. ***Appl surf sci,*** *256*(11), pp.3369-3373.

37. Fleischmann, M., Hendra, P.J. and McQuillan, A.J., 1974. ***Chem. Phys. Lett***, *26*(2), pp.163-166.

38. Michota, A. and Bukowska, J., 2003. ***J. Raman Spectrosc***, *34*(1), pp.21-25.

39. Wei, H., Rodriguez, K., Renneckar, S., Leng, W. and Vikesland, P.J., 2016. ***Analyst***, *141*(6), pp.2072-2072.

40. Guo, S. and Dong, S., 2011. ***J. Mater. Chem***, *21*(42), pp.16704-16716.

41. Sharma, B., Frontiera, R.R., Henry, A.I., Ringe, E. and Van Duyne, R.P., 2012. ***Mater. Today***, *15*(1), pp.16-25.

42. Creighton, J.A., Albrecht, M.G., Hester, R.E. and Matthew, J.A.D., 1978. ***Chem. Phys. Lett,*** *55*(1), pp.55-58.

43. Philpott, M.R., 1975. ***J. Chem. Phys***, *62*(5), pp.1812-1817.

44. Mueller, M., Tebbe, M., Andreeva, D.V., Karg, M., Alvarez Puebla, R.A., Pazos Perez, N. and Fery, A., 2012. ***Langmuir***, *28*(24), pp.9168-9173.

45. Chen, Y.R., Chung, C.L., Chen, G. and Tzeng, Y., 2016. **In *Nanotechnology (IEEE-NANO), 2016 IEEE 16th International Conference*** *on* (pp. 759-762). IEEE.

46. Tao, A., Sinsermsuksakul, P. and Yang, P., 2007. ***Nat. Nanotechnol***, *2*(7), pp.435-440.

47. Lu, L., Luo, Z., Xu, T. and Yu, L., 2012. ***Nano Lett***, *13*(1), pp.59-64.

48. Hu, L., Chen, M., Fang, X. and Wu, L., 2012. ***Chem. Soc. Rev***, *41*(3), pp.1350-1362.

49. Ma, H. and Hao, J., 2011. ***Chem. Soc. Rev***, *40*(11), pp.5457-5471.

50. Fojtik, A. and Henglein, A., 1993. ***Phys. Chem. Chem. Phys***, *97*(2), pp.252-254.

51. Neddersen, J., Chumanov, G. and Cotton, T.M., 1993. ***Appl. Spectrosc***, *47*(12), pp.1959-1964.

52. Agarwal, N.R., Fazio, E., Neri, F., Trusso, S., Castiglioni, C., Lucotti, A., Santo, N. and Ossi, P.M., 2011. ***Cryst. Res. Technol***, *46*(8), pp.836-840.

53. Canamares, M.V., Garcia-Ramos, J.V., Sanchez-Cortes, S., Castillejo, M. and Oujja, M., 2008. ***J. Colloid Interface Sci***, *326*(1), pp.103-109.

54. Ahern, A.M. and Garrell, R.L., 1987. ***Anal. Chem***, *59*(23), pp.2813-2816.

55. Sato-Berrú, R., Redón, R., Vázquez-Olmos, A. and Saniger, J.M., 2009. ***J. Raman Spectrosc***, *40*(4), pp.376-380.

56. Creighton, J. A., Blatchford, C. G. and Albrecht, M.G, 1979. ***J Chem. Soc. Faraday Trans. 2***, 75(6), pp.790-798.

57. Frens, G., 1973. ***Nature***, *241*(105), pp.20-22.

58. Lee, P.C. and Meisel, D., 1981. ***J. Catal***, *70*(1), pp.160-167.

59. Van Lierop, D., Krpetić, Ž., Guerrini, L., Larmour, I.A., Dougan, J.A., Faulds, K. and Graham, D., 2012. ***Chem. Comm***, *48*(66), pp.8192-8194.

60. Wang, Y. and Asefa, T., 2010. ***Langmuir***, *26*(10), pp.7469-7474.

61. Rodríguez-Fernández, J., Pérez-Juste, J., García de Abajo, F.J. and Liz-Marzán, L.M., 2006. ***Langmuir***, *22*(16), pp.7007-7010.

62. Camargo, P.H., Rycenga, M., Au, L. and Xia, Y., 2009. ***Angew. Chem., Int. Ed***, *48*(12), pp.2180-2184.

63. Zhang, Q., Li, W., Moran, C., Zeng, J., Chen, J., Wen, L.P. and Xia, Y., 2010. ***J. Am. Chem. Soc***, *132*(32), pp.11372-11378.

64. McLellan, J.M., Li, Z.Y., Siekkinen, A.R. and Xia, Y., 2007. ***Nano lett***, *7*(4), pp.1013-1017.

65. Langille, M.R., Personick, M.L., Zhang, J. and Mirkin, C.A., 2012. ***J. Am. Chem. Soc***, *134*(35), pp.14542-14554.

66. Lu, X., Rycenga, M., Skrabalak, S.E., Wiley, B. and Xia, Y., 2009. ***Annu. Rev. Phys. Chem***, *60*, pp.167-192.

67. Peng, P., Huang, H., Hu, A., Gerlich, A.P. and Zhou, Y.N., 2012. ***J. Mater. Chem***, *22*(31), pp.15495-15499.

68. Wei, H., Hao, F., Huang, Y., Wang, W., Nordlander, P. and Xu, H., 2008. ***Nano lett***, *8*(8), pp.2497-2502.

69. Khoury, C.G. and Vo-Dinh, T., 2008. ***J. Phys. Chem. C***, *112*(48), pp.18849-18859.

70. Orendorff, C.J., Gearheart, L., Jana, N.R. and Murphy, C.J., 2006. ***Phys. Chem. Chem. Phys*** *8*(1), pp.165-170.

71. Nikoobakht, B., Wang, J. and El-Sayed, M.A., 2002. ***Chem. Phys. Lett*** *366*(1), pp.17-23.

72. Brust, M., Walker, M., Bethell, D., Schiffrin, D.J. and Whyman, R., 1994. ***Chem. Commun***, (7), pp.801-802.

73. Quester, K., Avalos-Borja, M. and Castro-Longoria, E., 2016. ***J biomater appl*** *7*(02), p.118.

74. Kimling, J., Maier, M., Okenve, B., Kotaidis, V., Ballot, H. and Plech, A., 2006. ***J. Phys. Chem. B***, *110*(32), pp.15700-15707.

75. Steinigeweg, D. and Schlücker, S., 2012. ***Chem Comm***, *48*(69), pp.8682-8684.

76. Link, S. and El-Sayed, M.A., 1999. ***J. Phys. Chem. B***, 103 (40), pp 8410–8426

77. El-Sayed, M.A., 2001. ***Acc. Chem. Res***, *34*(4), pp.257-264.

78. Link, S. and El-Sayed, M.A., 2003. ***Annu. Rev. Phys. Chem***, *54*(1), pp.331-366.

79. Eustis, S. and El-Sayed, M.A., 2006. ***J. Phys. Chem. B***, *35*(3), pp.209-217.

80. Jain, P.K., Lee, K.S., El-Sayed, I.H. and El-Sayed, M.A., 2006. ***J. Phys. Chem. B***, *110*(14), pp.7238-7248.

81. Rosi, N.L. and Mirkin, C.A., 2005. ***Chem. rev***, *105*(4), pp.1547-1562.

82. Alivisatos, P., 2004. ***Nat. biotechnol***, *22*(1), p.47.

83. Alkilany, A.M., Thompson, L.B., Boulos, S.P., Sisco, P.N. and Murphy, C.J., 2012. *Adv.* ***Drug Delivery Rev***, *64*(2), pp.190-199.

84. Quester, K., Avalos-Borja, M., Vilchis-Nestor, A.R., Camacho-López, M.A. and Castro-Longoria, E., 2013. ***PLoS One***, *8*(10), p.e77486.

85. Kalmodia, S., Harjwani, J., Rajeswari, R., Yang, W., Barrow, C.J., Ramaprabhu, S., Krishnakumar, S. and Elchuri, S.V., 2013. ***Int. J. Nanomedicine***, *8*, p.4327.

86. Patra, S., Mukherjee, S., Barui, A.K., Ganguly, A., Sreedhar, B. and Patra, C.R., 2015. ***Adv mater res-switz***, *53*, pp.298-309.

87. Kottmann, J.P., Martin, O.J., Smith, D.R. and Schultz, S., 2001. ***Phys. Rev. B, PRB***, *64*(23), p.235402.

88. Sau, T.K. and Rogach, A.L., 2010. ***Adv Mat***, *22*(16), pp.1781-1804.

89. Pastoriza-Santos, I. and Liz-Marzán, L.M., 2008. ***J. Mater. Chem***, *18*(15), pp.1724-1737.

90. Xie, J., Zhang, Q., Lee, J.Y. and Wang, D.I., 2008. ***ACS nano***, *2*(12), pp.2473-2480.

91. Li, J. and Zhang, J.Z., 2009. ***acs sym ser***, *253*(23), pp.3015-3041.

92. Cao, Y.C., Jin, R., Nam, J.M., Thaxton, C.S. and Mirkin, C.A., 2003. ***J. Am. Chem. Soc***, *125*(48), pp.14676-14677.

93. Morones, J.R., Elechiguerra, J.L., Camacho, A., Holt, K., Kouri, J.B., Ramírez, J.T. and Yacaman, M.J., 2005. ***Nanotechnology***, *16*(10), p.2346.

94. Agnihotri, S., Mukherji, S. and Mukherji, S., 2014. ***RSC Adv***, *4*(8), pp.3974-3983.

95. Graham, D. and Goodacre, R., 2008. ***Chem Soc Rev***, *37*(5), pp.883-884.

96. Schlücker, S., 2014. ***Angew. Chem. Int. Ed***, *53*(19), pp.4756-4795.

97. Guo, Q., Xu, M., Yuan, Y., Gu, R. and Yao, J., 2016. ***Langmuir***, *32*(18), pp.4530-4537.

98. Levin, C.S., Kundu, J., Barhoumi, A. and Halas, N.J., 2009. ***Analyst***, *134*(9), pp.1745-1750.

99. Tam, F., Piotti, M.E. and Freeman, R.G., 2011. ***Cabot Security Materials Inc***., U.S. Patent Application 13/163,392.

100. Jing, C. and Fang, Y., 2007. ***Chem. Phys***, *332*(1), pp.27-32.

101. Pagliai, M., Caporali, S., Muniz-Miranda, M., Pratesi, G. and Schettino, V., 2012. ***J. Phys. Chem. Lett***, *3*(2), pp.242-245.

102. Harris, R.A., Mlambo, M. and Mdluli, P.S., 2016. ***RSC Adv***, *6*(15), pp.12131-12142.

103. Hay, P.J. and Wadt, W.R., 1985. ***J. Chem. Phys***, *82*(1), pp.299-310.

104. Matousek, P. and Stone, N., 2016. ***Chem Soc Rev***, *45*(7), pp.1794-1802.

105. Grubisha, D.S., Lipert, R.J., Park, H.Y., Driskell, J. and Porter, M.D., 2003. ***Anal chem***, *75*(21), pp.5936-5943.

106. Sha, M.Y., Xu, H., Natan, M.J. and Cromer, R., 2008. ***J. Am. Chem. Soc***, *130*(51), pp.17214-17215.

Chapter 3

The effect of chain-length on the SERS of 1-alkanethiols functionalized on AuNPs

3.1 Introduction

Alkanethiol protected gold nanoparticles (AuNPs) are among the most studied and used systems in science and technology. These systems have attracted a great interest in research due to simple synthetic methods, their stability and unique electronic, chemical and optical properties [1-3]. In fact, co-ordination of AuNPs with alkanethiols results in the formation of self-assembled monolayer (SAMs) which has a major contribution towards their properties [4, 5]. The SAMs of alkanethiols on AuNPs have attracted most interest in applications such as plasmonic photovoltaic, photo-catalysis, and photo-thermal heating [1, 6]. Recently, thiol SAMs are utilized as Raman reporters during SERS experiments for Raman signal enhancement [6]. Their strong chemical affinity towards AuNPs plays a major role in the improvement of Raman cross-section as a result of charge transfer between the molecular orbitals and the conduction bands of the metal.

Anyway, it is well known that shapes, sizes and dielectric environment of NPs can be tuned to manipulate their properties in order to open more gates for various applications including SERS [1, 7, 8]. For instance, nanorods, nanospheres, and other nanostructured materials have been reported to show a variety of optical and electronic properties which make them desirable to use in SERS applications [9, 10]. However, little has been reported on how the surface chemistry of these NPs can be utilised to manipulate their optical and electronic properties, without ruling out the theories of inorganic chemistry about the effects of metal-ligands interactions on the electronic structure and properties of metal surface. It was found that 1-alkanethiols on AuNPs can influence their electronic properties [11]. Cirri *et al.* showed that adsorbing 1-alkanethiol on AuNPs has an influence on their electronic

properties. They further explained the way the charge density of the metallic core is affected by 1-alkanethiols of various chain-lengths in various solvents [11]. Therefore by taking advantage of these properties which are possessed by 1-alkanethiols, Raman scattering cross-section of various molecules can be improved.

It is lately appreciated that changing a head group of ligand (i.e. amine to thiol or vice versa) can also affect the physical and chemical properties of AuNPs including dampening of SPR and increased electron−lattice coupling [12, 13], which is more advantageous in SERS experiments. Even though there is a lot of information on the effect of AuNPs-alkanethiols SAMs on Raman signal enhancement; not much has been done on the effect of specific chain-length of 1-alkanethiol. Herein, we aim to show the effect of chain-length of 1-alkanethiols on Raman signal enhancement. Pentanethiol (PT), decanethiol (DT), dodecanethiol (DDT), and pentadecanethiol (PDT) on AuNPs were used as Raman reporters. The effect of chain-lengths was investigated by comparing the Raman spectrum of each 1-alkanethiols with their SERS spectrum. A SERS spectrum is a Raman spectrum of each 1-alkanethiols after they were adsorbed on AuNPs. Furthermore we investigate the interaction of the 1-alkanethiols with the AuNPs through DFT and Molecular Dynamics modelling. The DFT calculations are important in the evaluation of the adsorption of different alkanethiols on the surface of AuNPs. The adsorption studies through computer modelling further helps in the determination of the effect of alkanethiol on the surface chemistry of AuNPs and the impact on SERS. Herein we further aim to use DFT and Molecular Dynamics modelling to calculate the theoretical spectra, charge densities on the surface of AuNPs, and the nucleophilic centres of the molecules for SERS EF evaluation.

3.2 Experimental

3.2.1 Chemicals

Hydrogen tetrachloroaurate (III) trihydrate ($HAuCl_4.\ 3H_2O$, 50 %), trisodium citrate ($C_6H_5Na_3O_7.\ 2H_2O$, 99.9%), Pentanethiol (PT, 98%), Decanethiol (DT, 96%), Dodecanethiol (DDT, 98%), and Petadecanethiol (PDT, 97%) were all purchased from Sigma Aldrich and used as received. All glassware was washed with aquaregia solution, and all the solutions were dissolved with distilled water.

3.2.2 Synthesis of and functionalization of AuNPs with 1-alkanethiols

Citrate capped AuNPs were synthesized following Turkevich method [13]. Typically, An aqueous solution of 1 mM $HAuCl_4$ (100 mL) was heated to boil (approximately 97 °C). To the boiling solution, 0.04 M of an aqueous solution of tri-sodium citrate was added. The mixture was stirred vigorously while heating, until color changes from colorless to deep ruby-red (7 min) which indicate the formation of AuNPs. The as-synthesized AuNPs were further functionalized with n-1-alkanethiols of various chain-lengths (1-pentanethiol, 1-decanethiol, 1-dodecanethiol and 1-pentadecanethiol) as shown in the schematic diagram in Figure 3.1. The colloidal solutions of AuNPs were centrifuged at 15000 rpm, for 15 min in order to concentrate the dispersed particles and to remove excess unreacted ions. The centrifuged solution of the AuNPs was divided into 3 aliquots of 10 mL. To each aliquot, 200 µL of 10 mM of each 1-alkanethiol dissolved in dimethyl sulphoxide (DMSO) was added and the mixtures were stirred for 3 h at room temperature. Figure 3.1 shows the schematic diagram representing the formation of citrate capped AuNPs followed by the substitution of citrate with 1-alkanethiols.

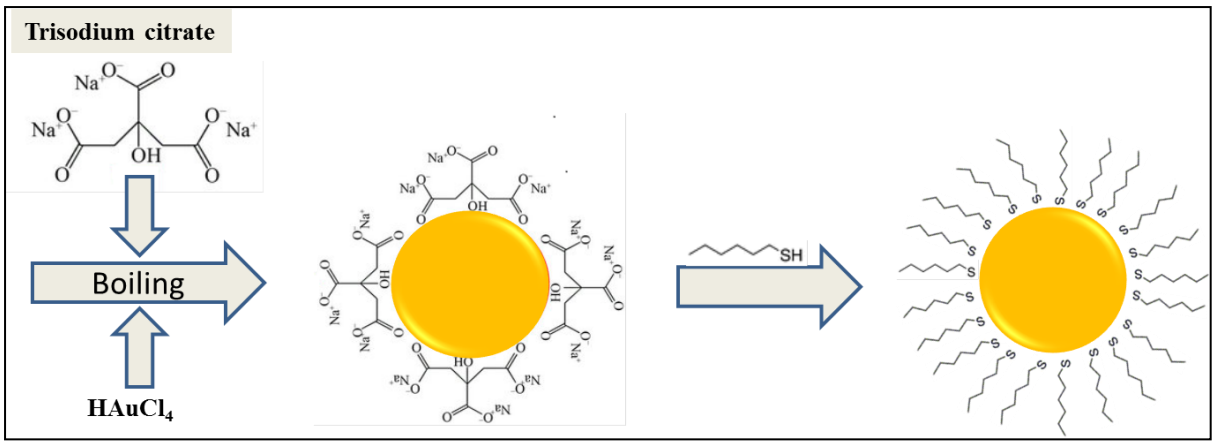


Figure 3.1: Schematic diagram representing the synthesis and functionalization of AuNPs.

3.2.3 Characterization

All excess impurities from colloidal solutions were removed using a universal 320R centrifuge at a maximum speed of 15000 rpm. The absorption spectra were acquired using a Varian Cary Eclipse (Cary 50) UV-Vis spectrophotometer. For spectral analysis, all the samples were diluted with distilled water until the optical density (OD) of 1 was reached. Transmission electron microscopy (TEM) images were obtained from FEI Tecnai-12 microscopy at an electron acceleration voltage of 200 KV and beam sport size of 10-100 nm. All SERS experiments were carried out using a PerkinElmer Raman Station 400 benchtop Raman spectrometer. The excitation laser with the near infrared wavelength of 785 nm, power of 100 mW and a spot size of 100 μm was used for all experiments. A spectral range of 100-3200 cm^{-1} was employed. The detector was a temperature controlled Charged Coupled Device (CCD) detector (-50 °C) incorporating a 1024 x 256 pixel sensor. The surface charge and the stability of substrate were investigated using the zetasizer potential.

3.3 Computer Simulation

3.3.1 Molecular Adsorption

Au 13 nanocluster was constructed and ligand adsorption was simulated. A trade-off exists between simulation accuracy and computational time. Since it becomes increasingly more difficult to do accurate molecular mechanics and dynamics calculations on large atomic systems, the aforementioned nanoclusters were selected and simulated. Although, in size, they are not exactly the same as those experimentally investigated, similar trends (small NPs *vs* large NPs) were observed on comparing their Raman spectra.

By using the Dmol3 of the *BioVia* ***Materials Studio*** 7.0 (MS 7.0), different number of ligand molecules were adsorbed onto the Au nanocluster surface. For the initial adsorption, a *universal forcefield* was used and the charges were assigned using the *QEq* charge equilibration method. As a check, the same experiment was repeated using the *charge consistent valence forcefield* (cvff) with charges assigned by the forcefield. Density functional theory (DFT) was used to determine the optimum geometries for each of the resulting ligand nanocluster systems using the Dmol3 – module of MS 7.0. The GGA: PBE, gradient-corrected functionals were used. Frequency calculation was done from the properties tab for computing a Hessian which is used for vibrational frequencies of the model.

3.4 Results and discussion

The absorption spectra of citrate and 1-alkanethiols capped gold AuNPs are presented in **Figure 3.2**. A sharp peak for citrate-capped AuNPs was observed at 521 nm due to the effect of coherent oscillation of conduction electrons when interacting with electromagnetic radiation [7, 14]. After the substitution reaction of citrate with 1-alkanethiols (DT, DDT and PDT), a red shift of the SPR band was observed, and the summary of these SPR peaks are

summarized in **Table 3.1**. However, there was no shift to higher wavelength for PT functionalized AuNPs as the peak remained at 521 nm in **Figure 3.2**, and this can be attributed to a negligible change in dielectric environment due to a shorter chain-length PT.

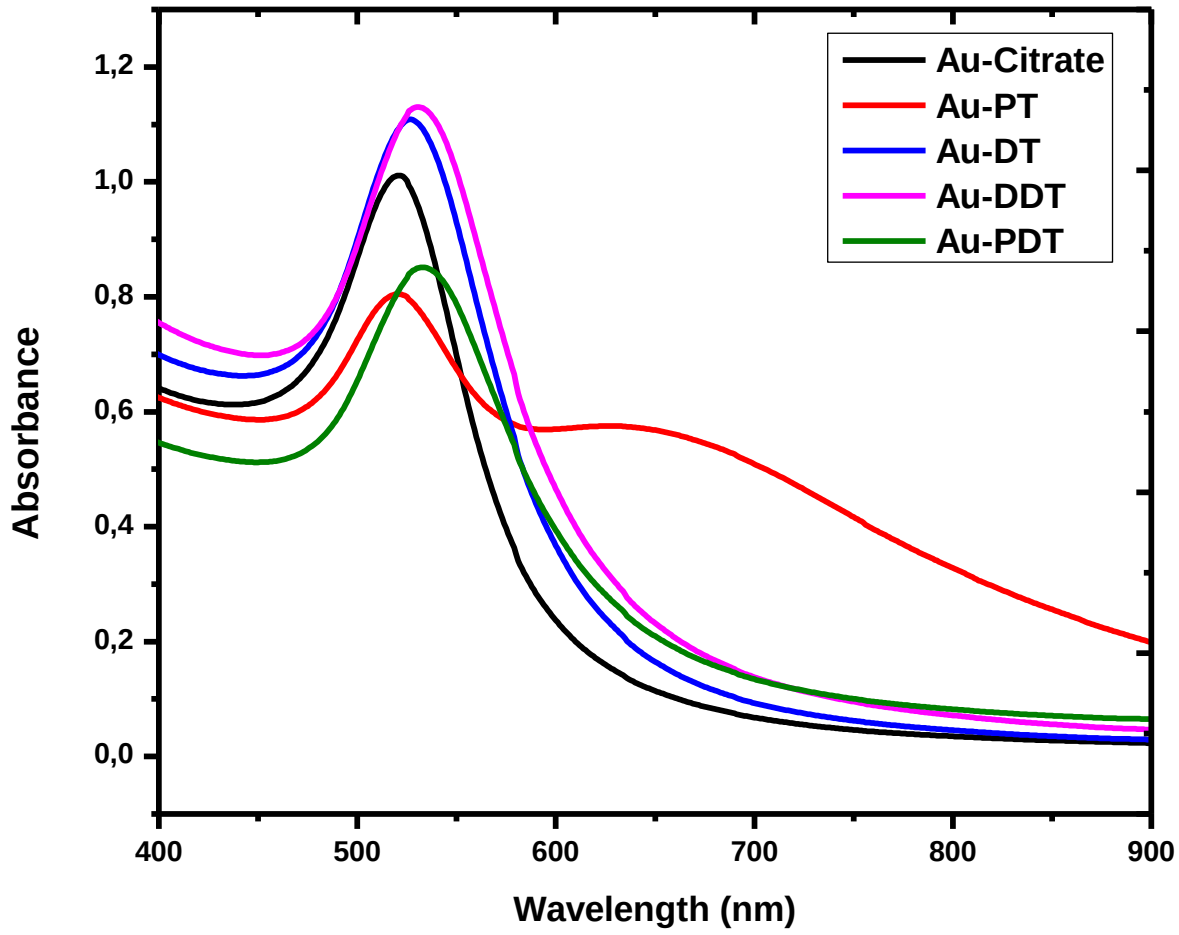


Figure 3.2: UV-Vis absorption spectra of citrate capped and 1-alkanethiols functionalized AuNPs.

The red shift in 1-alkanethiols functionalized AuNPs of longer chain-lengths (DT, DDT, and PDT) from 521 nm to 526, 531, and 533 nm, respectively as seen in **Figure 3.2**, are attributed to the change in dielectric constant of the medium through the introduction of 1-alkanethiols. These observations agree with what have been reported in literature [7]. Additionally, the chemisorption (resulting in charge transfer between metal and 1-alkanethiols orbitals) of 1-alkanethiol on the surface also played a role in the shift in SPR band. The appearance of a

secondary peak at longer wavelengths as seen at 650 nm for the Au-PT NPs usually suggests the formation of more anisotropic nanoparticles or is an indication of broad size distribution possibly caused by agglomeration. **Table 3.1** also shows the calculated full width at half maximum (FWHM) values of the SPR peaks. The FWHM values clearly indicate the broadening of the SPR bands as the 1-alkanethiols are introduced to the solution. This broadening effect is an indication of a slight agglomeration of AuNPs. Introducing 1-alkanethiols within the colloidal solution reduces the suspension ability of NPs due to the replacement of negative charged ions of citrate surrounding the surface, hence the slight agglomeration and aggregation of particles. The values of FWHM decreased with an increase in chain-length of 1-alkanethiols. This is a result of less steric hindrance provided by shorter chain PT as compared to its longer chain counterparts (DT, DDT, and PDT). The small length of PT molecules has resulted to the particles to move closer to each other, hence the agglomeration of NPs.

Table 3.1: Summary of SPR bands of citrate capped and 1-alkanethiols functionalized AuNPs and their corresponding FWHM values

Sample name	SPR bands wavelength (nm)	FWHM (nm)
Au-citrate	**521**	**104**
Au-PT	**521**	**169**
Au-DT	**526**	**124**
Au-DDT	**531**	**130**
Au-DDT	**533**	**131**

Figure 3.3 shows the particle size distribution of citrate and 1-alkanethiols capped gold nanoparticles, and their corresponding TEM images used to measure the average diameter are shown in **Figure 3.4**. The citrate capped AuNPs were observed to be spherical with good dispersity and an average diameter of 15±3 nm as shown in **Figure 3.4 (a)** and **Figure 3.3** respectively. There was no significant change in average particle size after functionalization of AuNPs with the different alkanethiols as observed in **Figure 3.3**. The observed change was due to a slight agglomeration of particles prior to functionalization with 1-alkanethiols; this is attributed to a slow substitution reaction of the citrate by the different chain-lengths 1-alkanethiols. Some bigger particles are noticeable in the TEM images shown in **Figure 3.4** (b) to (e). Another notable feature was the influence of chain-length in the inter-particle distance during SAMs formation. The shortest chain (PT) resulted into shorter inter-particle distance as seen in **Figure 3.4 (b)**, which caused particle to agglomerate and this is also evident from the absorption spectrum which showed a second broad peak around 650 nm in **Figure 3.2**. The inter-particle distance was observed to increase with an increase in chain-length as can be clearly seen in **Figure 3.4 (b-e).**

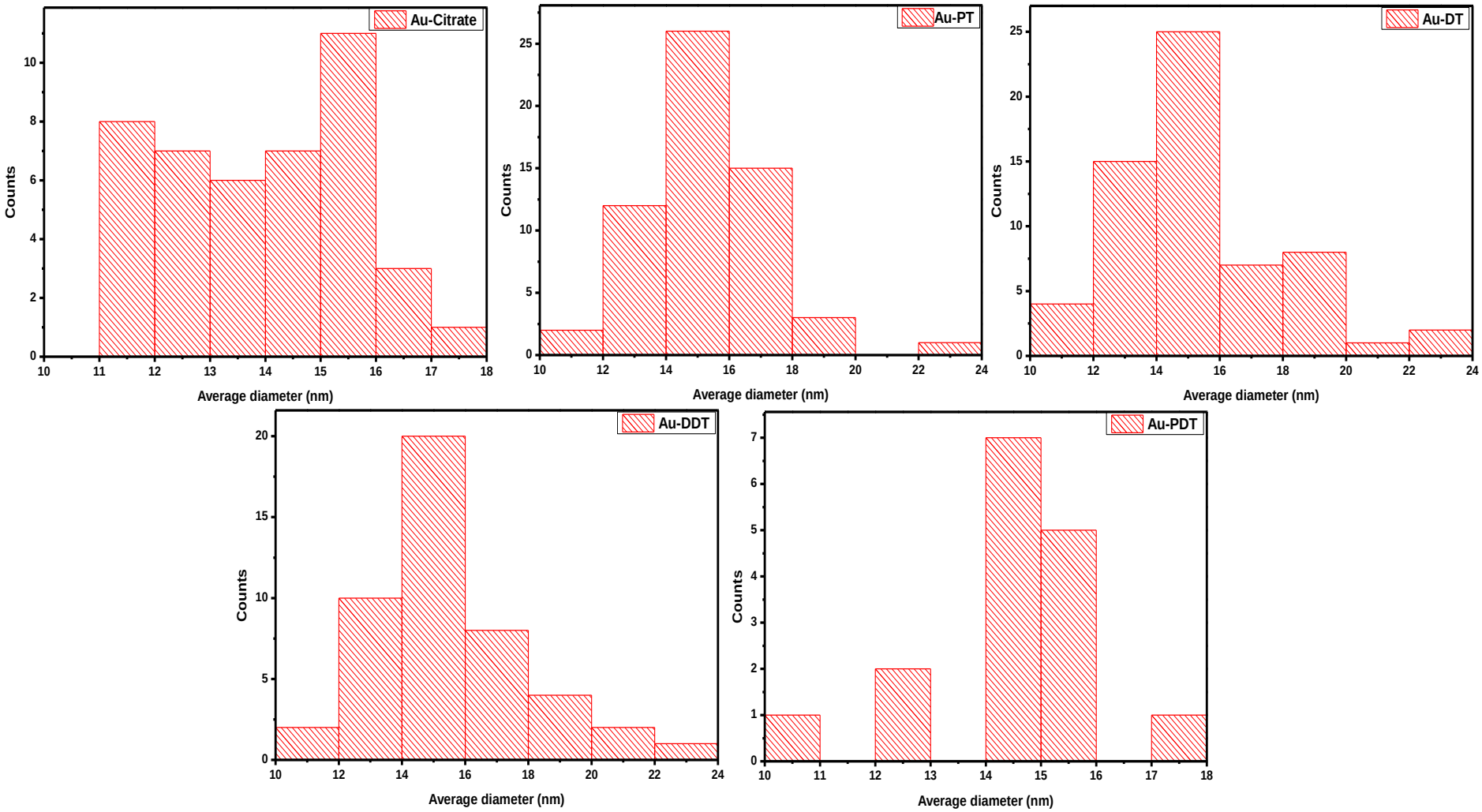


Figure 3. 3: Particle size distribution of citrate capped and 1-alkanethiols functionalized AuNPs.

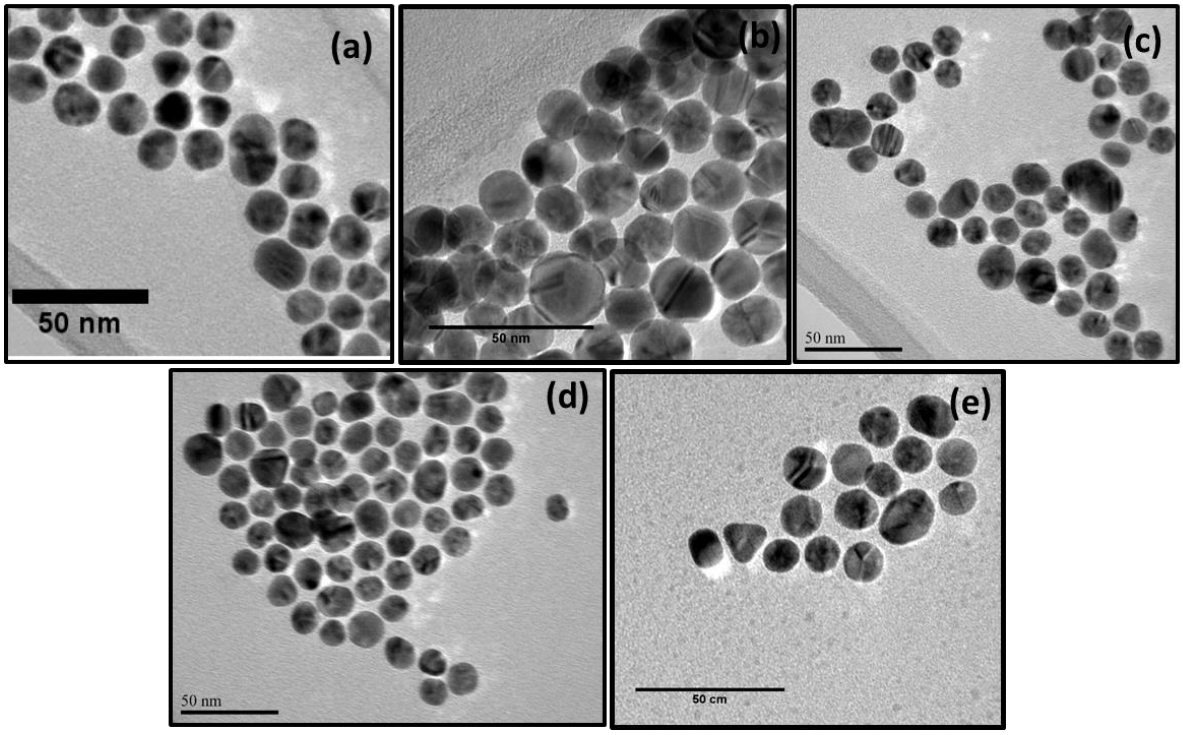


Figure 3.4: TEM images of (a) citrate-capped, (b) PT, (c) DT, (d) DDT, (e) PDT functionalized AuNPs.

Functionalization of AuNPs with alkanethiols is understood to occur via substitution reaction, where citrate ions are replaced by alkanethiols of different chain-lengths using their thiol head group [15]. The displacement of citrate ions can lead to a change in surface charge or agglomeration of nanoparticles, thus a stability investigation of these functionalized AuNPs is vital for their SERS evaluation study. Zetasizer was used to evaluate their stability, and all the functionalized AuNPs were found to have a negative potential. The thiol capped nanoparticles have a surface charge values that were less negative compared to the citrate-capped AuNPs (-60 mV), and the Zeta potential values are summarized in **Table 3.2**. The zeta potentials distributions are shown in **Figure S3.1-S3.5**. The high negative value of zeta potential for citrate capped AuNPs confirms good stability and dispersion of particles as compared to the 1-alkanethiol functionalized particles in solution. A decrease in potential value of the functionalized AuNPs also confirms the displacement of citrate ions with

alkanethiols which possess a thiol group with strong affinity for metal surface. The longer chain-length (PDT) showed a lesser potential (-18 mV) as compared to shorter chain-lengths; this is attributed to long chain's ability to form more stable and dense SAMs [5, 14, 16, 17]. The potential values of DDT and DT functionalized AuNPs were found to -54 and -42 mV, respectively, while PT functionalized AuNPs was -32 mV. These two potential values of DDT and DT functionalized AuNPs were close to citrate-capped AuNPs (-60 mV), this might be due to the manner in which these alkanethiols interact with metal surface, and the resulting orientation.

Table 3.2: The values of zeta potentials of citrate capped and 1-alkanethiols functionalized AuNPs

Sample name	Zeta potential (mV)
Au-citrate	-60
Au-PT	-32
Au-DT	-42
Au-DDT	-54
Au-PDT	-18

The EF dependence on the chain-length of alkanethiols (PT, DT, DDT and PDT) functionalized on AuNPs was investigated through SERS experiments. **Figure 3.5** shows the normal Raman (NR) spectra of 1-alkanethiols (black) and SERS spectra (red) of all 1-alkanethiols adsorbed on AuNPs respectively. The SERS effect on all 1-alkanethiols was

clearly evidenced by the enhanced and appearance of some vibrational bands which were supressed on the NR spectra. The SERS spectra of all 1-alkanethiols are dominated by strong bands at 2900 cm^{-1} (*) and 1450 cm^{-1} (#) which are assigned to υ(C-H) symmetrical and asymmetrical vibrations, respectively. On the other hand the vibrational bands at a range of 2500 cm^{-1} to 2700 cm^{-1} (circled peaks) were observed from all NR spectra. These bands were all assigned to the vibration of υ(S-H) group of each 1-alkanethiol. The dissociation of S-H group prior to the binding of 1-alkanethiols on the surface of AuNPs (as was expected) was evidenced by the disappearance of υ(S-H) vibrational bands in the SERS spectra. The binding of 1-alkanethiolates on the surface of AuNPs was further evidenced by the appearance of new vibrational bands 280 cm^{-1} which are assigned to υ(Au-S) vibrations denoted by &. **Table 3.3-3.6** summarise the assignment of Raman bands of 1-alkanethiol before and after they were adsorbed on AuNPs. The positions of the observed peaks of all 1-alkanethiols agree with what have been reported on literature [18-20].

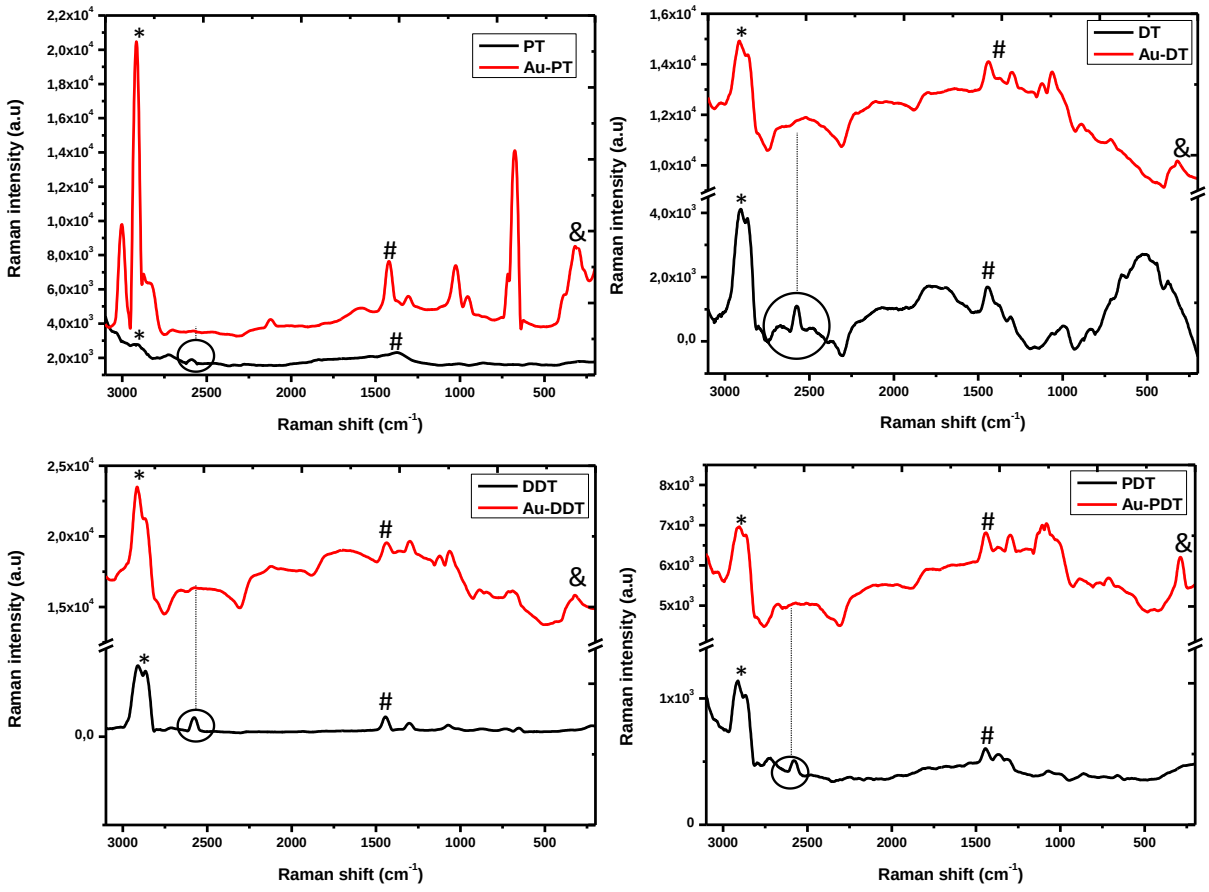


Figure 3.5: Raman spectra of 1-alkanethiols (black) and their corresponding SERS spectra (red). * denotes υ(C-H) *sym*, # denotes υ(C-H) *asym* and & denotes υ(Au-S).

Table 3.3: A Summary of the experimental and theoretical bands assignment of PT adsorbed on AuNPs

Band assignment	υ(Au-S)	υ(C-S)	υ(CC) aliph	δ(CH2) asym	υ(-S-H)	υ(C-H) sym
PT (experimental)	no peak	-	-	1450	2610	2941
Au-PT (experimental)	280	720	970, 1020, 1250	1420	no peak	2941
PT (theoretical)	No peak	650,700, 780	1050, 1250	1470	2550	2900, 300
Au-PT (theoretical)	250	700	1200	1490	no peak	2900, 3100

PT = Pentanethiol, Au = Gold, Aliph = aliphatic, sym = symmetric, asym=asymmetric

Table 3. 4: A Summary of the experimental and theoretical bands assignment of DT adsorbed on AuNPs

Band assignment	υ(Au-S)	υ(C-S)	υ(CC) aliph	δ(CH2) asym	υ(-S-H)	υ(C-H) sym
DT (experimental)	no peak	700, 950	1060, 1300	1480	2588	2890
Au-DT (experimental)	320	650, 820	1020	1480	no peak	2990
DT (theoretical)	No peak	750, 800	1100, 1250	1550	2600	2990
Au-DT (theoretical)	-	-	1050, 1150	-	no peak	2950

DT = Decanethiol, Au = Gold, Aliph = aliphatic, sym = symmetric, asym=asymmetric

Table 3.5: A Summary of the experimental and theoretical bands assignment of DT adsorbed on AuNPs

Band assignment	υ(Au-S)	υ(C-S)	υ(CC) aliph	δ(CH2) asym	υ(-S-H)	υ(C-H) sym
DDT (experimental)	no peak	748	1050, 1250	1490	2620	2980
Au-DDT (experimental)	290	750	1100	1470	no peak	2980
DDT (theoretical)	No peak	750, 800	1120	1480	2680	2860, 3050
Au-DDT (theoretical)	300	740, 880	1200	1450	no peak	2860, 3050

DDT = Dodecanethiol, Au = Gold, Aliph = aliphatic, sym = symmetric, asym=asymmetric

Table 3. 6: A Summary of the experimental and theoretical bands assignment of PDT adsorbed on AuNPs

Band assignment	υ(Au-S)	υ(C-S)	υ(CC) aliph	δ(CH2) asym	υ(-S-H)	υ(C-H) sym
PDT (experimental)	no peak	740	1230	1450	2620	2880
Au-PDT (experimental)	270	750	1000, 1250	1472	no peak	2885
PDT (theoretical)	no peak	750, 800	1150, 1250	1480	2500	2900
Au-PDT (theoretical)	250	500, 550; 650	1170, 1300	1500	no peak	2850, 3000

PDT = Pentadecanethiol, Au = Gold, Aliph = aliphatic, sym = symmetric, asym=asymmetric

The calculated EFs of all alkanethiols on AuNPs are shown in the form a bar graph in **Figure 3.6.** Equation 1 was used to do all the calculations, Where I_{SERS} and I_{NR} are the intensities of the vibrational modes in SERS and native Raman spectrum respectively. N_{NR} represents the number of molecules probed on the Raman spectrum (free 1-alkanethiol), while N_{SERS} represents the number of molecules probed using SERS (1-alkanethiol with Au substrate).

$$EF = \frac{I_{SERS}N_{NR}}{I_{NR}N_{SERS}} \quad (1)$$

N_{NR} can be expressed further using equation (2):

$$N_{NR} = \frac{Ah\rho}{m} \quad (2)$$

Where A, h, ρ, and m are the laser spot area, the focal length, the density of 1-alkanethiols (PT, DT, DDT and PDT) and their molecular weights respectively. N_{SERS} can also be expressed as in equation (3):

$$N_{SERS} = 4\pi r^2 CAN \quad (3)$$

Where r, C, A and N are the average radius of the AuNPs, the surface density of the 1-alkanethiol, the area of the laser spot, and the surface coverage of the AuNPs (particles μm^{-2}), respectively.

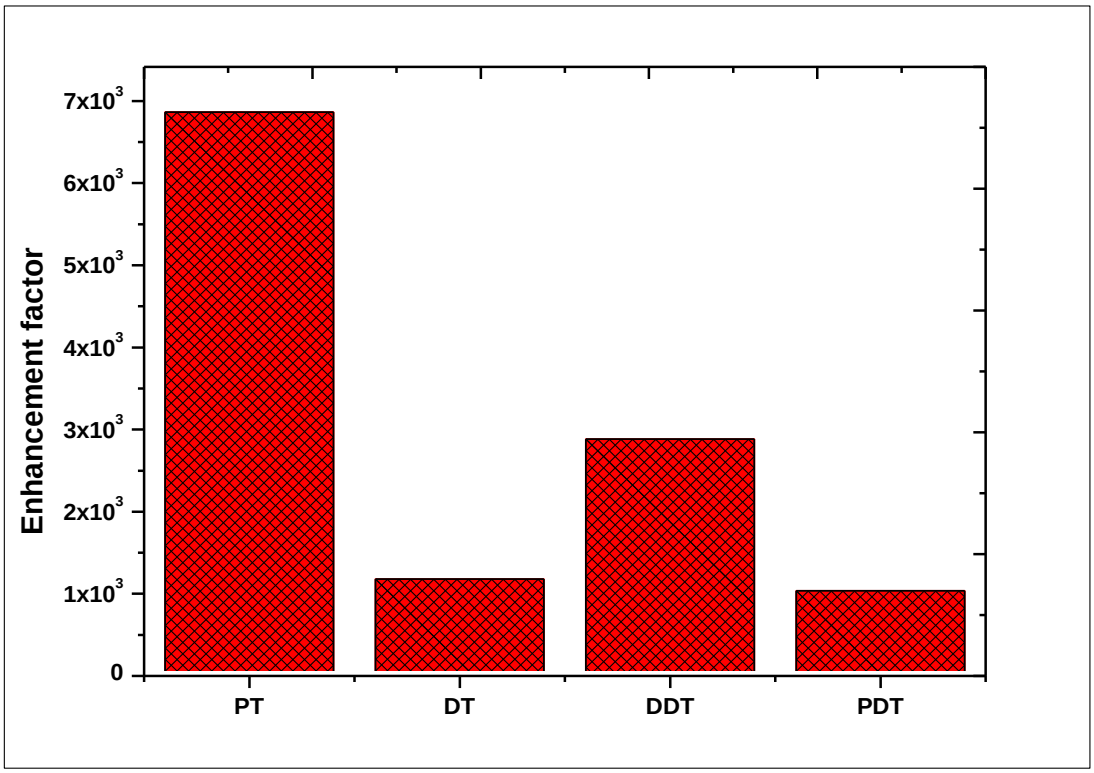


Figure 3.6: Relationship between the enhancement factor and chain-length of 1-alkanethiols.

In all calculations, the peak at 2900 cm^{-1} (C-H symmetric vibration) was used to determine the EF since it exhibits the highest intensity. The EF dependency on the chain-length of 1-alkanethiol is shown in **Figure 3.6**. The bar graph is clearly indicating a decreasing trend of EF with an increase in 1-alkanethiol chain-length. PT was found to possess largest EF among

the other thiols (DT, and DDT and PDT). A related study by Kennedy *et al.* also showed a decrease in enhancement factor as the chain-length of 1-alkanethiol increased [16]. This can be attributed to the fact that the shorter chain-length of n-1-alkanethiol is likely to result in less stable and weakly packed SAM which lead to a slight agglomeration of NPs and the creation of hot spots. This is also confirmed by TEM image in **Figure 3.4 (b)**, where particles tend to clump together. In addition, PT has higher chance for spectral multiplexing than DT, DDT and PDT since it has shorter chain-length. The other factor which might have played a role on the Raman signal enhancement is the orientation of 1-alkanethiols on the surface of gold nanoparticles. The obtained EF values were 3.8×10^3, 1.6×10^3, 2.0×10^3 and 1.5×10^3 for PT, DT, DDT and PDT, respectively. However, the EFs larger than these ones can be obtained using dyes molecules as Raman reporters. This is because dye molecules result in a resonance Raman scattering (RRS) effect as a result of a strong charge transfer in the visible region. However, most dye molecules cannot form SAMs around the surface of SERS substrate due to their bulkiness; which can also affect the stability of substrate and uniformity of SERS results [21-24]. The reported EF values in this study were expected, small as they are, since 1-alkanethiols used in this project didn't have any functional group which will further influence the charge transfer between the metal and the molecules. However, critical to this study is to also investigate whether other factors such as the geometry of the RRs on the surface of the nanoparticles play a role in the enhancement of the Raman signal. Hence the evaluation of the effect of chain-length on SERS was further carried out using theoretical modelling. In this case density functional theory (DFT) calculations were carried out using Material studio (Dmol3 module), through which the theoretical Raman spectra, chain-length, nucleophilic centres and the charge density of each alkanethiol was determined. The modelled 1-alkanethiols and their chain-lengths are shown in **Figure 3.7**.

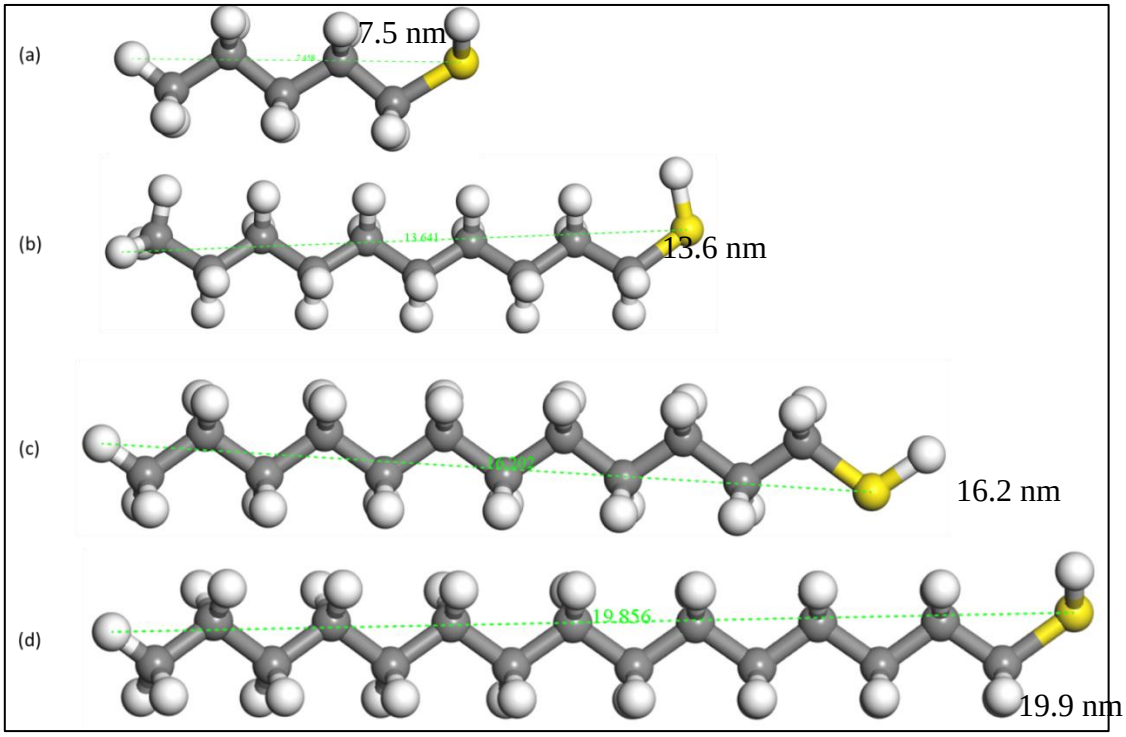


Figure 3.7: The modelled 1-alkanethiols and their chain-lengths (a) 1-PT, (b) 1-DT, (c) 1-DDT, (d) 1-PDT.

The Raman spectra of these alkanethiols were modelled both before and after they were adsorbed on a cluster made of 19 Au atoms which represent AuNPs as shown in **Figure 3.8**; and were further compared with the experimental spectra. These modelled spectra offered more information on the validation of adsorption of 1-alkanethiols on AuNPs. Shown in **Figure 3.8** are the modelled normalized Raman spectra of the NR (prior to the attachment to Au) and SERS spectra (attached to the Au surface) of the alkanethiols. There is a disappearance of υ(S-H) vibration peak at 2600 cm^{-1} in the Au-PT spectrum as opposed to the PT spectrum. This suggested that there was a strong attachment of the PT ligand on the surface of the Au through the thiol moiety. This was also observed for the Au-PDT spectrum.

On the other hand, the NR spectra of DDT and PDT showed the absence of the υ(S-H) peak. This was attributed to the deprotonation of 1-alkanethiols prior to their adsorption on AuNPs surface. Generally a vibrational peak around 200 cm^{-1} - 350 cm^{-1} accounts for the formation υ(Au-S) and this was observed in SERS spectra for all but the Au-PDT spectrum. This was indicative of the poor interaction of the PDT ligand with the Au surface. The increase in the intensity of some of the peaks in the SERS spectra and the appearance of new peaks gave an insight on the enhancement of Raman scattering possessed by each 1-alkanethiol. The small chain 1-alkanethiol (PT) was found to possess more intense Raman peaks than the long chain 1-alkanethiol in the 200 cm^{-1} - 350 cm^{-1} region. Just like in the experimental study, PDT possesses the lowest peak intensity.

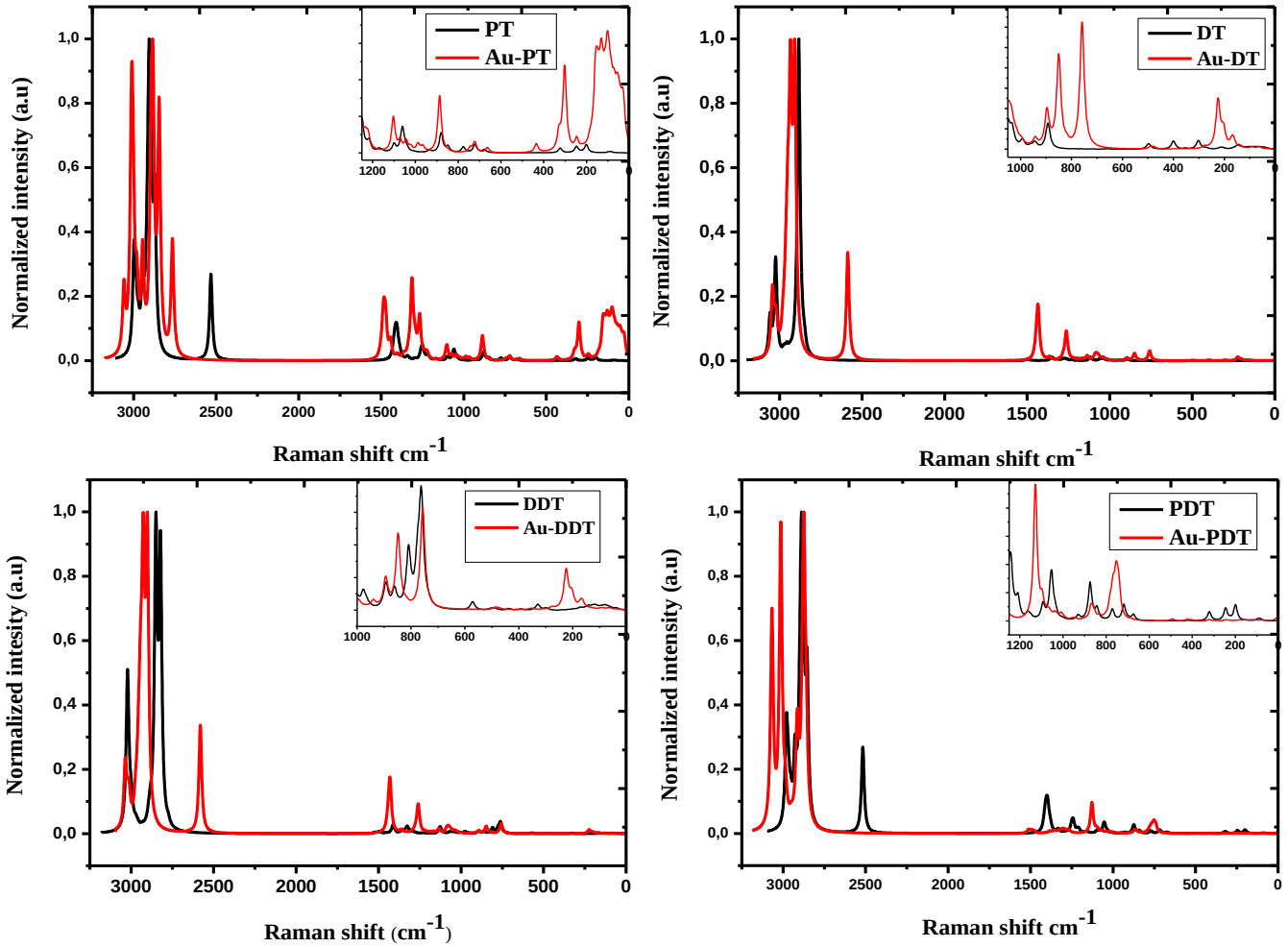


Figure 3.8: DFT calculated Raman spectra of (a) PT, (b) DT, (c) DDT, and (e) PDT together with the insert of the zoomed lower region of the spectra.

DFT calculations were further used to determine the nucleophilic centres of 1-alkanethiols. For alkanethiols, the nucleophilic centre is around the S atom. The larger the cross-section of the nucleophilic centre, the more strongly the RR will bind to the Au surface. **Table 3.7** shows the measured cross-sectional lengths of nucleophilic centres for all the molecules. The nucleophilic centres were found to increase with an increase in chain lengths of the 1-alkanethiol. This means that the longer chain, PDT will have more effect on the electron density of the metal. Due to this, it is expected that there will be a high charge transfer from the HOMO to the LUMO of PDT or to the metallic surface as compared to the shorter chain 1-alkanethiols. This therefore suggests that PDT will have a higher enhancement factor as compared to the other alkanethiols, however this is contrary to the previous findings.

Table 3. 7: DFT calculated nucleophilic centres of PT, DT, DDT, and PDT

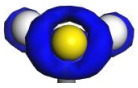
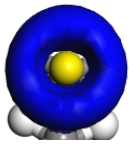
Raman reporters	**Nucleophilic centres**	**Diameters (Å)**
1-Pentanethiol		1.9
1-Decanethiol		2.8
1-Dodecanethiol		3.2
1-Pentadecanethiol		3.7

Figure 3.9 shows the molecular geometry of the alkanethiols on the Au surface as well as the charge density on the surface of AuNPs functionalized with various 1-alkanethiols. The simulated geometry showed that the longer the chain length, the more bent the geometry. This however might hinder the charge transfer to the metal. Based on the size of the nucleophilic centres, an increase in charge density with an increase in chain-length was expected. Even though an exact trend can't be deduced from Figure 3.9, it is clear that the 1-alkanethiols of different chain-length have an effect on the electronic properties of the metallic surface which is good for SERS effects. Nevertheless, the shorter chain PT seemed to have a higher charge transfer on the metal signified by the red area in the metal as compared to other alkanethiols. In particular, the longer chain PDT has weaker charge transfer to the metal. This is consistent with the experimental findings that suggest that PDT has a weaker EF.

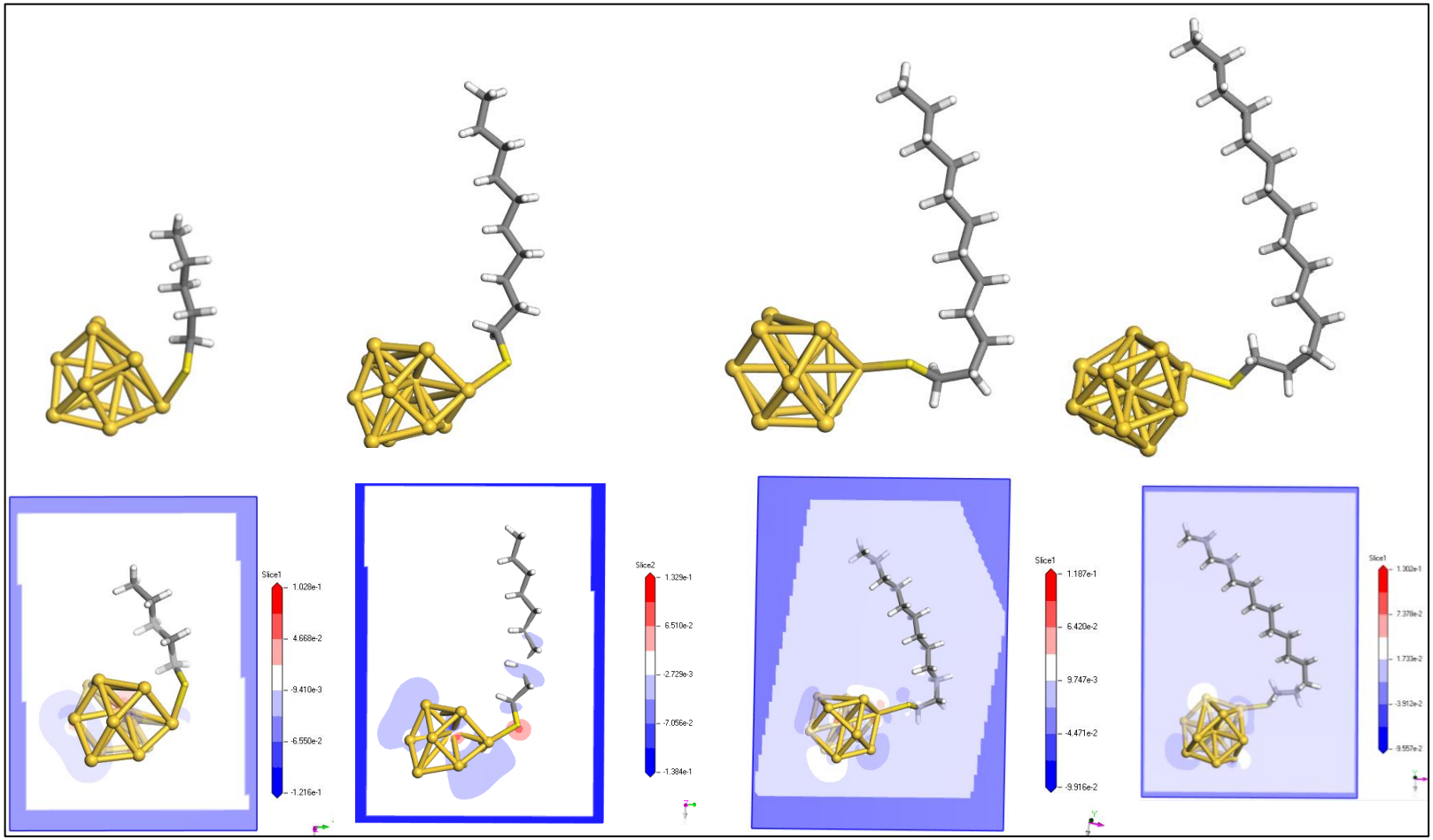


Figure 3.9: The calculated molecular geometry on the surface of AuNPs and their effect on the charge density (blue means lower charge density and red higher charge density)

The charge transfer to the LUMO of PT or the conduction band of the metal (Au) will be limited as a result of small nucleophilic centre. PDT should possess high Raman signal enhancement however it is very clear that the geometry of the ligand does play an important role. The total SERS EF results from both chemical (charge) and electromagnetic enhancement mechanisms. Since chemical enhancement mechanism is dominated by the electromagnetic enhancement mechanism on the total EF, the chemical effects might not have a significant influence on the total EF. The reason why PDT possesses lowest total EF might also be due to the fact that it forms well-ordered SAMs on the surface which results in a large inter-particle distance between the NPs. It is also important to note that smaller inter-particle distance and slight agglomeration of NPs caused by small chain 1-alkanethiols will result in strong hot spots that significantly enhance the laser electromagnetic field. The EF is widely dependent on the enhanced EM field than the charge transfer contribution.

3.5 Conclusion

Stable AuNPs were successfully prepared and further functionalized by PT, DT, DDT and PDT. The TEM micrographs revealed monodispersed AuNPs with spherical morphologies. There was no significant agglomeration or morphological change of NPs after functionalization as was evidenced from TEM micrographs. The UV-Vis showed sharp SPR bands around 520 nm, which confirmed the presence of stable and spherical AuNPs in the colloidal solution. The zeta potentials for both 1-alkanethiol functionalized and unfunctionalized AuNPs were further obtained in order to identify surface charge and the stability of AuNPs. The strong negative potential confirmed the negatively charged surface with good stability. SERS experiments showed an improvement in the intensity of all 1-alkanethiols spectra as compared to the ones obtained from the NR studies. The calculated EF of Raman scattering was found to decrease with an increase in the chain-length of 1-

alkanethiols, with PT possessing the highest EF and PDT the lowest. The modelling studies corroborated the findings of the experimental studies where PT had the highest EF and PDT the lowest in spite of the free PDT having the largest nucleophilic centre cross-sectional area. The geometry of the RR on the surface of Au had an influence on charge transfer from the RR to the metal and this resulted in PT having the highest EF also evident from the simulated Raman spectra.

3.6 References

1. Daniel, M.C. and Astruc, D., 2004. ***Chem rev,*** *104*(1), pp.293-346.
2. Harris, R.A., Mlambo, M. and Mdluli, P.S., 2016. ***RSC Adv***, *6*(15), pp.12131-12142.
3. Malinsky, M.D., Kelly, K.L., Schatz, G.C. and Van Duyne, R.P., 2001. ***J. Am. Chem. Soc***, *123*(7), pp.1471-1482.
4. Zhang, L., Goddard III, W.A. and Jiang, S., 2002. ***J. chem. phys***, *117*(15), pp.7342-7349.
5. Freeman, R.G., Grabar, K.C., Allison, K.J. and Bright, R.M., 1995. ***Science,*** *267*(5204), pp.1629.
6. Mlambo, M., Harris, R.A., Mashazi, P., Sabela, M., Kanchi, S., Madikizela, L.M., Shumbula, P.N., Moloto, N., Hlatshwayo, T.T. and Mdluli, P.S., 2017. ***Appl Surf Scie***, *396*, pp.695-704.
7. Quester, K., Avalos-Borja, M. and Castro-Longoria, E., 2016. ***J biomater appl*** 7(02), pp.118.
8. Jiang, L., Qian, J., Cai, F. and He, S., 2011. ***Anal. Bioanal. Chem***, *400*(9), pp.2793.
9. Xie, J., Zhang, Q., Lee, J.Y. and Wang, D.I., 2008. ***ACS nano***, 2(12), pp.2473-2480.
10. Bindhu, M.R. and Umadevi, M., 2014. ***Mater. Lett***, 120, pp.122-125.

11. Cirri, A., Silakov, A., Jensen, L. and Lear, B.J., 2016. ***J. Am. Chem. Soc***, *138*(49), pp.15987-15993.

12. Trudel, S., 2011. ***Gold Bull***, *44*(1), pp.3-13.

13. Kimling, J., Maier, M., Okenve, B., Kotaidis, V., Ballot, H. and Plech, A., 2006. ***J. Phys Chem B***, *110*(32), pp.15700-15707.

14. Quester, K., Avalos-Borja, M., Vilchis-Nestor, A.R., Camacho-López, M.A. and Castro-Longoria, E., 2013. ***PLoS One***, 8(10), pp.77486.

15. Kleinman, S.L., Frontiera, R.R., Henry, A.I., Dieringer, J.A. and Van Duyne, R.P., 2013. ***Phys. Chem. Chem. Phys***, *15*(1), pp.21-36.

16. Kennedy, B.J., Spaeth, S., Dickey, M. and Carron, K.T., 1999. ***J. Phys Chem B***, 103(18), pp.3640-3646.

17. Boca, S., Rugina, D., Pintea, A., Barbu-Tudoran, L. and Astilean, S., 2010. ***Nanotechnology,*** *22*(5), pp.055702.

18. Li, J. and Zhang, J.Z., 2009. ***Coord. Chem. Rev.***, *253*(23), pp.3015-3041.

19. Morones, J.R., Elechiguerra, J.L., Camacho, A., Holt, K., Kouri, J.B., Ramírez, J.T. and Yacaman, M.J., 2005. ***Nanotechnology***, *16*(10), pp.2346.

20. Agnihotri, S., Mukherji, S. and Mukherji, S., 2014. ***RSC Adv***, *4*(8), pp.3974-3983.

21. Kottmann, J.P., Martin, O.J., Smith, D.R. and Schultz, S., 2001. ***Phys. Rev B***, *64*(23), pp.235402.

22. Sau, T.K. and Rogach, A.L., 2010. ***Adv Mat***, *22*(16), pp.1781-1804.

23. Sau, T.K., Rogach, A.L., Jäckel, F., Klar, T.A. and Feldmann, J., 2010. ***Adv Mat***, *22*(16), pp.1805-1825.

24. Pastoriza-Santos, I. and Liz-Marzán, L.M., 2008. ***J. Mat. Chem***, *18*(15), pp.1724-1737.

Chapter 4

The effect of chain-length on the SERS of 1-alkanethiols functionalized on AgNPs

4.1 Introduction

Silver nanoparticles (AgNPs) have shown the highest commercialization level, accounting for approximately 55% of the noble nano material-based products in 2011 [1-4]. AgNPs have been utilised in a number of applications including catalysis, biosensors, optical devices, antimicrobials and surface-enhanced Raman scattering (SERS) [5-9]. Most importantly, the exploitation of AgNPs in SERS applications (as SERS substrate) has attracted lot of research owing to their simple synthetic method, tuneable size and shapes, stability and most critically their strong inter-transition band in the Infrared-visible (Ir-Vis) range of electromagnetic (EM) spectrum. Characteristically, AgNPs possess a very strong absorption band as a result of interaction with incident EM radiation that is in resonant with the collective oscillation of free electrons commonly known as surface plasmon resonance (SPR) on their surface. The excitation of SPR results in the enhancement of EM field around the surface of nanoparticles (NPs), which is responsible for the intense Raman scattering that is observed in SERS. However, various parameters have to be controlled in order to obtain SPR excitations which include; the size, shape, dielectric properties, and local environment of the nanoparticle.

1-alkanethiols molecules on the other hand were found to alter the optical properties of AgNPs in the sense that they form self-assembled monolayer (SAMs) on the surface [10, 11]. 1-alkanethiol SAMs on AgNPs are of great interest for the creation of new functional materials due to the formation of dense, tightly bonded and well-ordered systems on the surface. They can further provide a simple functionality for selective tailoring of surface

electronic and optical properties which are more critical to many areas of scientific study [12, 13] including SERS applications. Although much focus has been done on synthesis and characterization of SAM-modified AgNPs, few investigations have been done on how the chain-lengths of 1-alkanethiols affect the surface chemistry of AgNPs and Raman signal enhancement. Kennedy *et al*. have demonstrated the effect of chain-length of 1-alkanethiol on Raman activity towards the detection of aromatic compounds. The best enhancement factor (EF) of 2.1 $*10^3$ was obtained for shorter chain-length 1-alkanethiol on AgNPs [14]. This was attributed to the fact that the enhanced electromagnetic (EM) field decrease exponentially with the distance from the SERS substrate. The chain-length of 1-alkanethiol was also found to have an effect on the chemical properties of nanoparticle. A study by Cirri *et al.* showed that longer chain 1-alkanethiols have a great effect on the chemical and electronic properties of nanoparticles [15]. An understanding of the effect of the 1-alkanethiol' chain-length on SERS could open many research gates in the nanotechnology, and more importantly in the application of SERS technique. The current project focused on the experimental and theoretical studies of the effect that the chain-length of 1-alkanethiol (i.e. 1-Pentanethiol, 1-Decanethiol, 1-Dodecanethiol and 1-Pentadecanethiol) has on surface of AgNPs and Raman scattering enhancement.

4.2 Experimental

4.2.1 Chemicals

Silver nitrate ($AgNO_3$, 99%), trisodium citrate ($C_6H_5Na_3O_7.2H_2O$, 99.9%), Pentanethiol (PT, 98%), Decanethiol (DT, 96%), Dodecanethiol (DDT, 98%), and Pentadecanethiol (PDT, 97%) were all purchased from Sigma Aldrich and used as received. All glassware was washed with aquaregia solution, and all the solutions were dissolved with distilled water.

Glycerol [$C_3H_5(OH)_3$] was purchased from Associated chemical enterprises (PTY) LTD, South Africa.

4.2.2 Instrumentations

All excess impurities from colloidal solutions were removed using a centrifuge and the characterization techniques used are described in Chapter 3.

4.2.3 Synthesis and functionalization of AgNPs

AgNPs were synthesized using a modified Lee and Meisel method [16]. In a typical procedure 10 mg of $AgNO_3$ was dissolved in 40% glycerol-water solution. The solution was the heated to a boiling temperature; about 97^{o}C. To a boiling solution 0.3 mL of 3% trisodium citrate solution was added. The mixture was then stirred vigorously while heating. A change in color of the mixture from colorless to pale yellow after 5 min was an indication of the formation of AgNPs. It is also important to note that the volumetric flask from which AgNPs where synthesized in, was rapped with aluminium foil to avoid the interaction of light with NPs. The as-synthesized AgNPs were further functionalized with 1-1-alkanethiols of various chain-lengths (1-pentanethiol, 1-decanethiol, 1-dodecanethiol and 1-pentadecanethiol). The colloidal solutions of AgNPs were centrifuged at 15000 rpm for 15 min in order to concentrate the dispersed particles and to remove access supernatants. The centrifuged solution was then divided into 3 aliquots of 10 mL. To each aliquot, 200 µL of 10 mM of each 1-alkanethiol was added and the mixtures were stirred for about 3 h at room temperature. The functionalized solutions were further centrifuged in order to remove the molecules which didn’t adsorb on the surface of AgNPs.

4.3 Results and discussion

AgNPs were prepared via citrate reduction of $AgNO_3$ in aqueous solution and then subsequently modified with 1-alkanethiols as described in the previous section. The colloidal solution turned yellow which was the indication of AgNPs formation. As a result of functionalization with 1-alkanethiols, the colloidal solution changed color to pale yellow. The change in color of colloidal solution can be attributed to the agglomeration or a change in dielectric environment of AgNPs. The SPR absorption peaks of citrate-capped and 1-1-alkanethiols functionalized AgNPs are shown in **Figure 4.1**. The absorption spectrum of citrate-capped AgNPs shows the SPR band at 414 nm, indicating the presence of spherical or spherical-like AgNPs. The summary of SPR bands for both citrate and 1-alkanethiols modified AgNPs are shown in **Table 4.1**. The 1-alkanethiol SPR bands were found to be slightly red-shifted to 419, 422, 425 and 424 nm for PT, DT, DDT and PDT-AgNPs from that of citrate-AgNPs (414 nm). This slight shift of the SPR bands to higher wavelength is attributed to a change in dielectric environment.

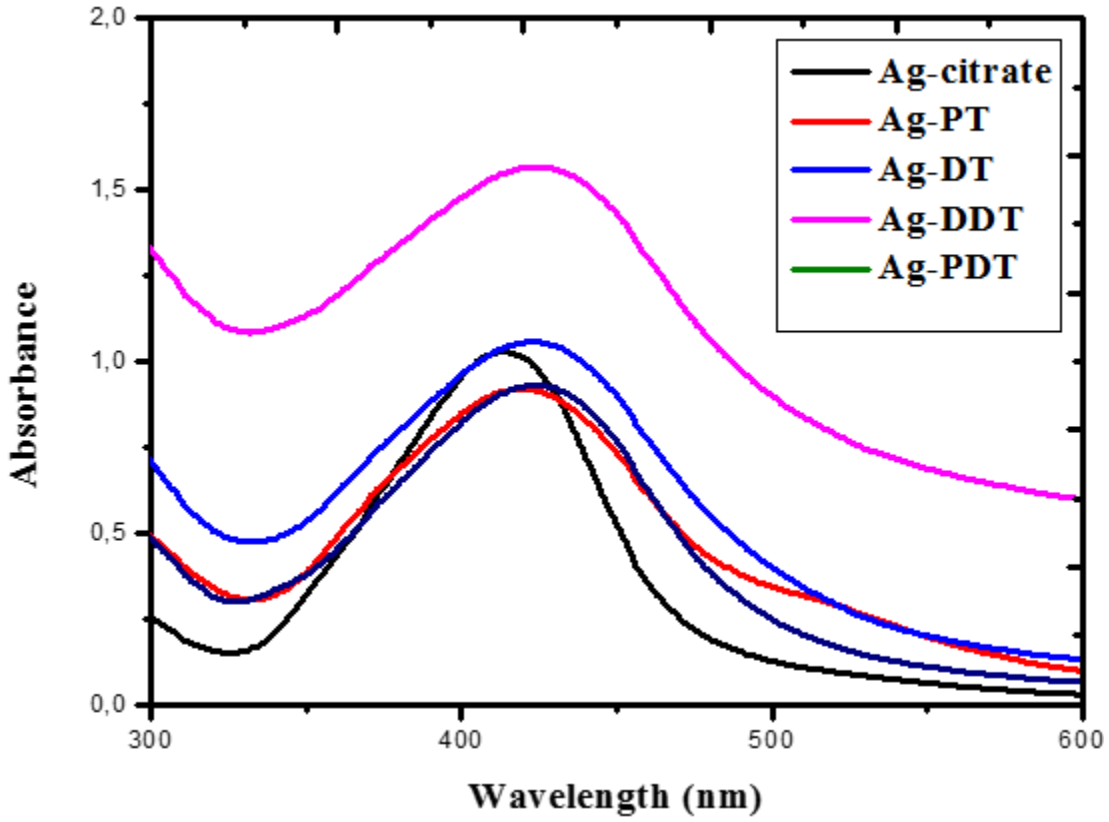


Figure 4.1: UV-Vis absorption spectra of citrate capped and 1-alkanethiols functionalized AuNPs.

Table 4.1: Summary of SPR bands of citrate capped and 1-alkanethiols functionalized AgNPs and their corresponding FWHM values

Sample name	SPR bands (nm)
AgNPs-citrate	414
AgNPs-PT	419
AgNPs-DT	422
AgNPs-DDT	425
AgNPs-PDT	424

Figure 4.2 depicts the particle size distribution, while **Figure 4.3** representing the corresponding TEM micrographs for citrate capped and 1-alkanethiol functionalized AgNPs. TEM micrographs show monodispersed AgNPs with spherical-like morphology and the average diameter of about 25 nm. There was no significant change in the diameters of AgNPs after the modification with 1-alkanethiols. However, a slight agglomeration and aggregation of NPs was observed in the functionalized AgNPs, more especially on the PT functionalized NPs. This effect is attributed to a slow substitution reaction during the replacement of citrate ions by 1-alkanethiols on the surface of AgNPs. The citrate capped AgNPs in colloidal solution characteristically possess anions adsorbed to the surface. These negative charges on the surface influence the repulsive force between the particles and further promote dispersion in solution. The displacement of citrate ions by alkanethiols was evidenced by the reduced inter-particle distance between NPs, and also the tendency of particles to clump together or a slight agglomeration more especially on the shorter chain-length alkanethiol (PT). Such changes in PT functionalized AgNPs might be due to a tendency of shorter chain length ligands to form less dense and weakly bonded SAMs on the surface [12]. Nevertheless, these results corroborate the red-shifting of the absorption spectra.

The zeta potential measurements were necessary for determining the surface potential and stability of NPs before and after functionalization with 1-alkanethiols. Both the citrate capped and 1-alkanethiol functionalized AgNPs show anionic surfaces as depicted in **Table 4.2**. In contrast, PDT functionalized AgNPs showed a cationic surface. The citrate capped AgNPs possesses a strong negative potential which was found to be -19 mV as compared to those for PT, DT and PDT which were found to be -0.174, -0.193, -0.657 and 0.351 respectively. This was due to the negatively charged citrate surrounding the surface of AgNPs. Upon addition of PT, DT, DDT and PDT, a covalent adsorption of thiolate ions is expected to occur since 1-

alkanethiols have a strong chemical affinity towards AgNPs' surface, and most citrate ions will be displaced from the surface. This explains the less negative values of zeta potential prior to the addition of 1-alkanethiols. Moreover, a decrease in zeta potential confirms the loss of stability and the ability of AgNPs to disperse in colloidal solution. In general, AgNPs both citrate and 1-alkanethiols modified showed a lack of stability based on the information from zeta potential measurements. This is because the measured potentials are much more less than -30 mV which is the minimum potential NPs should possess in order to be stable in colloidal solution. **Figure S4.1-S4.5** indicates the zeta potential distribution for both citrate capped and 1-alkanethiols functionalized AgNPs.

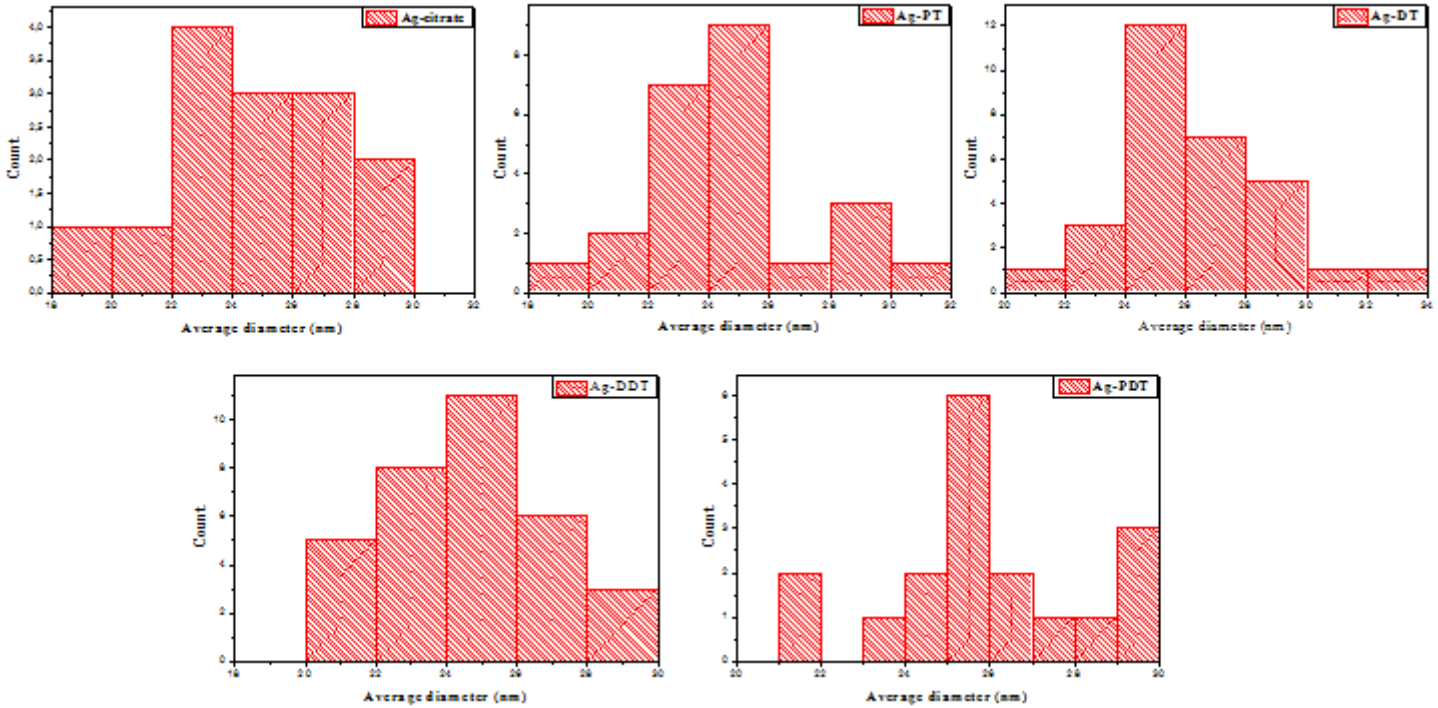


Figure 4.2: Particle size distribution of citrate capped and 1-alkanethiols functionalized AgNPs

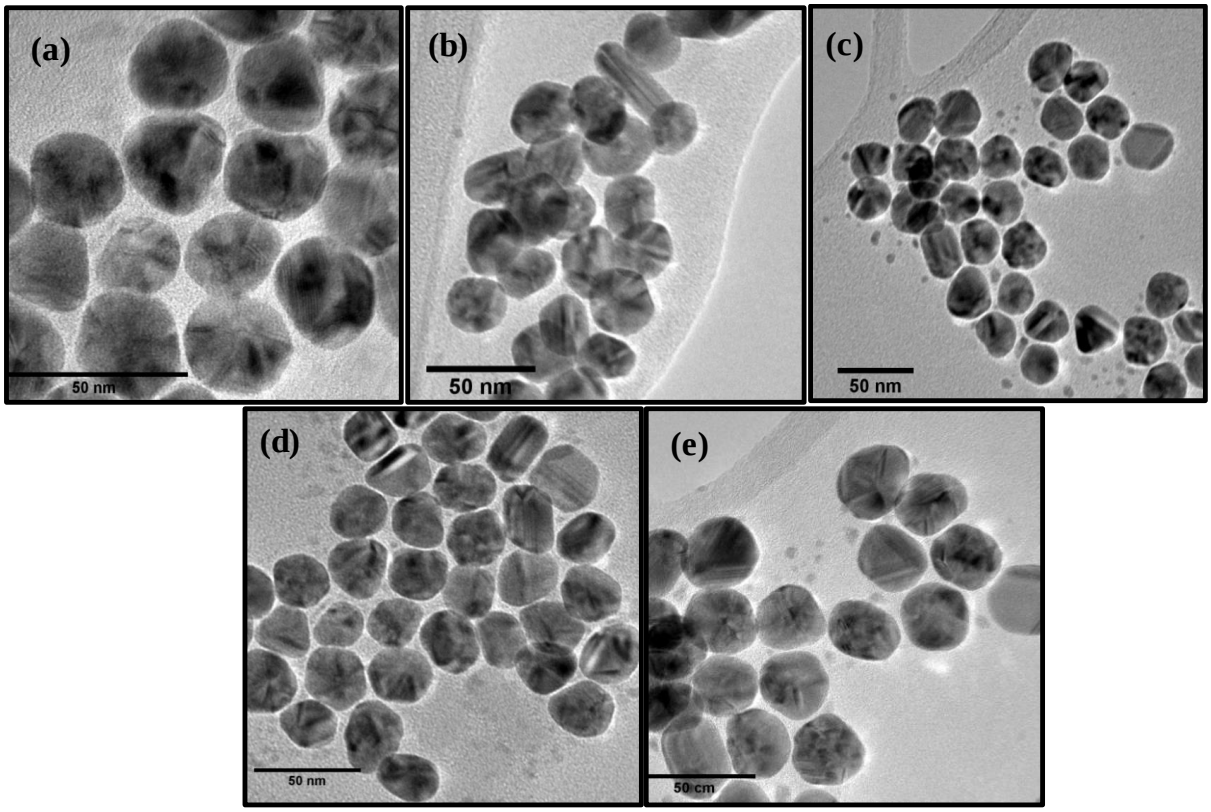


Figure 4.3: TEM images of (a) citrate-capped, (b) PT, (c) DT, (d) DDT, (e) PDT functionalized AgNPs.

Table 4. 2: The values of zeta potentials of citrate capped and 1-alkanethiols functionalized AgNPs.

Sample name	Zeta potential (mV)
Ag-citrate	-19.3
Ag-PT	-0,174
Ag-DT	-0,193
Ag-DDT	-0,657
Ag-PDT	0,351

The SERS spectra (red) of PT, DT, DDT, and PDT together with their normal Raman (NR) spectra (black) are presented in **Figure 4.4**. The significant changes in SERS spectra were observed, with an enhancement of almost all the Raman bands compared to those in the NR spectra. Moreover, some Raman bands (between 800 and 1000 cm^{-1}) which were not observed in NR spectra were observed in SERS spectra. The most significant feature in SERS spectra is the absence of a weak band around 2600 cm^{-1} assigned to υ(S-H) vibration. The disappearance of this band in SERS spectra suggests that S-H group was directly involved in the interaction with the surface of AgNPs. Most interestingly, a new Raman band around 250 cm^{-1} was observed in the SERS spectra (&). This band was assigned to υ(Ag-S) vibration, confirming the interaction between the 1-alkanethiols and AgNPs. Strong SERS bands were also observed around 1550 cm^{-1} (#) and 2900 cm^{-1} (*) assigned respectively to asymmetrical and symmetrical υ(C-H) vibration. **Tables 4.3 - 4.6** show the assignment of other Raman bands which were observed in the NR and SERS spectra.

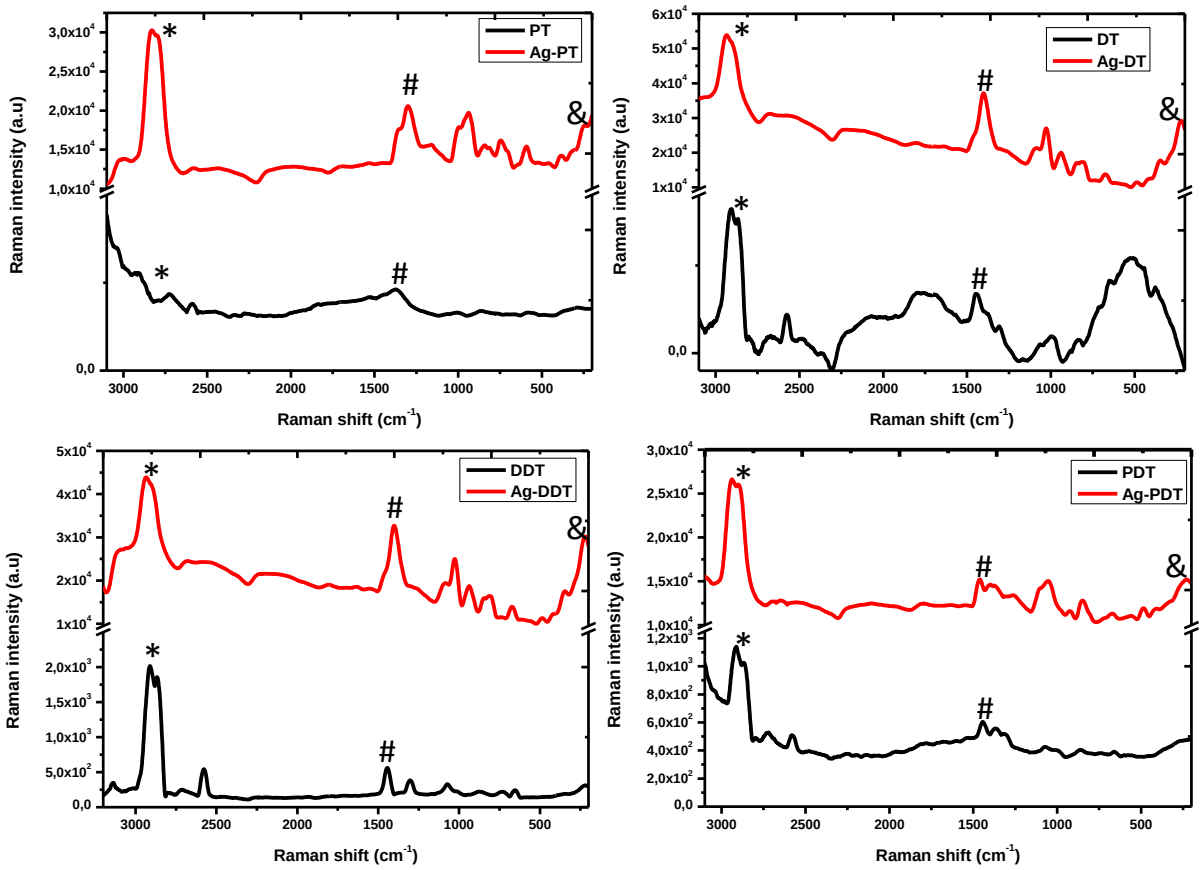


Figure 4.4: Raman spectra of 1-alkanethiols (black) and their corresponding SERS spectra (red).

Table 4. 3: A Summary of the experimental and theoretical bands assignment for PT adsorbed on AgNPs

Band assignment	υ(Ag-S)	υ(C-S)	υ(CC) aliph	δ(CH2) asym	υ(-S-H)	υ(C-H) sym
PT (experimental	no peak	no peak	no peak	1450	2610	2941
Ag-PT (experimental)	250	650, 780, 980	no peak	1420	no peak	2900
PT (theoretical)	no peak	650,700, 780	1050, 1250	1470	2550	-
Ag-PT (theoretical)	250, 300	450, 720, 850	1150, 1350	1510	no peak	2890

PT = Pentanethiol, Ag = Silver, Aliph = aliphatic, sym = symmetric, asym=asymmetric

Table 4. 4: A Summary of the experimental and theoretical bands assignment for DT adsorbed on AgNPs

Band assignment	υ(Ag-S)	υ(C-S)	υ(CC) aliph	δ(CH2) asym	υ(-S-H)	υ(C-H) sym
DT (experimental)	no peak	700, 950	1060, 1300	1480	2588	2890
Ag-DT (experimental)	240	720, 850)	1000	1450	no peak	2980
DT (theoretical)	No peak	750, 800	1100, 1250	1550	2600	2990
Ag-DT (theoretical)	-	-	-	-	No peak	2800

DT = Decanethiol, Ag = silver, Aliph = aliphatic, sym = symmetric, asym=asymmetric

Table 4. 5: A Summary of the experimental and theoretical bands assignment for DDT adsorbed on AgNPs

Band assignment	υ(Au-S)	υ(C-S)	υ(CC) aliph	δ(CH2) asym	υ(-S-H)	υ(C-H) sym
DDT(experimental)	no peak	748	1050, 1250	1490	2620	2980
Ag-DDT (experimental)	240	640, 780, 920	1010	1450	no peak	3000
DDT (theoretical)	no peak	750, 800	1120	1480	2680	2860, 3050
Ag-DDT (theoretical)	-	750	-	-	no peak	2800, 3000

DDT = Dodecanethiol, Ag = Silver, Aliph = aliphatic, sym = symmetric, asym=asymmetric

Table 4. 6: A Summary of the experimental and theoretical bands assignment for PDT adsorbed on AgNPs

Band assignment	υ(Ag-S)	υ(C-S)	υ(CC) aliph	δ(CH2) asym	υ(-S-H)	υ(C-H) sym
PDT (experimental)	no peak	740	1230	1450	2620	2880
Ag-PDT (experimental)	250	600, 850	1100	1450	no peak	2900
PDT (theoretical)	no peak	750, 800	1150, 1250	1480	2500	2900
Ag-PDT (theoretical)	-	750	1150	-	no peak	2900, 3050

PDT = Pentadecanethiol, Ag = silver, Aliph = aliphatic, sym = symmetric, asym=asymmetric

The relationship between the calculated EF and the chain-length of 1-alkanethiol is presented in **Figure 4.5**. The EF for each 1-alkanethiol was calculated using equation 1 in Chapter 3. The symmetrical υ(C-H) vibrational band around 2900 cm^{-1} was used to calculate the EF for all 1-alkanethiols since it acquired the highest intensity. PT was found to possess the highest EF as compared to DT, DDT and PDT. In general, the EF decreased with an increased in chain-length of 1-alkanethiol, however with the exception of DDT. The calculated EFs for all 1-alkanethiols were found to be $3.8*10^3$, $1.6*10^3$, $2.0*10^3$ and $1.5*10^3$ for PT, DT, DDT and PDT, respectively. A similar trend of decreasing EF with an increase in chain-length of 1-alkanethiol was also observed for 1-alkanethiols functionalized AuNPs in Chapter 3.

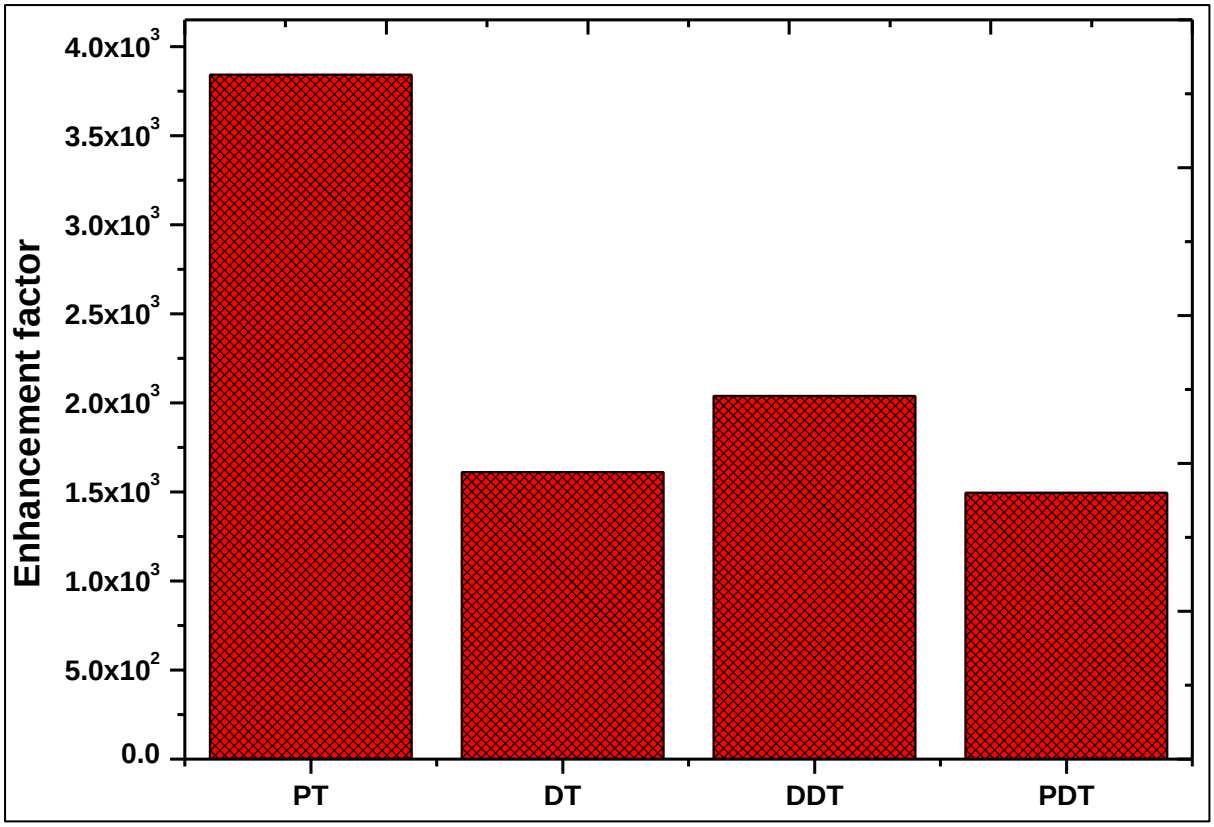


Figure 4. 5: Relationship between the enhancement factor and chain-length of 1-alkanethiols.

The DFT calculations were carried out using Material studio (Dmol3 module) in order to model the theoretical spectra, the chain lengths, the charge densities and nucleophilic centres of 1-alkanethiols. **Figure 4.6** represents the modelled 1-alkanethiols and their chain-lengths; while **Figure 4.7** showing the manner through which the 1-alkanethiols adsorb on the surface of AgNPs. It was clear from **Figure 4.7** that the 1-alkanethiols adsorb on the surface through thiolate group. These results were expected since there were no other functional groups from 1-alkanethiols which could've competed with sulphur atoms towards binding with Ag. Moreover, the geometry of the alkanethiols on the surface of the AgNPs was different as compared to AuNPs. The Ag-PT is more bent than the Au-PT whilst the Ag-DT is more linear compared to Au-DT. This might have an influence on the observed EF trend.

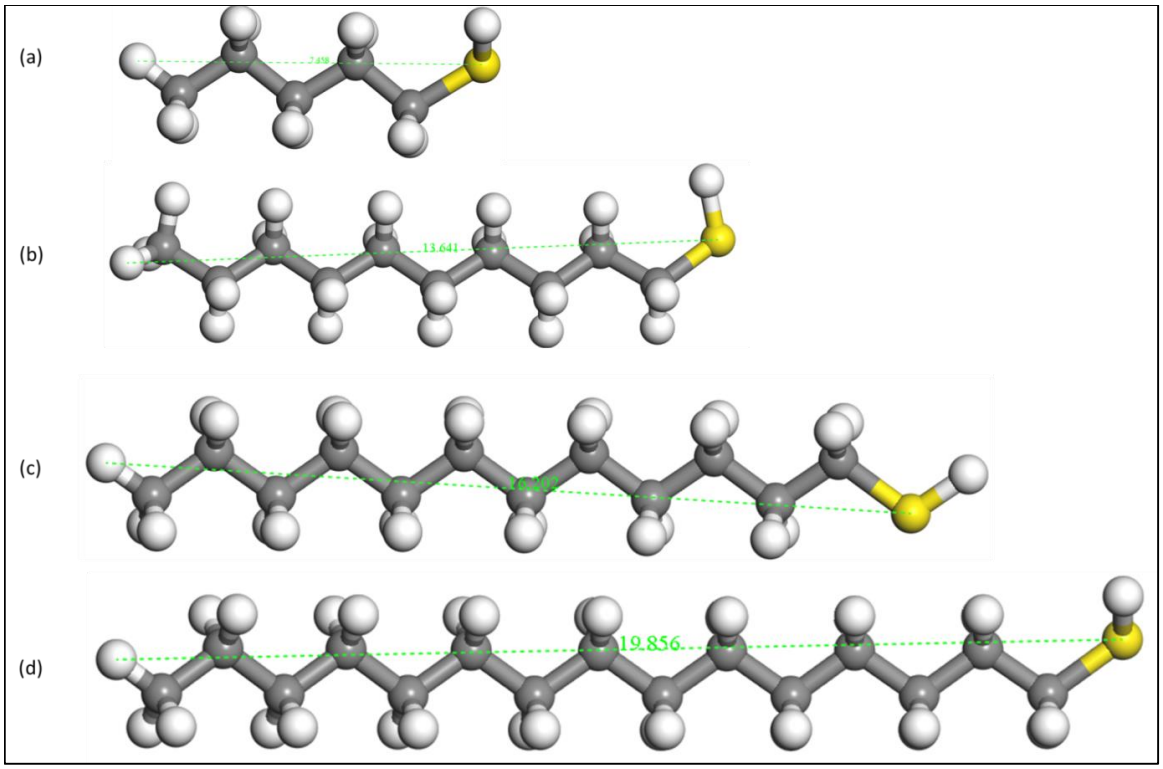


Figure 4. 6: The modelled 1-alkanethiols and their chain-lengths (a) 1-PT, (b) 1-DT, (c) 1-DDT, (d) 1-PDT.

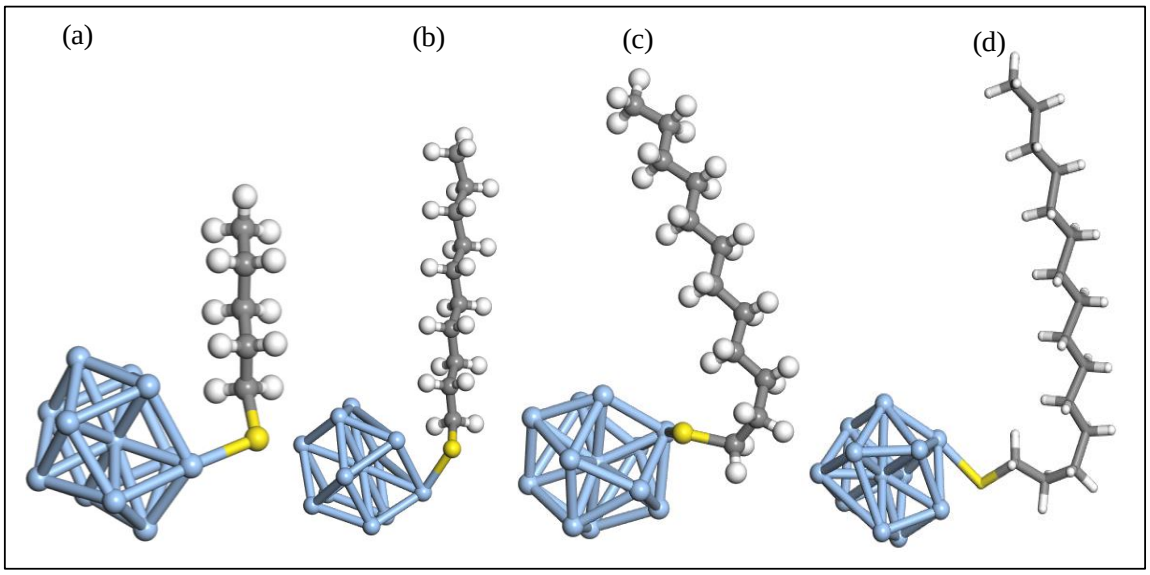


Figure 4.7: Optimized geometries of (a) Ag-PT, (b) Ag-DT, (c) Ag-DDT and (d) Ag-PDT.

The Raman spectra of modelled 1-alkanethiols both before and after they were adsorbed on AgNPs are shown in **Figure 4.8**. The disappearance of υ(S-H) vibrational band around 2600 cm^{-1} was observed from all the 1-alkanethiols functionalized AgNPs spectra. The emergence of a new vibrational peak around 0 - 200 cm^{-1} which is assigned to υ(Ag-S) vibrational band was observed for the Ag-PT spectrum hence confirming the adsorption of PT through sulphur atoms as shown in **Figure 4.8**. Ag-DT, Ag-DDT and Ag-PDT showed no evidence of the new peak however the peak at 3000 cm^{-1} was enhanced as compared to the NR spectra. In fact, Ag-PDT showed the highest intensity suggesting the highest EF.

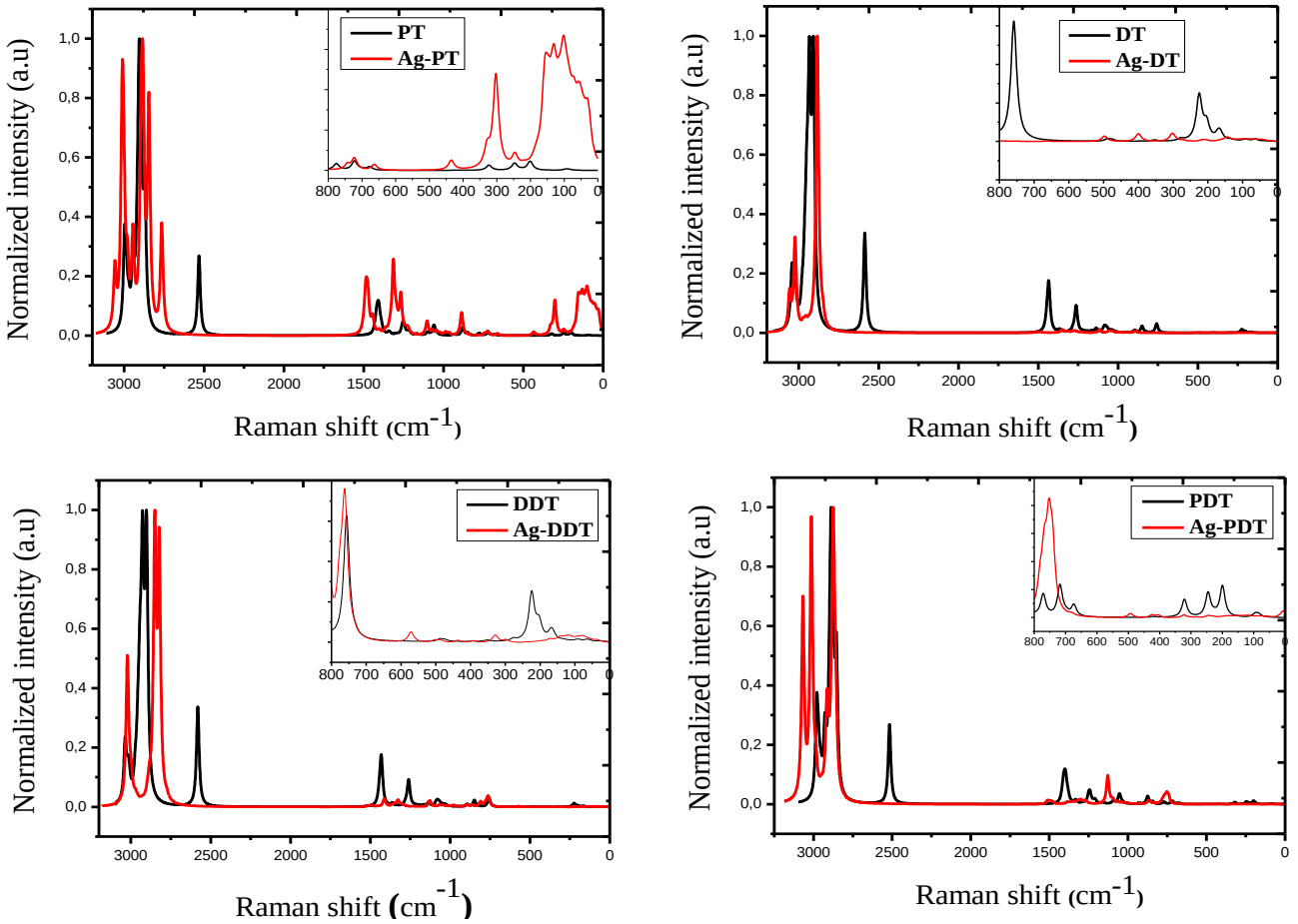
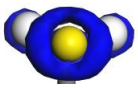
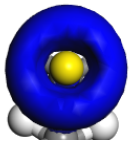


Figure 4.8: DFT calculated Raman spectra of (a) PT, (b) DT, (c) DDT, and (e) PDT together with the insert of the zoomed lower region of the spectra.

Nonetheless, it was difficult to establish a defined trend between the chain-length and the EF of the Raman scattering. This undefined trend might be due to the way 1-alkanethiols were adsorbed on the surface during the modelling process. It is important to adsorb the molecule on the same site or atom for all calculations, since different sites possess different surface energy. The way 1-alkanethiols were adsorbed on the surface might've played a vital role in this inconsistency. The calculated nucleophilic centres for each 1-alkanethiols are also shown in **Table 4.7**. The increase in the length of the nucleophilic centres with an increase in the chain-length was observed, suggesting that the PDT will bind strongly to the metal surface and therefore would likely have the highest EF.

Table 4. 7: DFT calculated nucleophilic centres of PT, DT, DDT, and PDT

Raman reporters	**Nucleophilic centres**	**Diameters (Å)**
1-Pentanethiol		1.9
1-Decanethiol		2.8
1-Dodecanethiol		3.2
1-Pentadecanethiol		3.7

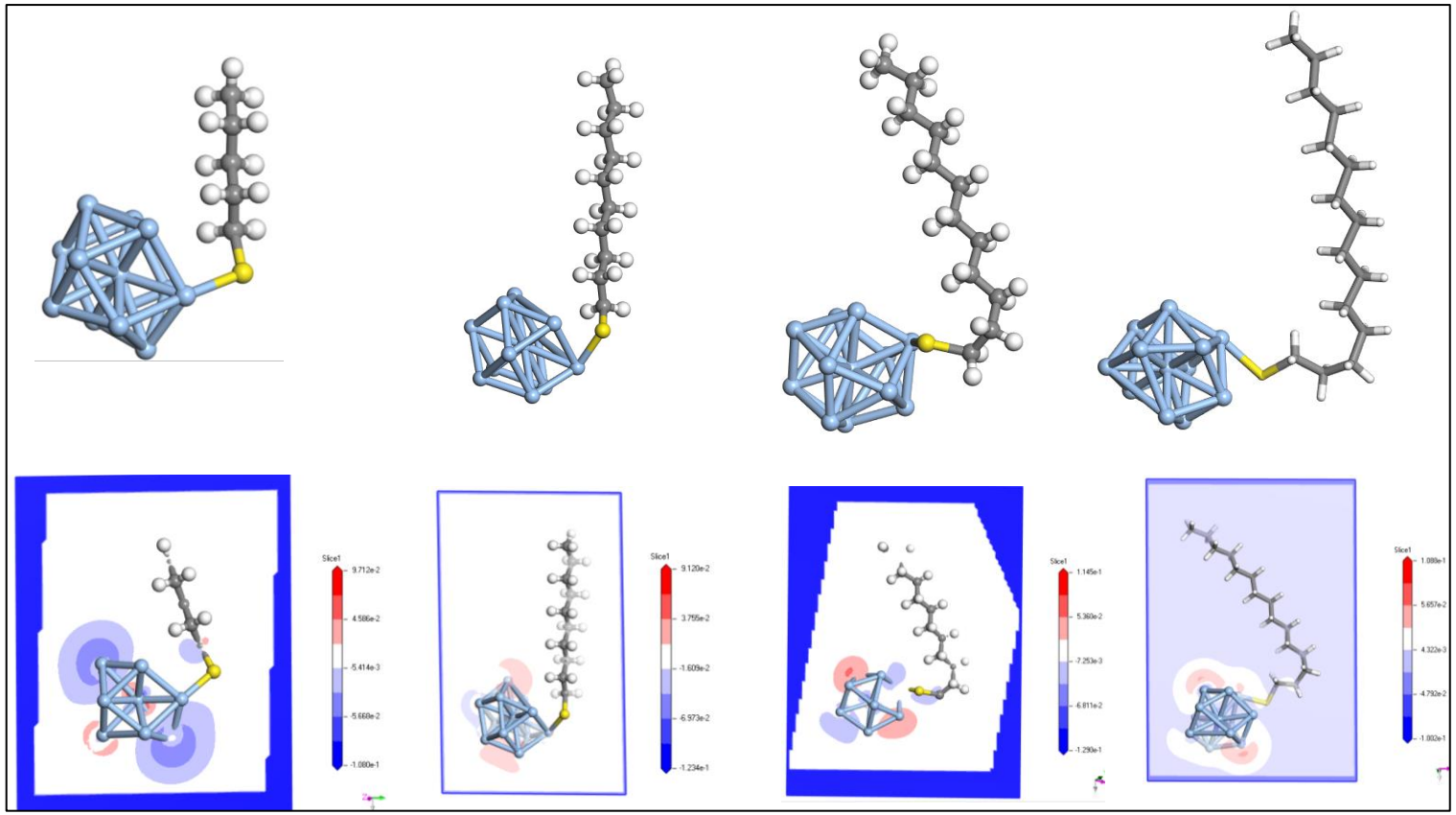


Figure 4.9: The calculated molecular geometry on the surface of AgNPs and their effect on the charge density

These observations were consistent with an increase in the charge density on the metallic surface (**Figure 4.9**) as a result of strong charge transfer by longer 1-alkanethiols. Unlike the shorter chain 1-alkanethiols, PDT will have a significant effect on the chemical properties of AgNP, which will further promote a charge transfer from its HOMO to the LUMO or to the conduction band of the metal. These effects are expected to influence the Raman signal in some ways. Therefore, by only considering a chemical enhancement mechanism, PDT should then possess a strong Raman signal enhancement. However, this was not the case in the calculation performed in the experimental session. These results were found to oppose the trend of SERS EF. This might be due to the fact that the calculated EF in the experimental session included both the chemical and electromagnetic effects. It is also important to note that the DFT calculation doesn't include the effect of hot spots caused by a slight agglomeration of nanoparticles which are functionalized with shorter chain 1-alkanethiols. In DFT, only one cluster is used as a substrate, which is why there won't be any hot spots creation. More understanding on the effects of 1-alkanethiols on electronic and chemical properties of nanoparticles can open more gates in understanding SERS effects, more especially in the chemical point of view.

4.4 Conclusion

AgNPs were successfully prepared and further functionalized by PT, DT, DDT and PDT. The spherical-like AgNPs ware obtained as was evidenced from TEM micrographs. There was no significant agglomeration or morphological change of NPs upon functionalization as was also evidenced from TEM micrographs. The UV-Vis showed sharp SPR bands around 420 nm, which confirmed the presence of stable and spherical AgNPs in the colloidal solution. The surface charge of AgNPs, both functionalized and unfunctionalized was found to be negative. SERS experiments showed an improvement in the intensity of all 1-alkanethiols spectra as

compared to the ones obtained from the NR studies. The calculated EF of Raman scattering was found to decrease with an increase in the chain-length of 1-alkanethiols, with PT possessing the highest EF and PDT the lowest. The modelling studies suggested that the Ag-PDT will have the highest contribution to EF from chemical effects due to the large nucleophilic centre, highest charge density transfer to the metal as well as highest intensity of the 3000 cm^{-1} peak in the simulated SERS spectrum. However it must be reiterated that EF is affected by both chemical effects and electromagnetic effects.

4.5 References

1. Wei, L., Lu, J., Xu, H., Patel, A., Chen, Z.S. and Chen, G., 2015. ***Drug Discov. Today***, *20*(5), pp.595-601.
2. Daniel, M.C. and Astruc, D., 2004. ***Chem rev***, *104*(1), pp.293-346.
3. Cirri, A., Silakov, A., Jensen, L. and Lear, B.J., 2016. ***J. Am. Chem. Soc***, *138*(49), pp.15987-15993.
4. Asghari, S., Johari, S.A., Lee, J.H., Kim, Y.S., Jeon, Y.B., Choi, H.J., Moon, M.C. and Yu, I.J., 2012. ***J. nanobiotech***, *10*(1), p.14.
5. Agnihotri, S., Mukherji, S. and Mukherji, S., 2013. ***Nanoscale***, *5*(16), pp.7328-7340.
6. Bindhu, M.R. and Umadevi, M., 2015. ***Spectrochim. Acta Mol. Biomol. Spectrosc***, *135*, pp.373-378.
7. Joseph, S. and Mathew, B., 2015. ***J Mol Liq***, *204*, pp.184-191.
8. Liu, K., Bai, Y., Zhang, L., Yang, Z., Fan, Q., Zheng, H., Yin, Y. and Gao, C., 2016. ***Nano lett***, *16*(6), pp.3675-3681.
9. Cao, Q., Liu, X., Yuan, K., Yu, J., Liu, Q., Delaunay, J.J. and Che, R., 2017. ***Appl. Catal. B Environ,*** *201*, pp.607-616.
10. Kreibig, U. and Vollmer, M., 1995. ***Mat. Scie. Springer-Verlag, Berlin***.

11. Mrksich, M. and Whitesides, G.M., 1996. ***Annu. Rev. Biophys,*** *25*(1), pp.55-78.
12. Piner, R.D., Zhu, J., Xu, F., Hong, S. and Mirkin, C.A., 1999. ***science***, *283*(5402), pp.661-663.
13. Kumar, A., Biebuyck, H.A., Abbott, N.L. and Whitesides, G.M., 1992. ***J. Am. Chem. Soc***, *114*(23), pp.9188-9189.
14. Kennedy, B.J., Spaeth, S., Dickey, M. and Carron, K.T., 1999. ***J. Phys. Chem. B,*** *103*(18), pp.3640-3646.
15. Cirri, A., Silakov, A., Jensen, L. and Lear, B.J., 2016. ***J. Am. Chem. Soc,*** *138*(49), pp.15987-15993.
16. Lee, P.C. and Meisel, D., 1982. ***J. Phys Chem***, *86*(17), pp.3391-3395.

Chapter 5

General Conclusions and Recommendations

5.1 Conclusions

5.1.1 Synthesis and functionalization of Au and Ag nanoparticles

Au and Ag nanoparticles with a spherical morphology were successfully synthesized by chemical reduction method. The resulting nanoparticles were further functionalized with 1-alkanethiols of various chain-lengths. Various spectroscopic and microscopic techniques were used to determine their optical and chemical properties. The SPR bands for both Au and Ag nanoparticles showed a slight red shift prior to functionalization with 1-alkanethiol as a result of change in dielectric environment. The measured zeta potentials confirm well dispersed nanoparticles with a medium to good stability. The surface charge of all nanoparticles was found to be negative as indicated by negative values of zeta potentials.

5.1.2 The dependence of Raman scattering cross-section on the chain-length of 1-alkanethiols

The effect of chain-length of 1-alkanethiols functionalized on the surface of Au and Ag nanoparticle on Raman activity was successfully investigated. The calculated EFs were found to be higher for shorter chain-length 1-alkanethiols as compared to 1-alkanethiols with long chain-length. This trend was clearly observed in all cases where Au and Ag nanoparticles were separately used as SERS substrate.

5.1.3 Modelling of SERS

The DFT calculations were successfully performed for the determination of the effect of 1-alkanethiols on electronic properties of SERS substrate and SERS EF. The calculated nucleophilic centre cross-sections were found to increase with an increase in the chain-length

of alkanethiol, resulting in an increase of charge density on the surface of SERS substrate. The calculated Raman spectra confirmed the adsorption of alkanethiols through sulphur atoms as was also observed on the experimental studies. The longer chain alkanethiols were found to contribute more to the SERS EF (SERS signals) through chemical effect as compared to the shorter chain alkanethiols.

5.2 Recommendations and future work

The study on the effect of concentration of each 1-alkanethiol is highly recommended for concentration optimization and determination of the limit of detection. More theoretical studies on the effect of 1-alkanethiols on the surface chemistry of metallic nanoparticles will be more significant in understanding their influence on Raman signal enhancement; more significantly on the CE mechanism. Careful attention on modelling the nanoparticles is probably required so that the molecules can be absorbed on the same active site. In fact an investigation on which site could yield the highest EF could also be done. The EME mechanism can also be investigated in order to determine if indeed high EF values can be obtained and whether these are independent of the chemical properties such as the chain-length of the RRs.

Appendix

Supplementary information

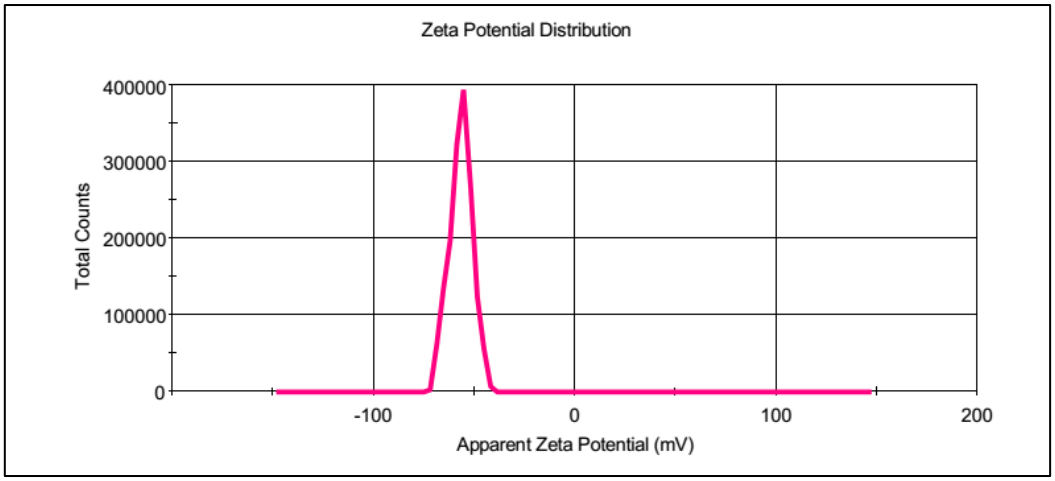


Figure S3. 1: Zeta potentials of AuNPs stabilized by tri-sodium citrate.

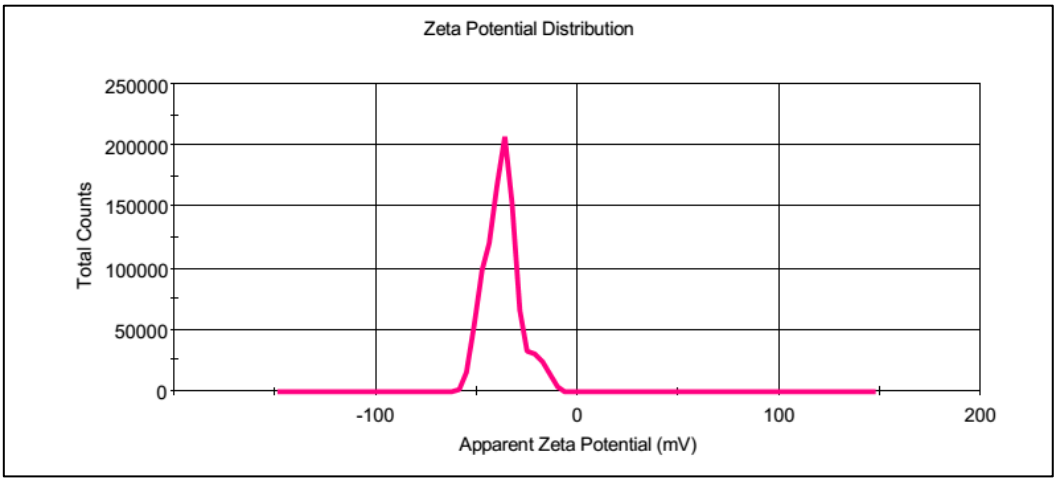


Figure S3. 2: Zeta potentials of AuNPs stabilized by PT.

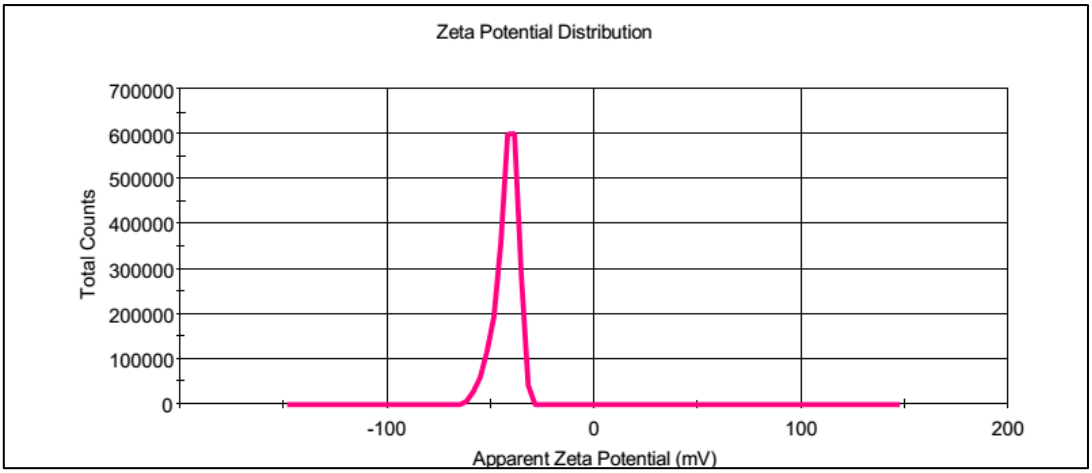


Figure S3. 3: Zeta potentials of AuNPs stabilized by DT.

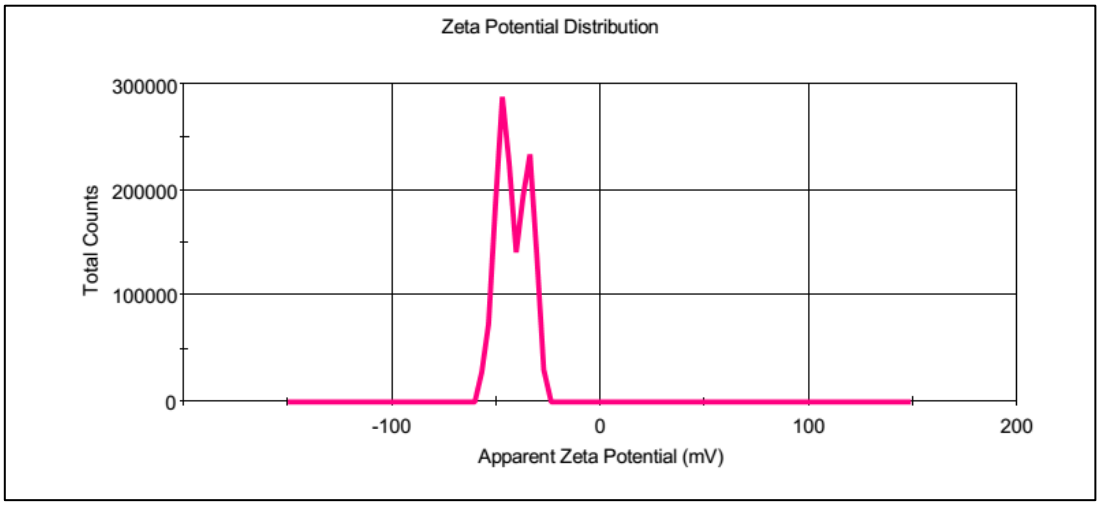


Figure S3. 4: Zeta potentials of AuNPs stabilized by DDT.

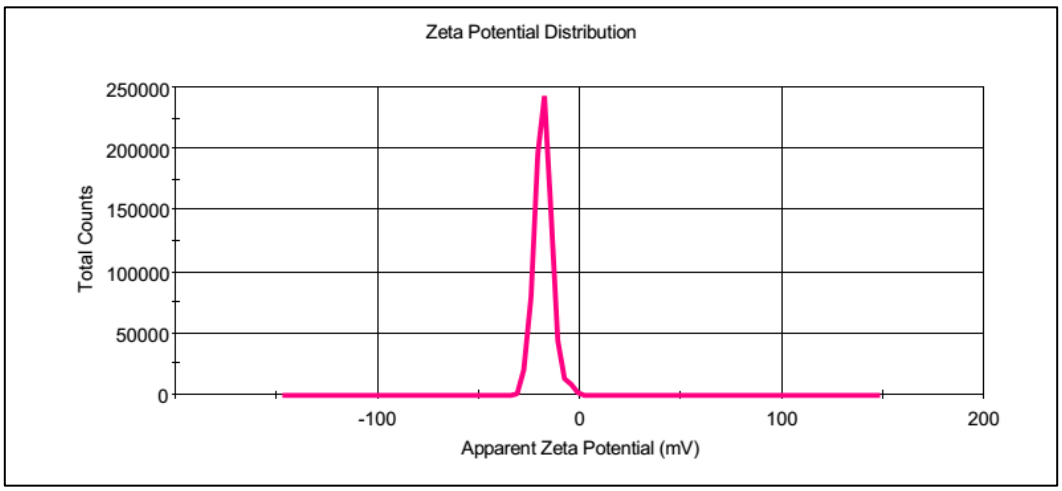


Figure S3. 5: Zeta potentials of AuNPs stabilized by PDT.

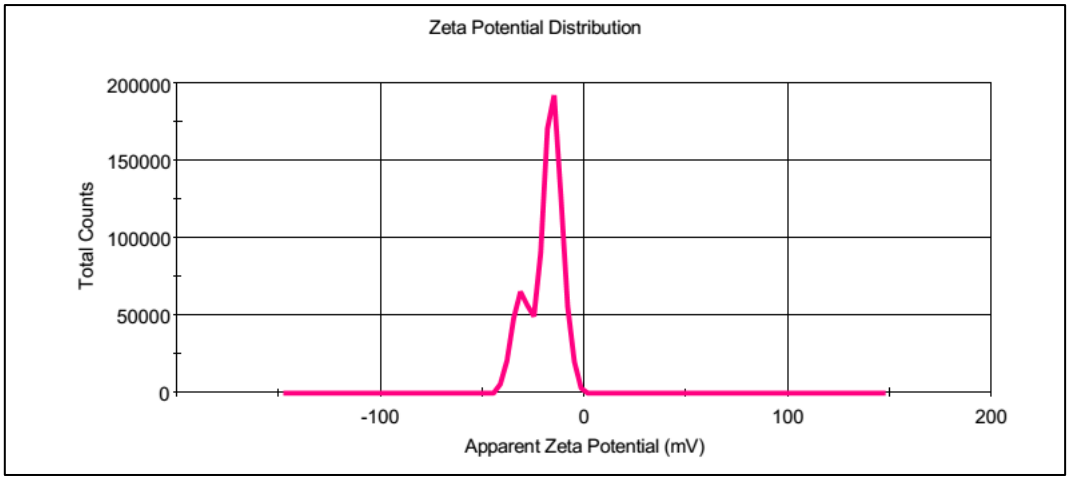


Figure S4. 1: Zeta potentials of AgNPs stabilized by tri-sodium citrate.

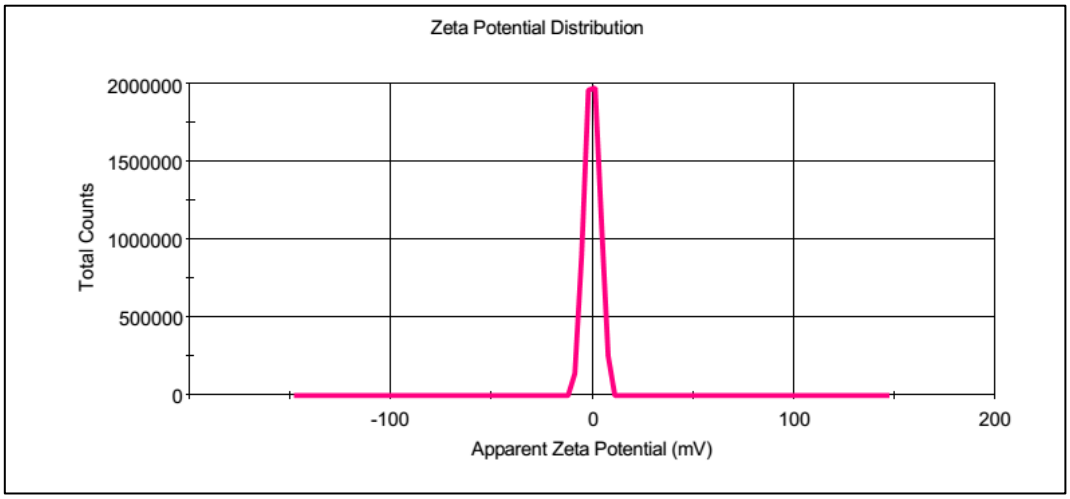


Figure S4. 2: Zeta potentials of AgNPs stabilized by PT.

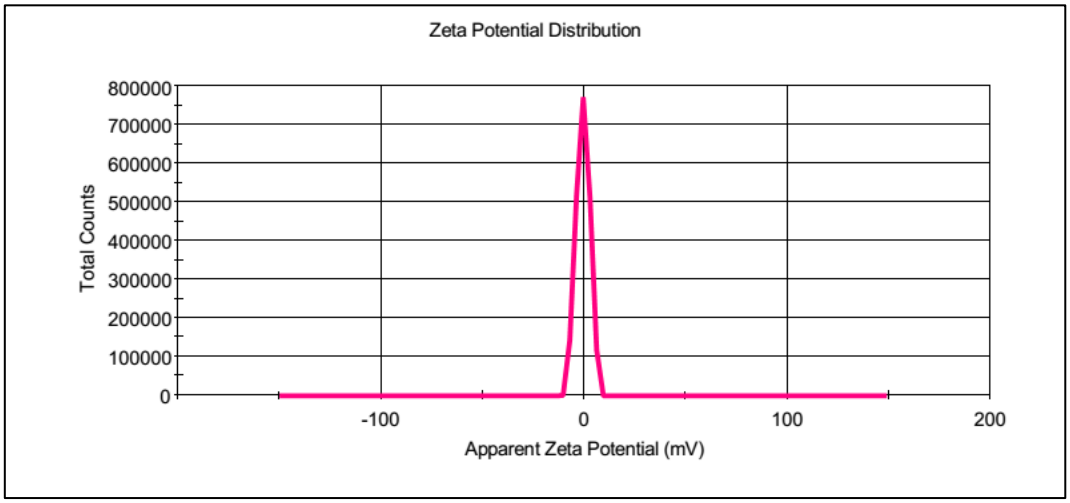


Figure S4. 3: Zeta potentials of AgNPs stabilized by DT.

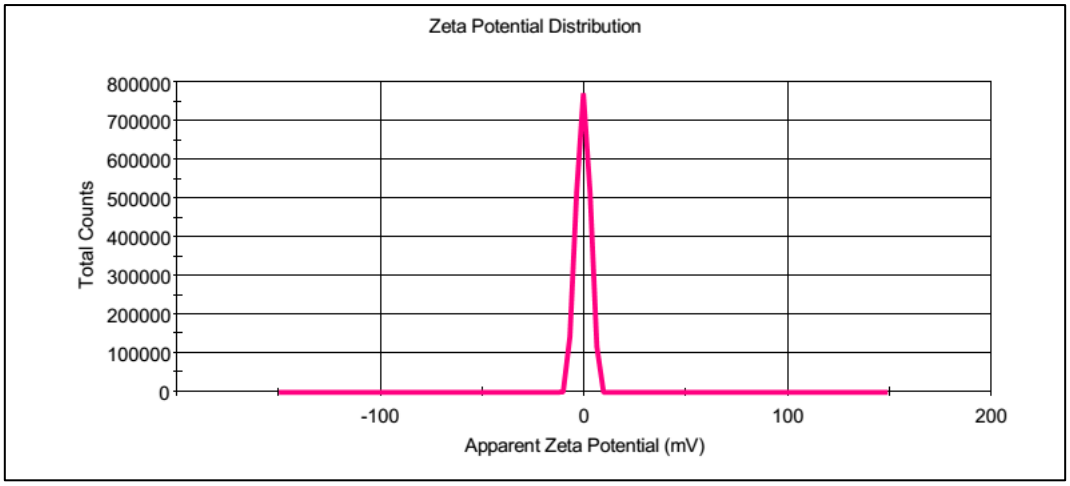


Figure S4. 4: Zeta potentials of AgNPs stabilized by DDT.

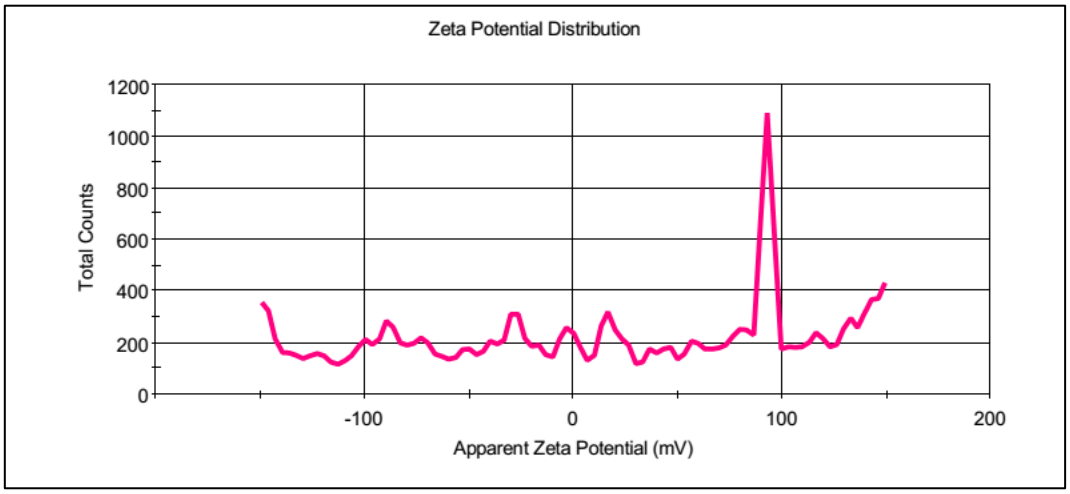


Figure S4. 5: Zeta potentials of AgNPs stabilized by PDT.